



NTNU – Trondheim
Norwegian University of
Science and Technology

Numerical Models for Dynamic Properties of a 14 Storey Timber Building

Ingunn Utne

Civil and Environmental Engineering

Submission date: December 2012

Supervisor: Kjell A Malo, KT

Norwegian University of Science and Technology
Department of Structural Engineering



MASTER THESIS 2012

| | | |
|--|-----------------------------|----------------------|
| SUBJECT AREA: Timber Structures, Dynamics | DATE: December 18th 2012 | NO. OF PAGES: 138 |
|--|-----------------------------|----------------------|

TITLE:

Numerical Models for Dynamic Properties of a 14 Storey Timber Building

Numeriske modeller for dynamiske egenskaper av et 14 etasjes trehus

BY:

Ingunn Utne



SUMMARY:

The world tallest timber building with height of 45 meters, is planned for Bergen, Norway. In this master thesis the dynamic properties of the case building, as proposed by Sweco and Artec, are investigated. The proposed structural concept with a glulam frame and power-storeys, have never previously been built, and it is desirable to develop and understanding of the dynamic problems concerning this building. Previous work have shown problems with acceleration levels for tall timber building, mostly due to the material properties of timber. Timber has high flexibility and strength combined with low weight.

The main aim of the work have been to build a 3D-model of the case building in a finite element program, where numerical methods can be used to find the dynamic properties of the building. The wind load and acceleration levels are investigated, and found to be reasonable compared to various criterions presented. The effect of the stiffness in the connections, as well as the use of apartment modules are investigated. In addition a dynamic analysis is run, and stochastic subspace state space system identification is used to verify the model. This can later be used for verification of the actual building when finished, and will be an important method to determine the actual damping and stiffness.

Based on the findings in this work, the concept is assumed feasible, possible with some changes an even better concept is achieved. It will be exciting to see how Sweco will develop the concept further in the next planning phase.

KEYWORDS: *dynamic response, timber buildings, system identification, acceleration requirements*

RESPONSIBLE TEACHER: Kjell Arne Malo

SUPERVISOR(S): Ole André Øiseth, Magne Bjertnes (Sweco),

CARRIED OUT AT: Department of Structural Engineering, NTNU

Masteroppgave 2012

Ingunn Utne

Numeriske modeller for dynamiske egenskaper til et 14 etasjes trehus (Numerical Models for dynamic Properties of a 14 Storey Timber Building)

Bakgrunn:

Vi ønsker å undersøke om limtre og massivtre kan danne stammen for høyere hus opptil for eksempel 20 etasjer. Som eksempelbygg benyttes byggesystemet som planlegges for et 14 etasjers høyhus i tre i Bergen. Dette byggeprosjektet forventes å bli verdens høyeste trehus (VHT) i en periode og er tegnet av arkitektfirmaet ARTEC og SWECO er byggeteknisk konsulent.

I denne masteroppgaven skal de dynamiske egenskapene til VHT kartlegges ved hjelp av numeriske simuleringer med elementmetoden (Abaqus). Det antas at det er nødvendig å benytte forenklete modeller av boligmodulene i dette arbeidet. Videre skal mulige plasseringer av måleinstrumenter for måling av dynamisk respons utredes. Måleresultatene fra disse instrumentene skal senere benyttes til systemidentifikasjon av ferdig byggverk. En numerisk modell kan også danne grunnlag for konstruktiv optimalisering og det er ønskelig at også denne muligheten utnyttes.

Forslag til gjennomføring av oppgaven:

1. Kandidaten foretar et studium med sikte på å skaffe seg oversikt over problematikken rundt vibrasjoner og dynamiske egenskaper av høye trehus.
2. Kandidaten setter seg inn i og sammenfatter tidligere studier med vekt på bæresystemer i limtre (og eventuelt massivtre) og forbindelser.
3. Kandidaten benytter VHT som case og modellerer dette bygget med FEM programmet Abaqus med en modell som kan benyttes til parameterstudier.
4. Kandidaten foretar et sensitivitetsstudium av VHT med spesiell vekt på stivhetsegenskaper av forbindelsene mellom komponenter.
5. Kandidaten utarbeider en oversikt over mulige plasseringer av måleinstrumenter for aksellerasjoner. Hensikten med plassering av måleinstrumenter er å instrumentere ferdig bygg og benytte måleresultatene for systemidentifikasjon.
6. Kandidaten kan foreslå endringer eller forbedringer av bæresystemet og dokumentere effekten av dette hvis tiden tillater det.
7. Kandidaten sammenfatter og lager en konklusjon på undersøkelsen.

Etter samråd med veiledere kan kandidaten konsentrere sitt arbeide til spesielle deler av oppgaven, eller trekke inn andre aspekter.

Generelt:

Besvarelsen skal ha form som en forskningsrapport hvor det legges vekt på en klar og oversiktlig presentasjonsform. Besvarelsen skal leveres ved Institutt for konstruksjonsteknikk innen 20. des 2012.

Faglærer: Kjell Arne Malo

Veiledere: Kjell Arne Malo (NTNU) og Magne Bjærtnes (SWECO)

Preface

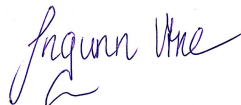
This master thesis is the end of the 5-year study programme *Master of Science in Civil Engineering*. It is carried out at the Department of Structural Engineering, under the Faculty of Engineering, Science and Technology at the Norwegian University of Science and Technology in Trondheim. The work presented in this thesis is a result of 20 weeks work, fall semester 2012, corresponding to 30 credits.

The master thesis is a collaboration between NTNU and Sweco, and I have had the possibility to follow the planning process of the "*soon to be*" world tallest timber building. This have been very instructive, but also challenging, partially due to the dissimilar time perspective between my work and Sweco's work. A lot of time is spent learning the FEM-program Abaqus/CAE, and from starting at scratch, with almost no prior knowledge, I can now say I master several of the possibilities and functions in the program. Also gaining knowledge on previously unknown theory such as system identification, acceleration requirements and the complexity of damping have been interesting. Hopefully, the work can be used for verification of the work done by Sweco.

I am very grateful to supervisor Kjell Arne Malo and associate professor Ole Øiseth, both at the Department for Structural Engineering, NTNU. They have supported me through my work, showed flexibility, and always helped me when I needed guidance.

I would also like to express my thanks to Magne Bjærtne at Sweco, he has showed an inspiring enthusiasm and knowledge, always willing to help. Finally a thank you to fellow student Anders Jørstad, for computer aid, good discussions and problem solving during the process.

Oslo, December 18th, 2012



Ingunn Utne

Abstract

The world tallest timber building with height of 45 meters, is planned for Bergen, Norway. In this master thesis the dynamic properties of the case building, as proposed by Sweco and Artec, are investigated. The proposed structural concept with a glulam frame and power-storeys, have never previously been built, and it is desirable to develop and understanding of the dynamic problems concerning this building. Previous work have shown problems with acceleration levels for tall timber building, mostly due to the material properties of timber. Timber has high flexibility and strength combined with low weight.

The thesis is divided into two parts, one theoretical treating the background theory, and where tall timber buildings, the dynamic challenges and methods used are presented. Next is the modeling part, where the case building is modeled, analyzed and results are discussed.

The main aim of the work have been to build a 3D-model of the case building in a finite element program, where numerical methods can be used to find the dynamic properties of the building. The wind load and acceleration levels are investigated, and found to be reasonable compared to various criterions presented. The effect of the stiffness in the connections, as well as the use of apartment modules are investigated. In addition a dynamic analysis is run, and stochastic subspace state space system identification is used to verify the model. This can later be used for verification of the actual building when finished, and will be an important method to determine the actual damping and stiffness.

Based on the findings in this work, the concept is assumed feasible, possible with some changes an even better concept is achieved. It will be exciting to see how Sweco will develop the concept further in the next planning phase.

Sammendrag

Verdens høyeste trehus, med høyde på 45 meter, er under planlegging i Bergen, Norge. I denne masteroppgaven vil de dynamiske egenskapene til eksempelbygget, slik som det er foreslått av Sweco og Artec, bli undersøkt. Det foreslåtte bæresystemet med limtre ramme og power-etasjer, har aldri tidligere blitt bygd, og det er ønskelig å utvikle en forståelse for de dynamiske problemene en kan møte på med dette bygget. Tidligere arbeid har vist at det kan bli problemer med aksellerasjonsnivåene for høye trehus, som regel på grunn av material egenskapene til tre. Treet har høy fleksibilitet og stivhet, kombinert med lav vekt.

Denne masteroppgaven er delt opp i to deler, en teoretisk del som behandler bakgrunnsteori, og der høye trebygg, dynamiske utfordringer og metoder blir presentert. Videre er en modellering del, hvor case bygningen blir modellert, analysert og resultater blir diskutert.

Hovedmålet med denne oppgaven har vært å lage en 3D-modell av eksempelbygget i et elementmetodeprogram, der numeriske metoder kan brukes for å kartlegge de dynamiske egenskapene til bygget. Vindlasten og aksellerasjonsnivåene blir undersøkt, og funnet til å være akseptable i henhold til ulike krav som blir presentert. Effekten av stivheten i knutepunktene, og bruken av leilighetsmoduler blir undersøkt. I tillegg er en dynamisk analyse kjørt, og stokastisk system identifikasjon blir brukt til å verifisere modellen. Dette kan senere brukes til å verifisere den faktiske bygningen når den er ferdigstilt, og vil være en viktig metode til å estimere den faktiske dempingen og stivheten.

Basert på dette arbeidet, antas konseptet å være brukbart, muligens vil det med noen få endringer kunne bli enda bedre. Det vil bli spennende å se hvordan Sweco utvikler konseptet videre i neste planleggingsfase.

Contents

| | | |
|----------|---|-----------|
| 1 | Introduction | 1 |
| 1.1 | Background | 1 |
| 1.2 | Scope of present Work | 1 |
| 1.3 | Project: <i>The World Tallest Timber Building</i> | 2 |
| 1.4 | Limitations | 2 |
| 2 | Building tall with Timber | 5 |
| 2.1 | Timber as construction Material | 5 |
| 2.1.1 | Glued laminated Timber - <i>Glulam</i> | 6 |
| 2.2 | Tall Timber Buildings | 8 |
| 2.2.1 | Examples | 8 |
| 3 | Dynamics | 11 |
| 3.1 | Dynamic Properties of a Structure | 11 |
| 3.2 | Dynamic Loads on Buildings | 12 |
| 3.2.1 | Representation of the Wind Load | 13 |
| 3.2.2 | Structural Response to dynamic Loads | 16 |
| 3.2.3 | Acceleration | 18 |
| 3.3 | Damping | 19 |
| 3.3.1 | Damping in Structures | 22 |
| 3.4 | Monitoring of tall Buildings | 23 |
| 3.4.1 | Sensors | 23 |
| 3.5 | System Identification | 25 |
| 3.5.1 | Mathematical Model of the System | 26 |
| 3.5.2 | The State Space Model | 27 |
| 3.5.3 | Algorithm for System Identification of an Output-only Model | 28 |
| 4 | Modelling and analysis | 31 |
| 4.1 | The case building | 31 |
| 4.2 | Model in <i>Abaqus</i> | 33 |
| 4.2.1 | Material properties | 34 |
| 4.2.2 | Modeling of damping | 35 |
| 4.3 | Analysis | 36 |
| 4.4 | Model for system identification | 37 |

| | | |
|----------|--|-----------|
| 4.4.1 | Retrieving measurement data | 37 |
| 4.4.2 | Preprocessing | 37 |
| 4.4.3 | Identification | 37 |
| 4.4.4 | Model updating | 39 |
| 5 | General results for simplified model | 41 |
| 5.1 | Eigenfrequency | 41 |
| 5.1.1 | Mass | 44 |
| 5.1.2 | Boundary Conditions at Foundation | 44 |
| 5.1.3 | Damping | 45 |
| 5.2 | Spectral Analysis | 48 |
| 5.3 | Serviceability | 50 |
| 5.3.1 | Maximum Displacement | 51 |
| 5.3.2 | Maximum Acceleration | 51 |
| 5.4 | Locations of Instruments | 56 |
| 5.4.1 | Verification of the Model using System Identification | 57 |
| 5.4.2 | Effect of damping in model on the results from system identification | 62 |
| 5.5 | Suggestions for improving the Superstructure | 65 |
| 5.5.1 | Increasing the mass in the concrete slabs | 65 |
| 5.5.2 | Using concrete slab as roof | 66 |
| 5.5.3 | Reducing the number of storeys | 67 |
| 5.5.4 | Coupling of CLT walls | 67 |
| 5.5.5 | Tuned mass damper at roof | 67 |
| 6 | Parametric study | 69 |
| 6.1 | Connections | 69 |
| 6.1.1 | Modeling of Connections | 70 |
| 6.1.2 | 2D-truss | 70 |
| 6.1.3 | Reducing A in Beam Segments | 72 |
| 6.1.4 | Reducing I in Beam Segments | 73 |
| 6.1.5 | Energy dissipation in Connections | 73 |
| 6.1.6 | Summary of Connection Study | 74 |
| 6.2 | Modules | 74 |
| 6.2.1 | Key Properties of the Modules | 74 |
| 6.2.2 | Modules tied to slab | 76 |
| 6.2.3 | Damping Ratio by Components | 79 |
| 6.2.4 | Modules connected to external frame with springs in top | 81 |
| 7 | Conclusion | 85 |
| 7.1 | Summary of Findings | 85 |
| 7.2 | Remarks | 86 |
| 7.3 | Further Work | 86 |
| | Bibliography | 91 |

| | |
|---|-------------|
| Appendix | 92 |
| A Mass properties of <i>Abaqus</i> model | i |
| A.1 Added mass in model for eigenfrequency analysis | i |
| A.1.1 Distribution of mass | ii |
| B Formulas for wind load and acceleration | iii |
| B.1 Wind load | iv |
| B.1.1 Distribution of wind load | vii |
| B.2 Calculation of acceleration at top floor: | ix |
| B.3 Spectral analysis | x |
| B.4 Displacements and accelerations | xii |
| C Calculation of the stiffness of the connection | xv |
| C.1 Axial stiffness | xvi |
| C.2 Rotational stiffness | xvi |
| D Digital appendix | xvii |
| E Matlab scripts | xix |
| E.1 Calculation of distributed static Wind Load | xix |
| E.2 Calculation of maximum Acceleration | xxii |
| E.3 Spectral Analysis | xxv |

List of Figures

| | | |
|------|--|----|
| 1.1 | Illustration of the case building [9] | 2 |
| 2.1 | Glulam [42] | 6 |
| 2.2 | Umeå Östra with glulam and steel structure [5] | 7 |
| 2.3 | Glulam girders at Oslo Airport Gardermoen [46] | 7 |
| 2.4 | Flisa bridge in Hedmark, Norway [34] | 7 |
| 2.5 | Tall timber buildings | 8 |
| 2.6 | Proposals for tall timber buildings | 9 |
| 3.1 | Frequency ranges for excitation of structures [21] | 12 |
| 3.2 | Wind load [44] | 13 |
| 3.3 | Fluctuating wind force for wind in Z-direction | 15 |
| 3.4 | Procedure for spectral analysis by Davenport, [21] | 17 |
| 3.5 | Background and resonant response from wind loading [21] | 18 |
| 3.6 | Acceleration criteria for buildings subjected to wind load | 19 |
| 3.7 | Free vibration of the three categories of damping [15] | 20 |
| 3.8 | Rayleigh-damping [29] | 22 |
| 3.9 | Examples of accelerometer locations, [26] | 24 |
| 3.10 | Example of inclinometer position [48] | 24 |
| 3.11 | Sketch of GPS monitoring concept [27] | 25 |
| 3.12 | Basic model of a system [31] | 26 |
| 4.1 | Model of the case building | 32 |
| 4.2 | A typical module [24] | 32 |
| 4.3 | Local axis of beam | 34 |
| 4.4 | Rayleigh-damping in frame structure | 36 |
| 4.5 | Choice of model order in MATLAB script | 38 |
| 4.6 | Example of estimation of eigenfrequencies from system identification | 38 |
| 5.1 | Mode 1, $f = 1.245Hz$ | 42 |
| 5.2 | Mode 2, $f = 1.351Hz$ | 42 |
| 5.3 | Mode 3, $f = 1.975Hz$ | 43 |
| 5.4 | Mode 4, $f = 2.223Hz$ | 43 |
| 5.5 | Illustration of truss end | 45 |

| | | |
|------|--|------|
| 5.6 | Rayleigh-damping in frame structure | 46 |
| 5.7 | Component wise damping in frame structure | 47 |
| 5.8 | Results from spectral analysis | 48 |
| 5.9 | Response spectrum | 49 |
| 5.10 | Resonance for different damping ratios | 49 |
| 5.11 | Acceleration criterions at top floor | 51 |
| 5.12 | Motion symptoms due to acceleration levels [12] | 52 |
| 5.13 | Acceleration at top floor with respect to damping | 53 |
| 5.14 | Acceleration at top floor in point A | 54 |
| 5.15 | Displacement at top floor in point A | 55 |
| 5.16 | Locations of accelerometers, <i>illustrations from BOB, [9]</i> | 56 |
| 5.17 | Results from fast fourier transform of measurement data | 57 |
| 5.18 | Effect of changing the sampling rate | 58 |
| 5.19 | Effect of choice of model order | 59 |
| 5.20 | Estimates from system identification, Z-direction | 60 |
| 5.21 | Estimates from system identification, X-direction | 62 |
| 5.22 | Estimates from system identification, Z-direction, $\xi = 3\%$ | 63 |
| 5.23 | Estimates from system identification, X-direction, $\xi = 3\%$ | 64 |
| 6.1 | Joint with slotted steel plates and dovels [33] | 69 |
| 6.2 | 2D-truss | 70 |
| 6.3 | Mode shape 1 for 2D-truss with tied connections | 71 |
| 6.4 | Effect on frequency for varying stiffness in beam segments | 72 |
| 6.5 | Simplified models of the apartment modules [24] | 75 |
| 6.6 | Mode shapes of the two-by-four module stack [24] | 76 |
| 6.7 | Mode 1, $f = 1.193Hz$ -4% compared to simplified model | 76 |
| 6.8 | Mode 2, $f = 1.311Hz$ -3% compared to simplified model | 77 |
| 6.9 | Mode 4, $f = 2.076Hz$ -7% compared to simplified model | 77 |
| 6.10 | Mode 5, $f = 2.363Hz$ | 78 |
| 6.11 | Mode 6, $f = 2.527Hz$ | 78 |
| 6.12 | Combined rayleigh-damping considering superstructure and modules | 80 |
| 6.13 | Comparison of the combination of component wise damping ratio | 80 |
| 6.14 | Effect on frequency for varying spring stiffness in connections | 82 |
| A.1 | Simplification of mass and live load in stories | ii |
| B.1 | Pressure zones on the building [44] | vi |
| B.2 | Applied wind load | viii |
| C.1 | Sketch of a connection in a timber bridge [32] | xv |

List of Tables

| | | |
|------|--|------|
| 2.1 | Material properties for concrete, steel and timber | 6 |
| 3.1 | Common damping ratios [44] | 22 |
| 4.1 | Material properties of CE L40C [2] | 35 |
| 4.2 | Material properties of massive wood panels [6] | 35 |
| 5.1 | Eigenfrequency of building with and without additional masses . . . | 44 |
| 5.2 | Eigenfrequency of building with respect to boundary conditions . . . | 45 |
| 5.3 | Effect of different damping ratios on the eigenfrequency | 48 |
| 5.4 | Displacement and acceleration from spectral analysis | 50 |
| 5.5 | Maximum values from the dynamic analysis | 55 |
| 5.6 | Eigenfrequencies detected by the FFT of acceleration time histories . | 57 |
| 5.7 | Results from system identification, Z-direction | 61 |
| 5.8 | Results from system identification, X-direction | 61 |
| 5.9 | Results from system identification, Z-direction, $\xi = 3\%$ | 63 |
| 5.10 | Results from system identification, X-direction, $\xi = 3\%$ | 65 |
| 5.11 | Frequencies and accelerations from increased mass in concrete slabs . | 66 |
| 5.12 | Frequencies and accelerations from adding slab at top level | 66 |
| 6.1 | Eigenfrequency of 2D-truss | 71 |
| 6.2 | Results for model with beam segments, $A_{segment} = 0.2 \cdot A_{beam}$. . . | 73 |
| 6.3 | Eigenfrequency of module stacks [24] | 75 |
| 6.4 | Damping ratios for different components | 79 |
| 6.5 | Acceleration for increased damping ratio | 81 |
| 6.6 | Acceleration when connecting modules | 83 |
| A.1 | Increased mass from non-structural components | i |
| B.1 | Properties for calculation of the wind load | iii |
| B.2 | Distribution of static wind forces | viii |
| B.3 | Applied static wind forces in z-direction | ix |
| B.4 | Applied static wind forces in x-direction | ix |

1 Introduction

The eagerness among both architects and engineers to build taller buildings, with new and path-breaking concepts have existed through all time. Currently the planning of a 14 storey timber building for Bergen, Norway is in the process. The building is expected to become the world tallest timber building when finished.

1.1 Background

Previous work on the feasibility of tall timber buildings have identified challenges regarding the serviceability limit state, especially concerning the acceleration levels at the top floor. The dynamic behavior of the planned building is therefore of high importance to determine the feasibility of the suggested concept. Since this type of timber building is the first of it's kind, it is desirable to instrument the building when finished, to identify the actual properties and response of the building.

1.2 Scope of present Work

In this master thesis the dynamic properties of the case building will be investigated by the development of numerical models and modal analysis. This work involves production of a model of the case building in the finite element program *Abaqus*, and consequently study the dynamic properties such as frequency, mode shapes, acceleration etc. In addition the location of instrumentation will be examined. The connections between members in the frame and the effect on the global response, will be discussed. Also the effect of the prefabricated apartment modules will be investigated.

The goal of this work is to develop an understanding of the dynamic problems associated with tall timber buildings, as well as investigate the dynamics concerning the case building.

1.3 Project: *The World Tallest Timber Building*

The case model for this thesis is a 14 storey timber building planned for Bergen in Norway. If built, this will be the tallest timber building, rising 44 meters above the foundation level. This pilot project is a collaboration between the housing cooperative *Bergen og Omegn Boligbyggelag - BOB*, the architects *Artec*, the consulting engineer firm *SWECO*, the building element factory *Kodumaja* in Estonia, and the timber processing group *Moelven*.



Figure 1.1: Illustration of the case building [9]

The residential building will be located in Damsundet in Bergen, and the apartments will be built in prefabricated modules. The substructure consist of a timber-frame, constructed as an external truss in glued laminated timber. To strengthen the frame, a power-story is introduced every fourth story. The modules are supported by concrete slabs on top of the power-storeys. The properties of the case building will be more thoroughly presented and discussed in chapter 4.1.

1.4 Limitations

The focus in this report is the dynamic properties of the case building. Thus this work will not cover subjects such as (but not limited to):

- Evaluation of ultimate limit state (ULS) performance

1.4. LIMITATIONS

- Fire safety
- Acoustics
- Seismic performance
- Detailing of members
- Economics and costs
- Construction and erection of structure

In addition, the modeling of the case building will as far as possible reflect the proposed design by SWECO and ARTEC, but some simplifications are made. To some extent, recent changes in the geometry and concept have been implemented. Nevertheless, due to limited time, the FEM- model used in this thesis is not entirely updated compared to the latest geometry, concept and recent changes done by Sweco.

2 Building tall with Timber

For many years structures of concrete and/or steel have been the first choice for mid-rise and tall buildings. Until the mid 1990's several countries, including Norway, restricted the height of timber buildings, especially due to fire risk. Previous work have shown that dynamics and vibrations create challenges for planners and structural engineers when considering tall timber buildings [39].

Recently years increased focus on environmental problems, and at the same time the eagerness to build higher, better and more exceptional than what is already done arises the challenge among engineers to build tall timber buildings. The United Nations has with several agreements tried to reduce the worlds CO_2 emission by 25-40% of the levels in 1990, within year 2020 [1]. Building with timber is an environmental alternative to concrete and steel, especially because timber stores carbon dioxide rather than polluting the atmosphere in the manufacturing process [39].

2.1 Timber as construction Material

Timber is a natural material, therefore the material properties will vary. Timber is composed of fibers of cellulose, with high tensile strength. The fibers are held together by the lignin surrounding the bundles of fibers. The fibers are usually aligned parallel to the length of the tree. Consequently timber is a composite material, where the cellulose fibers are the reinforcement of the lignin material [28, 37]. The result is a material with high strength and stiffness, and low weight. Due to the fiber orientation, the strength parallel or normal to the grain is vastly different, thus timber must be considered an orthotropic material. The strength might be reduced by defects such as knots, and the humidity will influence the quality.

Compared to concrete and steel the modulus of elasticity, and thus the resistance to bending is usually low. On the other hand the ratio between stiffness and weight is high. Table 2.1 shows the material parameters, as well as the mass-to-stiffness ratio. The parameters used in this comparison are for the longitudinal direction of timber. Timber with strength grade C24 (ref. NS-EN 338) is used in the comparison [37].

CHAPTER 2. BUILDING TALL WITH TIMBER

Table 2.1: Material properties for concrete, steel and timber

| Material | Density [kg/m^3] | Young's modulus [MPa] | specific strength |
|--------------|-------------------------|------------------------------|-------------------|
| Concrete | 2 500 | 35 000 | 14 |
| Steel | 7 800 | 210 000 | 27 |
| Timber (C24) | 350 | 11 000 | 31 |

Even though the Young's modulus of timber is only equivalent to 30% of the stiffness of concrete and 5% of the stiffness of steel, the specific strength, is significantly higher. The specific strength is defined as the strength divided by the density. Another advantage with timber is the orthotropic material definition, and thus high efficiency.

2.1.1 Glued laminated Timber - *Glulam*



Figure 2.1: Glulam [42]

Glulam is a versatile timber product, produced from several layers of laminates. The laminates are chosen based on strength and humidity, and glued together and finally compressed. This process allows for several different cross sections, as well as curved shapes. The range of use varies from girders to truss members or strengthening of the superstructure. Glulam is commonly used in both bridges as well as large buildings.

The strength of glulam is dependent on the materials and glue used. The beams are either homogeneous, with same strength grade in all laminates, or in-homogenous with varying strength grade [28]. The stiffness and densities for common strength classes of glulam are given in *NS-EN 1194 Timber structures, glued laminated timber - strength classes and determination of characteristic values*. The modulus of elasticity is in the range of $11600 - 14700 MPa$, and the density is in the range of $380 - 450 kg/m^3$ [43].

Umeå Östra: The train station in Umeå was finished in 2010, and is a 16 meters tall building. The lateral load bearing system is a steel structure, combined with a glulam frame in a pattern of X's for horizontal loading [5]. The frame structure is visible through the glass facade.

2.1. TIMBER AS CONSTRUCTION MATERIAL



Figure 2.2: Umeå Östra with glulam and steel structure [5]

Oslo Airport Gardermoen: Glulam was used for the main girders at Oslo Airport Gardermoen, finished in 1998 and designed by Avioplan AS. The main girders are 133 meters, and the free span is 52 meters [46]. The glulam beams are supported on steel structures, on top of concrete columns.

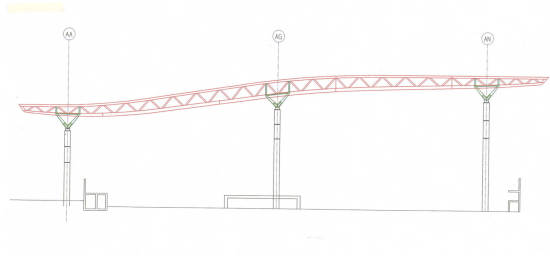


Figure 2.3: Glulam girders at Oslo Airport Gardermoen [46]

Bridges: Bridges are also often built with glulam due to the flexibility in cross sections, possibilities for curved shapes and length of each member. One example of this is Flisa bridge, which was the longest modern timber bridge when finished in June 2003. The longest span is 70.5 meters, and the total length is 196 meters [34].



Figure 2.4: Flisa bridge in Hedmark, Norway [34]

2.2 Tall Timber Buildings

Building tall with timber is thought to be a challenge due to the low weight and the flexibility of timber, creating dynamic challenges. Compared to tall buildings in steel and concrete, built as high as 800meters, a 45 meters tall building is "*nothing*". The issues concerning tall buildings become relevant for lower heights when building with timber [39]. Timber is a strong material, thus the ultimate limit state is usually not the problem.

Common structural systems for multi story timber buildings are [19]:

- **Frame structure** - Conventional frames with beams and columns, usually in combination with walls increasing the horizontal stiffness is a good solution for medium tall buildings in timber.
- **Truss structure** - Usually used for bridges, a truss structure gives high stability and good load distribution. The architectural flexibility is also good.
- **Element structure** - Elements of massive wood can be used as the load bearing system, both in vertical and horizontal direction. Often the elements are used in combination with either a frame or truss structure.

2.2.1 Examples

During the last decade, there are several similar projects with tall timber buildings, and some of them will be presented here.



Stadthaus [4]



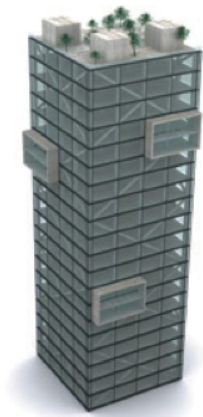
Forté [3]

Figure 2.5: Tall timber buildings

2.2. TALL TIMBER BUILDINGS

Stadthaus: At this moment, Stadthaus in London is the world tallest timber building. The construction is of massive wood and CLT, and the building is 9 storeys tall. Both the load bearing walls, the floor slabs and the central cores are built in timber. The building was built in 49 weeks, and stores 186 tones of carbon during it's lifetime [4].

Forté: When finished in 2012/2013, the apartment building in Melbourne, Australia will be the world tallest timber building, with 10 storeys, stretching 32.17 meters. This building will be constructed with cross laminated timber (CLT) [3].



Barentshus [10]



The Case for Tall Wood [20]

Figure 2.6: Proposals for tall timber buildings

Barentshus: In 2009 the planning of Barentshus in Kirkenes, Norway started. The proposal was a 20 story timber house, where a glulam frame should constitute the substructure. Sweco acted as the consulting engineers, and found the solution feasible, but the dynamics were challenging. As of fall 2012, the planning has not been finished, and the building will probably never be built. Nevertheless, more or less the same concept is used in the proposal for Damsundet [38], [10].

The Case for Tall Wood: This research project is a collaboration between the architects in *mgb Architecture + design* and the engineers in *Equilibrium Consulting* among others, proposed several concepts for tall timber buildings in the range of 12 - 20 storeys tall [20]. The proposed building is a system with structural wood core walls and glulam perimeter columns, and in addition some supplementing interior walls [20].

3 Dynamics

A dynamic problem is a time-dependent problem, usually as a result of a load that varies over time. This will in most cases produce oscillations of the structure, and precautions when designing the building should be made. Dynamic response can result in design problems due to [8]:

- Exceeding of functional requirements such as acceleration or displacement of a building
- Mechanical damage or collapse due to high loading from dynamic effects
- Fatigue due to repeated load cycles

For dynamic problems, *four* properties are important for the structural performance:

- stiffness
- geometry and distribution of mass
- damping properties
- load intensity and distribution of load over time

The properties will be discussed in the following. When considering wind loading on the building, the strength of the structure must be sufficient to resist the wind-induced forces. In addition the stiffness of the building must be high enough such that occupant comfort and serviceability criterions are satisfied [13]. Finally, the dynamic wind load may produce a dynamic response, which in many cases amplify the wind-induced forces and the deformations and motions.

3.1 Dynamic Properties of a Structure

A dynamic system is usually described with the equation of motion, where u represents the displacement and thus its time derivatives, \mathbf{m} the mass matrix, \mathbf{c} the damping matrix, \mathbf{k} the stiffness matrix and $\mathbf{p}(\mathbf{t})$ the external loading. The theory and equations describing a multi degree of freedom system is assumed to be

CHAPTER 3. DYNAMICS

familiar knowledge, the equations are therefore just stated here for reference.

$$\mathbf{m}\ddot{\mathbf{u}} + \mathbf{c}\dot{\mathbf{u}} + \mathbf{k}\mathbf{u} = -\mathbf{p}(\mathbf{t}) \quad (3.1)$$

The dynamic properties of a building is in general described with the eigenfrequency ω , damping ratio ζ , and mode shapes ϕ given in equation 3.2.

$$\omega_n = \sqrt{\frac{\mathbf{k}}{\mathbf{m}}} \quad (3.2a)$$

$$\zeta = \frac{c}{2m\omega_n} \quad (3.2b)$$

$$[\mathbf{k} - \omega_n^2 \mathbf{m}] \phi_n = \mathbf{0} \quad (3.2c)$$

3.2 Dynamic Loads on Buildings

A dynamic load is defined as a time-varying load. The magnitude, direction or point of application may vary with time. Examples of dynamic loads are wind, earthquakes, rotating or vibrating equipment and ocean waves. For a residential building (without any special equipment) only wind and earthquake loading are considered. Eurocode 8 treats the design of buildings for earthquake loads, and this will not be evaluated in this thesis. Figure 3.1 shows how the dominant frequency in earthquakes and wind are different, thereby affecting different types of structures. Wind is usually decisive for tall buildings with low natural frequencies, while earthquake will set the design criteria for low buildings with high natural frequencies.

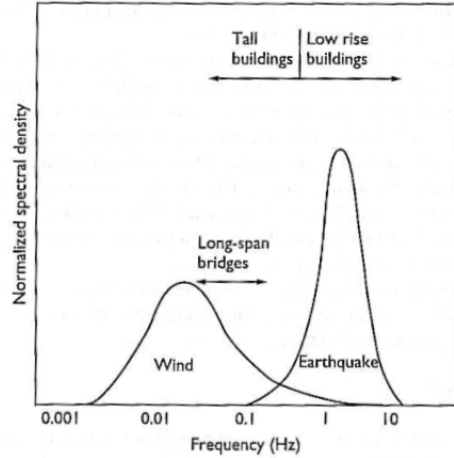


Figure 3.1: Frequency ranges for excitation of structures [21]

3.2. DYNAMIC LOADS ON BUILDINGS

3.2.1 Representation of the Wind Load

Since the wind load is varying over time, the best representation is done with stochastic time-series, based on the wind force spectrum. Eurocode 1 allows for a simplified calculation, where the wind load is treated as a static load. This gives reasonable results for deflections, but will not include the time-varying effect that might cause fatigue or vibrations. In this thesis, both a wind spectra and a static load is generated and applied to the building. The static load gives results for the maximum displacement and acceleration of the building. For the system identification used to verify the model, a wind spectra is generated with a MATLAB code provided by Ole Øiseth [35]. This gives a time-varying load, similar to the nature of the wind load, and it is possible to examine the dynamic response. This is not a good approximation to the actual wind load, as very few structural factors are implemented, thus it represents the variation of wind load above the actual force.

The response of the structure due to wind load is a function of the geometry, shape and dynamic properties of the building, as well as the wind conditions at the site. The wind conditions are a result of the surrounding terrain, the mean wind velocity, the return period, and the most common wind direction at the site. The mean wind velocities are given for all municipalities in Norway in the national annex of Eurocode 1-4.

3.2.1.1 Wind Load based on Eurocode 1

The static wind force distributed over the height of the building is found based on formulas given in chapter 4 and 5 in Eurocode 1 [44]. An assessment of the different factors are done, trying to represent the actual building and surrounding conditions.

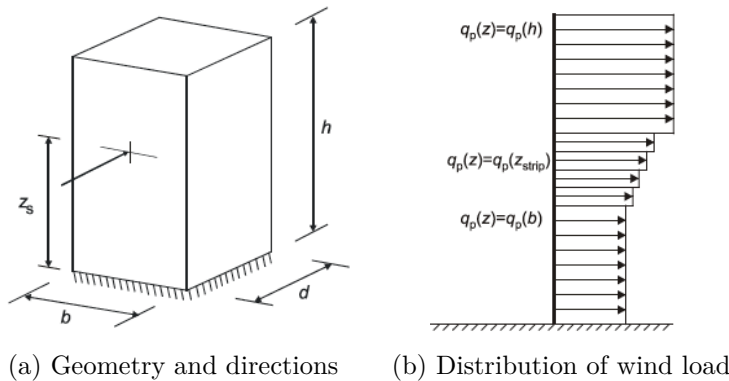


Figure 3.2: Wind load [44]

Figure 3.2 (a) shows how the depth, width and height of a building is defined

CHAPTER 3. DYNAMICS

with respect to the wind direction given by the arrow. Figure 3.2 (b) shows the distribution of wind load with respect to height of the building. The wind load increases for increasing height, based on the distribution of the wind velocity.

The wind force F_w is a sum of outward and inward pressure and friction forces on a building. Since the building is almost quadratic, the friction forces are neglected [44].

$$F_w = c_s c_d \cdot \sum_{surfaces} w_e \cdot A_{ref} \quad (3.3)$$

where:

- $c_s c_d$ is the structural factor, see appendix B
- w_e is wind pressure at a reference height z
- A_{ref} is the reference area

The formulas for calculating the wind load are given in appendix B, and the MATLAB script used to calculate the static wind load can be found in appendix E in addition to the the digital appendix.

3.2.1.2 Generated Wind Load from MATLAB

The turbulent wind-induced drag force due to wind can be expressed as:

$$F_D = \frac{1}{2} \cdot \rho \cdot C_D \cdot A \cdot U^2(t) = \frac{1}{2} \cdot \rho \cdot C_D \cdot A \cdot w(t) \quad (3.4)$$

where:

- U is the wind velocity, $U = \bar{U} + w(t)$
- ρ is the air density, usually 1.25 kg/m^3
- A is the area of the face where the wind load is applied
- C_D is the force factor

The wind speed U can be divided into the mean wind speed \bar{U} , and a randomly fluctuating wind speed $w(t)$. Only the fluctuating term of the wind load is wanted for the dynamic calculations, and the terms with $w(t)^2$ are neglected due to very low contributions. The load resulting from the mean wind speed \bar{U} is analogous to the static wind load treated in the previous section.

To include across-wind load generated by the turbulence, the matrix given in equation 3.5 can replace C_D in equation 3.4.

$$\begin{bmatrix} 2(\frac{d}{b}) \cdot C_D & -C_L \\ 2C_L & (\frac{d}{b}) \cdot C_D \end{bmatrix} \quad (3.5)$$

where:

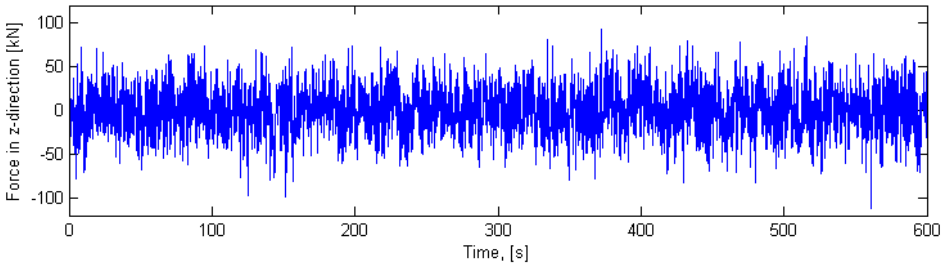
- C_D is the drag coefficient
- C_L is the lift coefficient

3.2. DYNAMIC LOADS ON BUILDINGS

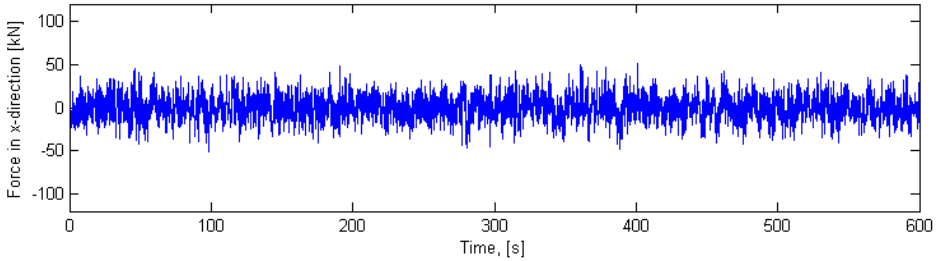
The drag coefficient is the same as the force coefficient in Eurocode 1-4, and is dependent on the geometry of the building. The lift coefficient accounts for the turbulence due to sharp edges on the building, giving forces in the across-wind direction. An experimental formula for the lift force is found in [30]:

$$C_L = 0.045\left(\frac{d}{b}\right)^3 - 0.335\left(\frac{d}{b}\right)^2 + 0.868\left(\frac{d}{b}\right) - 0.174 \quad (3.6)$$

The MATLAB script provided by Ole Øiseth gives the wind force both the along-wind and across-wind direction in two different points. The wind force applied at point 1 - at level with top of power story 1, when the wind direction is parallel to the z-axis is shown here for reference. [35]



(a) Wind force in along-wind direction (Z)



(b) Wind force in across-wind direction (X)

Figure 3.3: Fluctuating wind force for wind in Z-direction

The fluctuation wind speed $w(t)$ is assumed to be a Gaussian random process and the variation in wind speed is simulated in the time domain analogous to equation 3.7, [45].

$$w(t) = \sum_{k=1}^N a \cdot \cos(\omega_k t + \phi_k) \quad (3.7)$$

where:

CHAPTER 3. DYNAMICS

a is the amplitude
 ϕ_k is the arbitrary phase angle
 ω_k is the eigenfrequency

The amplitude is defined by the spectral density. For further discussion of the simulation of time series, the reader is referred to chapter A.3 in reference [45].

3.2.1.3 Methods for better Representation of the Wind Load

Both the static wind load based on the formulas in Eurocode 1-4, and the generated wind forces from the wind spectra are wrong. The main reason for this is all the simplifications done when reducing all the aerodynamic data, both concerning the building and the wind field, to a few plots and coefficients. Especially the distribution of the wind pressure over the buildings surface, and turbulence effects around corners are poorly represented. An important aspect when considering wind forces calculated from Eurocode 1 is that the wind is assumed to blow orthogonal to the building face. An actual wind will hit the building from different directions, often varying with time. To accomplish a better representation of the actual wind force on the building, this should also be accounted for. The dynamic wind load calculated include the across-wind force with the lift coefficient, but does not account for the time variation of the direction.

A more accurate procedure to represent the response from wind loading may be achieved by using wind tunnels. For example database-assisted design or the high frequency force balance method can then be used to determine the wind load on a structure [40]. The methods are described briefly here based on chapter 4.3 *Flexible Buildings* in the book *Design of Buildings and Bridges for wind* [40].

Database-Assisted Design Approach to estimate Wind Effects (DAD)

The concept is based on using a rigid model of the building in a wind tunnel. The aerodynamic pressure in a large number of taps on all four faces of the building are recorded for several directions of several applied mean wind speed.

High-Frequency Force Balance Method to estimate Wind Effects (HFFB)

The models used in this approach are rigid, and supported by a high-frequency force balance. Thus the base shear and moments can be measured. The wind forces on the building can then be found from the support reactions. HFFB is a good approach for buildings with linear fundamental mode shapes.

3.2.2 Structural Response to dynamic Loads

The wind velocities, and therefore also the wind load on a structure, are highly fluctuating over time. For structures with low natural frequencies, usually less

3.2. DYNAMIC LOADS ON BUILDINGS

than 1 Hz, the dynamic wind load may excite resonant dynamic response [21]. The response can be divided into three parts [40]:

1. *Static response* due to the mean wind load
2. *Background response* due to fluctuating wind force with natural frequencies different from the building's eigenfrequencies
3. *Resonant response* due to fluctuating wind force components with natural frequencies close to the building's eigenfrequencies.

To determine the structural response, a spectral analysis is very useful. Davenport have outlined a procedure for the spectral analysis shown in figure 3.4.

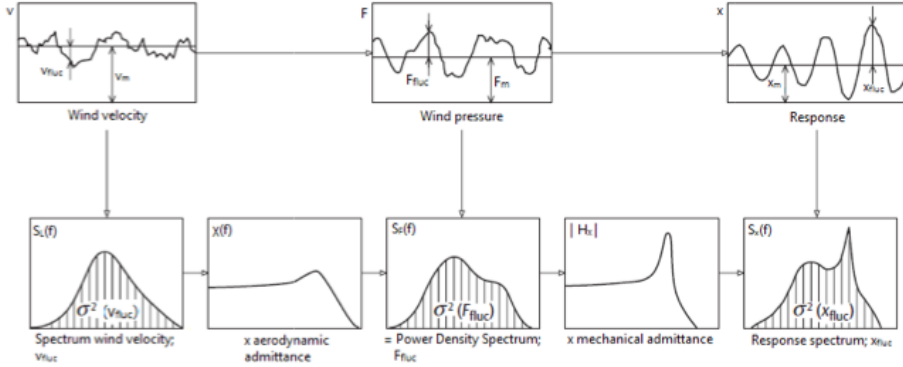


Figure 3.4: Procedure for spectral analysis by Davenport, [21]

The formulas used to calculate the response spectrum are given in Appendix B and are mainly from Eurocode 1-4. For a comparison of the different formulas used in spectral analysis of wind loading, the reader is referred to the article on this subject by Geert P.C. van Oosterhout, see reference [36].

The spectral analysis can be used to calculate the dynamic response, such as displacement and acceleration due to dynamic loads. In addition, the spectral density function of the response can be used to generate a time-history of the fluctuating wind forces using formulas for simulation of stochastic processes. This is not used in this thesis, as a already written MATLAB script was used to generate the dynamic wind load instead.

For structures with low natural frequency, the structural response is dominated by the background response, while for higher natural frequency the resonant response becomes more significant [21]. This is illustrated in figure 3.5.

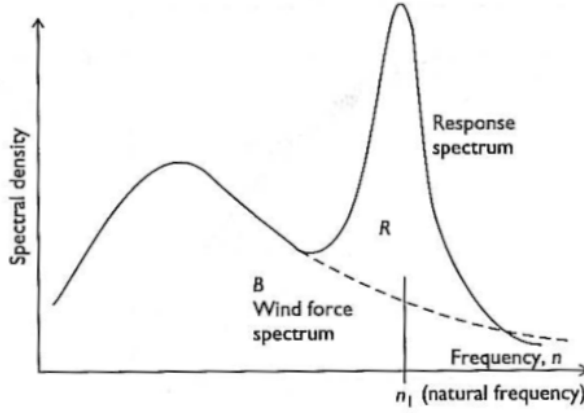


Figure 3.5: Background and resonant response from wind loading [21]

3.2.3 Acceleration

An important aspect concerning tall and flexible buildings is the *serviceability*. When considering dynamic loads such as wind load on buildings, collapse or fatigue is usually not at problem. The governing factor is usually if humans will experience discomfort due to swaying in the upper floors. This is measured with the acceleration of the top floor.

The accepted acceleration is dependent on the eigenfrequency f_0 of the building. Figure 3.8 shows the limits for (1) office buildings, and (2) residential buildings due to wind load with a 1-year return period. According to Boggs and Dragovich, a typical limit for human perception of acceleration at 1-10 years recurrence, is $0.005g$, and for comfort the typical criteria is $0.015g - 0.020g$ [13]. This corresponds to a perception limit at $0.049m/s^2$ and a comfort limit in the area of $0.147m/s^2 - 0.1965m/s^2$.

In addition Boggs have studied the human perception of acceleration, and his findings are summarized in figure 3.8 (b). The figures gives lower limits for the perception of acceleration levels at $0.002g$, while only 2% of the population will feel this. When a human is walking, the acceleration will feel disturbing if above $0.008g$, corresponding to $0.0785m/s^2$ for a 1-year return period. The limit for nausea, or seasickness symptoms, is for $0.01g$. [12]

3.3. DAMPING

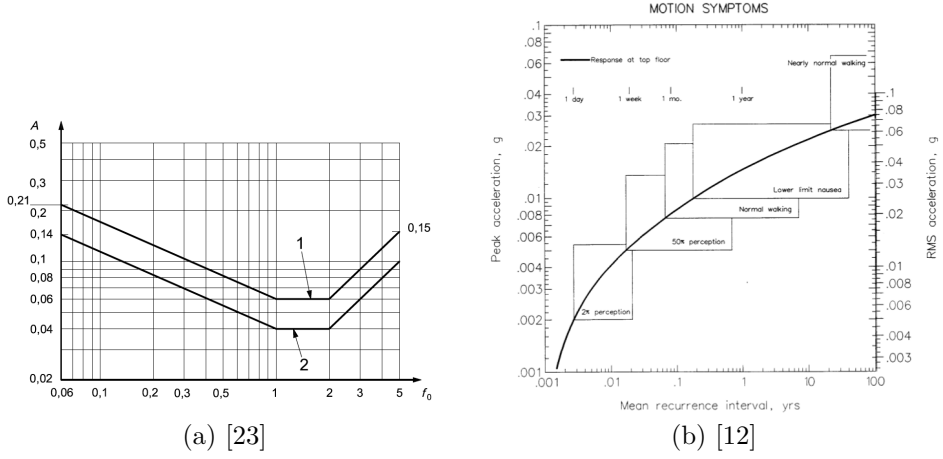


Figure 3.6: Acceleration criteria for buildings subjected to wind load

The acceleration of the top floor is calculated according to annex B in Eurocode 1-4. The probability factor c_{prob} allow for a different return period than the given 50 years. For a 1-year return period the formula is not valid, consequently a return period of 2 years is used.

The peak acceleration for the direction corresponding to the first mode shape, is found from equation 3.8, [44].

$$acc_x = \sigma_{a,x}(z) \cdot k_p \quad (3.8)$$

where:

- $\sigma_{a,x}$ is the standard deviation of the acceleration, see equation B.15
- k_p is the peak factor, where $\nu = n_{1,x}$
- z is the height where the acceleration is wanted

The formulas for calculating the acceleration is given in appendix B.

3.3 Damping

Damping is the process where the energy of a vibrating system is dissipated [15]. When a system is damped, the amplitude of free vibration will decay with time, and the resonance amplitude is limited [17]. Textbooks on the subject categorizes damping in structural dynamics as follows [15, 17]:

- **Viscous damping** occurs when a system is vibrating in a fluid or gas. The motion is resisted due to the viscous friction which absorbs energy.
- **Hysteresis damping** is the material damping, resulting from for example plasticity. The dissipated energy is then independent of the frequency

CHAPTER 3. DYNAMICS

- **Coulomb damping** is damping from friction. For example when two dry surfaces are sliding against each other. Special frictional devices can be installed in the structure to achieve higher frictional damping.
- **Radiation damping** is defined as energy loss to a surrounding medium. This can be for example dissipation of motion through soil that supports a structure.

Consequently it is unlikely to be able to identify and mathematically represent all the mechanisms that dissipates energy of an actual structure. The damping in structural dynamics is therefore represented by viscous damping, either in form of Rayleigh damping or modal damping. The damping coefficient c is chosen such that the dissipated vibration energy from the dashpot is equivalent to the total energy dissipation of the actual structure [15]. The damping force f_D is given in equation 3.9.

$$f_D = c \cdot \dot{u} \quad (3.9)$$

Damping of free vibrations The damping is usually expressed as a fraction of the critical damping. The critical damping value represents the smallest value of c that will restrain oscillations. The system will return to its equilibrium position without oscillation. See figure 3.7. Buildings, bridges, dams, offshore structures and so on will all be underdamped structures, where $\zeta < 1$, and the system will oscillate about its equilibrium position with decaying amplitudes. [15]

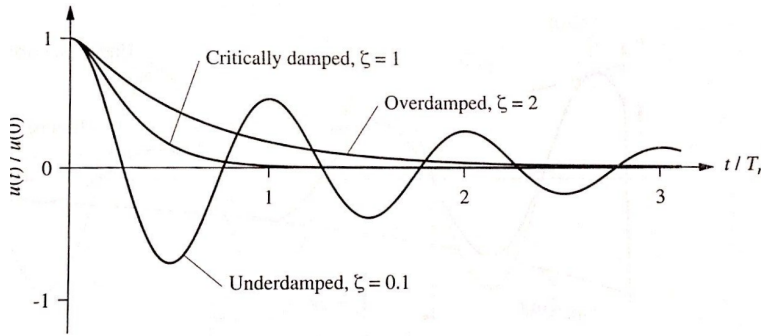


Figure 3.7: Free vibration of the three categories of damping [15]

The critical damping is expressed as:

$$c_{cr} = 2 \cdot m \cdot \omega_n \quad (3.10)$$

Thus, the damping ratio can be expressed as:

$$\xi = \frac{c}{c_{cr}} = \frac{c}{2m\omega_n} \quad (3.11)$$

3.3. DAMPING

The damping is also commonly expressed with the logarithmic decrement, expressing the decay in amplitude of two successive peaks when the structure is subjected to free vibration.

$$\delta = \ln \frac{u_i}{u_{i+1}} = \frac{2\pi\xi}{\sqrt{1-\xi^2}} \quad (3.12)$$

Modal damping If the method of modal superposition is used to achieve the response history, modal damping can be used. An individual damping ratio ξ is assigned to each natural frequency of the structure. The damping is expressed in a diagonal matrix, where the i th diagonal coefficient is $2\xi_i\omega_i$. The damping ratio ξ_i must be prescribed and estimated. When using modal damping ratios, ξ_i can be chosen to selectively damp higher modes. [17]

Composite modal damping allows for different damping ratios for each material. The modal damping ratio is then found as a weighted average of the mass associated with each material [41].

$$\xi_i = \frac{\phi_i}{m_i} \left(\sum_m \xi_m M_m \right) \phi_i \quad (3.13)$$

where:

- ϕ_i is the eigenvector of mode i
- m_i is the generalized mass for mode i : $m_i = \phi_i M \phi_i$
- M_m is the mass matrix for material m
- ξ_m is the damping ratio for material m

Rayleigh damping Also known as proportional damping, this type of damping is represented by a global damping matrix, as a combination of the stiffness-proportional part, and the mass-proportional part. The damping ratio ξ , the fraction of critical damping, is then represented by equation 3.14

$$\xi = \frac{1}{2} \left(\frac{\alpha}{\omega} + \beta\omega \right) \quad (3.14)$$

For linear analysis, the damping matrix is time-independent and represented by the initial stiffness and mass matrix [29]. Léger and Dussault suggest using the first natural frequency ω_i and the frequency of the highest mode with significant contribution to the response as ω_j . Thus the constants a and b_0 can be computed from equation 3.15 for a specific damping ratio ξ . a and b_0 corresponds to respectively α and β in equation 3.14.

$$\alpha = a = \frac{2 \cdot \xi \cdot \omega_i \cdot \omega_j}{\omega_i + \omega_j} \quad (3.15a)$$

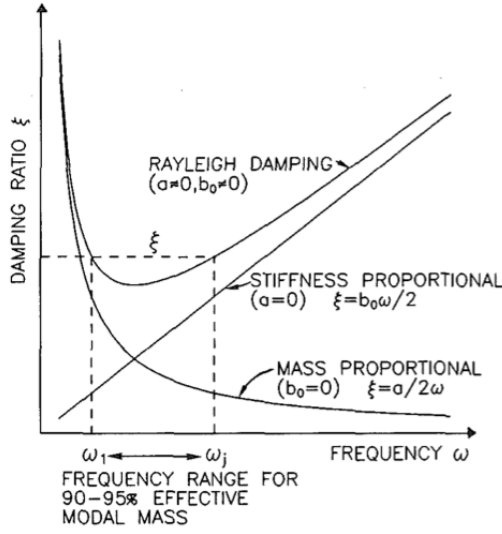


Figure 3.8: Rayleigh-damping [29]

$$\beta = b_0 = \frac{2 \cdot \xi}{\omega_i + \omega_j} \quad (3.15b)$$

3.3.1 Damping in Structures

The mechanisms that dissipates energy in vibrating systems are many, for example: friction in connections, cracking of concrete, inelastic behavior, etc [15]. It is difficult to identify all the active mechanisms, and therefore also difficult to estimate the damping in a structure. To evaluate the damping ratio in a structure, a vibration experiment must be executed on the actual structure. Since the damping is important to evaluate the dynamics of the structure, the damping ratio is usually assumed based on previous experiments on similar buildings. Common damping ratios for different structures are given in table 3.1, based on table F.2 in Eurocode 1-4 [44].

Table 3.1: Common damping ratios [44]

| Structure | ξ | δ_s |
|-------------------------------|---------------|-------------|
| Reinforced concrete buildings | 1.59% | 0.10 |
| Steel buildings | 0.80 % | 0.05 |
| Composite buildings | 1.28 % | 0.08 |
| Timber bridges | 0.96 - 1.91 % | 0.06 - 0.12 |

3.4 Monitoring of tall Buildings

The dynamic response of a building is mainly a result of wind loading. Since this is a natural phenomena, no analysis or calculations can predict the actual deformations and motions. Therefore, evaluating the dynamic response with field measurements may give valuable insight. The results from the field measurements are important to verify the computational models, and to optimize future models.

Monitoring of a building can also be used to study the structural health, and to discover collapse or defects in the building after a large impact, such as an earthquake or extreme wind loading. When comparing the properties of the structure before and after the impact, lack of stiffness may be a result of collapse or damage in for example a connection. This might be useful to prevent further damage and loss of lives.

Especially damping in structures is difficult to predict. Field measurements can give an estimation of the actual energy dissipation in the structure. This is important for new concepts, since the damping ratio is estimated based on experience from similar buildings. The damping is usually higher than expected due to the complexity of the structure and numerous connections.

3.4.1 Sensors

Different sensors for monitoring the motions can be used. It is important to place the sensors according to expected motions, such that all elements are detected. The sensors should be distributed both in plan and height, to achieve results for all motions.

Accelerometer An accelerometer is a device that measures the acceleration of a structure. The vibrating motion of the structure will be recorded for each direction. The accelerometers are easy to install, and can produce continuous measurements. The data are available instantly after measuring. Using several accelerometers over time, this can produce good results for the motion in the building. Accelerometers are the most common used sensors for monitoring of buildings.

Figure 3.9 (a) shows locations of accelerometers at a 244 meters high steel-frame building in Boston, USA, where accelerations were collected from eight locations in the building, four sensors on each plan. Two sensors orthogonal to each other, and parallel to the axis of the building were placed in pairs in two opposite corners of the building. The sensors were located on the 57th and 35th floor.

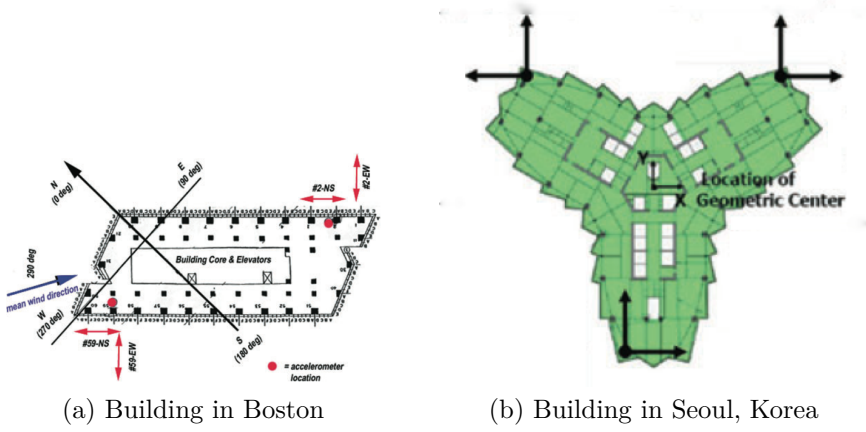


Figure 3.9: Examples of accelerometer locations, [26]

Figure 3.9 (b) shows the locations of accelerometers at a 73-storey tower reaching 264meters above ground in Seoul, Korea. The building is stiffened with a reinforced concrete core and exterior columns. Six accelerometers are located in orthogonal pairs distributed on the 64th floor.

Inclinometer A different approach is to measure the inclination or angle of the building at a given point and over time. Also the direction of the inclination is measured. Compared to acceleration the amplitudes of the inclination measurements will usually be lower, possibly resulting in increased error.

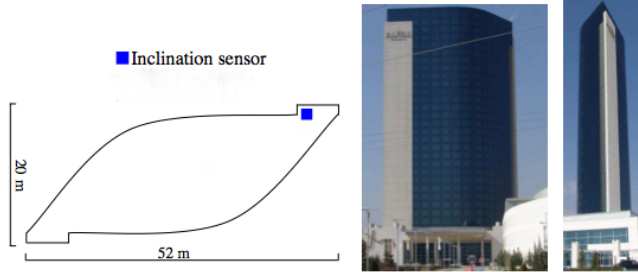


Figure 3.10: Example of inclinometer position [48]

GPS-monitoring The newest solution is to monitor the relative displacement at a given point in reference to a steady point on the ground. The signals are sent to a GPS, and the data collected. This is usually only used for a set time interval, as it is expensive with continuous measurements. GPS-monitoring is the most expensive of the three sensors presented here, and may also give poor data due to interference

3.5. SYSTEM IDENTIFICATION

from other stations in dense urban areas. The data are only collected from one point, and will not give a good representation of the total motion of the building.

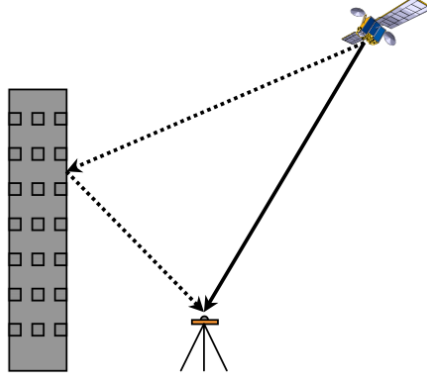


Figure 3.11: Sketch of GPS monitoring concept [27]

3.5 System Identification

System identification is an important aspect of the structural design and monitoring of a building. A good finite element model must represent the real behaviour of complex structures. Most design codes and formulas are based on extensive testing and measurements of similar buildings [7]. Knowing how to implement these records to improve the data-model is therefore of high importance.

System identification is the process where the output of the structure, for example displacement over time, generates the input of the structure, such as stiffness, damping and load matrices. There are several methods for system identification of a structure.

The dynamic properties of a structure must be described by mathematical models. Common models in structural engineering are [22]:

- differential equations
- transfer functions
- state space model
- ARMAX model

Furthermore there are several algorithms for the parameter estimation:

- Least squares method
- Maximum likelihood method
- Extended Kalman filter

In this thesis, only the N4SID method will be described. N4SID is short for *Numerical Subspace State Space System Identification*. In this algorithm, first

a singular value decomposition is done, followed by the least squares method to achieve a solution. In the *System Identification Toolbox* in MATLAB, the N4SID method is implemented.

3.5.1 Mathematical Model of the System

According to Ljung, a system is *"an object in which variables of different kinds interact and produce observable signals"* [31]. Figure 3.12 shows a simplified system where y is the output. The external signals that the observer can control is the input u , and w and v are the measured and unmeasured disturbances, respectively. A dynamic system is a system where the output depends on earlier input. It is therefore necessary with a state space model, describing the dynamic properties of the system, as well as all earlier input values [25].

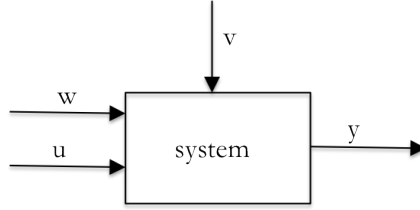


Figure 3.12: Basic model of a system [31]

The classical formulation of the multi degree of freedom system subjected to oscillations, is:

$$M_0 \ddot{y}(t) + C_{eff} \dot{y}(t) + K_{eff} y(t) = u(t) \quad (3.16)$$

where:

- $u(t)$ is the load vector, analogous with the input vector
- $y(t)$ is the stochastic response
- M_0 is the mass matrix
- C_{eff} is the damping matrix
- K_{eff} is the stiffness matrix

The matrices will in the following be expressed by capital letters only, not the usual bold print.

Rewriting equation 3.16 to a system of first order differential equations give [47]:

$$\begin{bmatrix} \dot{y}(t) \\ \ddot{y}(t) \end{bmatrix} = \begin{bmatrix} 0 & I \\ -M_0^{-1} K_{eff} & -M_0^{-1} C_{eff} \end{bmatrix} \begin{bmatrix} y(t) \\ \dot{y}(t) \end{bmatrix} + \begin{bmatrix} 0 \\ M_0^{-1} \end{bmatrix} u(t) \quad (3.17)$$

3.5. SYSTEM IDENTIFICATION

3.5.2 The State Space Model

The state space formulation for a linear time-invariant system in continuous time is then [7], [47]:

$$\dot{x}(t) = A_c x(t) + B_c u(t) + w_c(t) \quad (3.18a)$$

$$y(t) = C x(t) + D u(t) + v(t) \quad (3.18b)$$

where:

| | |
|--------|---|
| $x(t)$ | is the state vector |
| A_c | is the system matrix in continuous time |
| B_c | is the load matrix |
| w_c | is the system disturbance |
| v_c | is the measurement disturbance |
| C | is the output matrix |
| D | is a direct transmission matrix |

The state-output influence matrix can be found from the following definition of the output vector $y(t)$ [47]:

$$y(t) = C_a \ddot{x}(t) + C_v \dot{x}(t) + C_d x(t) \quad (3.19)$$

Where C_a , C_v and C_d are the output matrices for measurements of acceleration, velocity and displacement respectively.

The output matrix C , and the direct transmission matrix D is [47]:

$$C = [C_d - C_a M_0^{-1} K_{eff} \quad C_v - C_a M_0^{-1} C_{eff}] \quad (3.20a)$$

$$D = C_a M_0^{-1} \quad (3.20b)$$

The general solution to the state space formulation in equation 3.18 is [14]:

$$x(t) = e^{A_c t} x(0) + \int_0^t e^{A_c(t-\tau)} (B_c u(\tau) + w_c(\tau)) d\tau \quad (3.21)$$

The discrete time formulation can be found by sampling all variables such that $y_k = y(k\Delta t)$. The system can then be described with the following equations [47]:

$$x_{k+1} = A_d x_k + B_d u_k + w_k \quad (3.22a)$$

$$y_k = C x_k + D u_k + v_k \quad (3.22b)$$

Where the subscript d indicates the discrete times version of the matrixes described

before. The expected values of the noise w and v is expressed as [18]:

$$E \left[\begin{bmatrix} w_p \\ v_p \end{bmatrix} \begin{bmatrix} w_q^T & v_q^T \end{bmatrix} \right] = \begin{bmatrix} Q & S \\ S^T & R \end{bmatrix} \delta_{pq} \geq 0 \quad (3.23)$$

where:

Q, S, R are the covariance matrices of the noise
 δ_{pq} is the Kroenecker delta

Comparing the discrete time formulation in equation 3.22a to the homogenous solution of the differential equation in continous time, given in equation 3.21, the homogenous solution becomes [25], [14]:

$$A_d = e^{A_c \Delta t} \quad (3.24a)$$

$$B_d = B_c \int_0^t e^{A_c(\Delta t - \tau)} d\tau \quad (3.24b)$$

$$w_k = w_c(k\Delta t) \int_0^t e^{A_c(\Delta t - \tau)} d\tau \quad (3.24c)$$

$$y_k = CA_d x_0 \quad (3.24d)$$

3.5.3 Algorithm for System Identification of an Output-only Model

The concept of system identification can be summarized as the process where the system matrices A, B, C, D are determined and the matrices Q, S, R are estimated from the given measurements of input u and generated output y . The algorithm uses the state space estimates \hat{X}_i and weighting matrices W_1 and W_2 to find the system matrices. For the N4SID algorithm, $W_1 = I_{li}$ and $W_2 = I_j$.

The process to identify the system matrices can be summarized as:

1. Find the block Hankel matrix
2. Find the orthogonal projection
3. Singular value decomposition
4. Solve equation system by least squares method
5. Find dynamic properties of the system identified

The steps will be shortly explained here, based on reference [16], [18] and [47]. No thorough explanations or derivations are done. For the system identification done in this thesis, a previously written MATLAB script will be used. To get a better understanding of the script and the methods used, the theory is looked into anyway.

Output-only For the case when considering a building subjected to an actual wind load, the input, e.g the load is assumed unknown. The stochastic forces are

3.5. SYSTEM IDENTIFICATION

unmeasurable. The state-space model can then be reduced to [47]:

$$x_{k+1} = A_d x_k + w_k \quad (3.25a)$$

$$y_k = C_c x_k + v_k \quad (3.25b)$$

For the following algorithms, the output-only model will be used. For the simplified model used in this thesis, where the measurements are generated from an applied dynamic load on the FE-model in *Abaqus*, there is no noise present. This is not the case for the actual measurements planned for the case building.

Step 1 First the output block Hankel matrix $Y_{0|2i-1}$ must be found. The block Hankel matrix is a combination of future and past measurements. The same approach is done to achieve the input block Hankel matrix $U_{0|2i-1}$ [16].

$$Y_{0|2i-1} = \begin{bmatrix} y_0 & y_1 & y_2 & \cdots & y_{j-1} \\ y_1 & y_2 & y_3 & \cdots & y_j \\ \vdots & \vdots & \vdots & \ddots & \vdots \\ u_{i-1} & u_i & u_{i+1} & \cdots & u_{i+j-2} \\ y_i & y_{i+1} & y_{i+2} & \cdots & y_{i+j-1} \\ y_{i+1} & y_{i+2} & y_{i+3} & \cdots & y_{i+j} \\ \vdots & \vdots & \vdots & \ddots & \vdots \\ y_{2i-1} & y_{2i} & y_{2i+1} & \cdots & y_{2i+j-2} \end{bmatrix} = \begin{bmatrix} Y_p \\ Y_f \end{bmatrix} \quad (3.26)$$

Where p denotes the past and f denotes the future. i is a user-defined index, chosen larger than the maximum order of the system. j is dependent on the number of data samples, usually $j = s - 2i + 1$, where s is the sampled data. [16]

To find Y_p^+ and Y_f^- the line between Y_p and Y_f in equation 3.26 is simply shifted down one row.

Step 2 Next step is to make a projection of the subspace generated from the data, and estimate the observability matrix [18].

The projection of $Y_f^- = Y_{i+1|2i-1}$ into the row space of $Y_p = Y_{0|i-1}$ is found by the LQ decomposition:

$$\begin{bmatrix} Y_{0|i-1} \\ Y_{i|i} \\ Y_{i+1|2i-1} \end{bmatrix} = L \cdot Q^T = \begin{bmatrix} L_{11} & 0 & 0 \\ L_{21} & L_{22} & 0 \\ L_{31} & L_{32} & L_{33} \end{bmatrix} \begin{bmatrix} Q_1^T \\ Q_2^T \\ Q_3^T \end{bmatrix} \quad (3.27)$$

Where L is the lower triangular matrix and Q is an orthogonal matrix.

CHAPTER 3. DYNAMICS

The two projections needed are the relation between the past and the future:

$$O_i = Y_f/Y_p = \begin{bmatrix} L_{21} \\ L_{31} \end{bmatrix} Q_1^T \quad (3.28a)$$

$$O_{i-1} = Y_f^-/Y_p^+ = \begin{bmatrix} L_{31} & L_{32} \end{bmatrix} \begin{bmatrix} Q_1^T \\ Q_2^T \end{bmatrix} \quad (3.28b)$$

The order of the system can be found as the rank of O_i .

Step 3 Singular value decomposition will then give the observability matrix Γ_i , and the state sequence \hat{X}_i .

$$\Gamma_i = U_1 S_1^{1/2} \quad (3.29a)$$

$$\hat{X}_i = S_1^{1/2} V_1^T Q_1^T \quad (3.29b)$$

Step 4 Finally, the system matrices can be found from solving the equation system [18]:

$$\begin{bmatrix} \hat{X}_{i+1} \\ Y_{i|i} \end{bmatrix} = \begin{bmatrix} A \\ C \end{bmatrix} \begin{bmatrix} \hat{X}_i \end{bmatrix} + \begin{bmatrix} \rho_w \\ \rho_v \end{bmatrix} \quad (3.30)$$

For an output-only system, the load matrix \mathbf{B} and the

The noise covariance can then be estimated from the residuals ρ_w and ρ_v [18]:

$$\begin{bmatrix} Q & S \\ S^T & R \end{bmatrix}_i = \frac{1}{j} \left(\begin{bmatrix} \rho_w \\ \rho_v \end{bmatrix} \cdot \begin{bmatrix} \rho_w^T & \rho_v^T \end{bmatrix} \right) \quad (3.31)$$

Step 5 When the system matrices are known, the dynamic properties of the system can be found. Combining equation 3.17 and 3.18 gives the mass, stiffness and damping matrices. The eigenvalues and the corresponding eigenfrequencies and damping ratios can then be calculated.

$$x(t) = \begin{bmatrix} y(t) \\ \dot{y}(t) \end{bmatrix} \quad (3.32a)$$

$$A = \begin{bmatrix} 0 & I \\ -M_0^{-1} K_{eff} & -M_0^{-1} C_{eff} \end{bmatrix} \quad (3.32b)$$

$$C = \begin{bmatrix} I \\ 0 \end{bmatrix} \quad (3.32c)$$

4 Modelling and analysis

The residential building planned for Damsundet in Bergen will be modeled in the finite element program *Abaqus/CAE*, considerations and assumptions made when creating the model are discussed in this chapter. The proposed solutions and geometry from the preliminary study by SWEKO will be used. Due to limited time, the model is not entirely updated with recently changes in layout and geometry. All the same, the model and therefore also the results, should be a good representation of the case building, as these changes mainly affect the member detailing and not the global responses.

4.1 The case building

The proposed design for the case model is of very complex geometry. The prefabricated modules will fit exactly into the substructure, and thus the geometry of the substructure depends on geometry of the modules. Figure 4.1 shows the proposed structure for the timber frame. The proposed design of the modules are shown in figure 4.2.

The proposed geometry from SWEKO's preliminary study have been used when possible. Recently changes of the design have not been implemented due to time limitations.

The structure can be partitioned into the following parts:

- External timber frame covering the first 4 storeys
- Power-structure in story 5
- External timber frame for story 6 to 9
- Power-structure in story 10
- External timber frame, story 11 to 14
- Massive wood slabs in corridors
- Concrete slabs in story 6, and 11

The building is 14 stories high, a total of 44.5 meters. The base area is approximately 21 meters x 22.5 meters. Figure 4.1 (a) shows the glulam timber frame and other structural components such as slabs and walls in massive wood, concrete

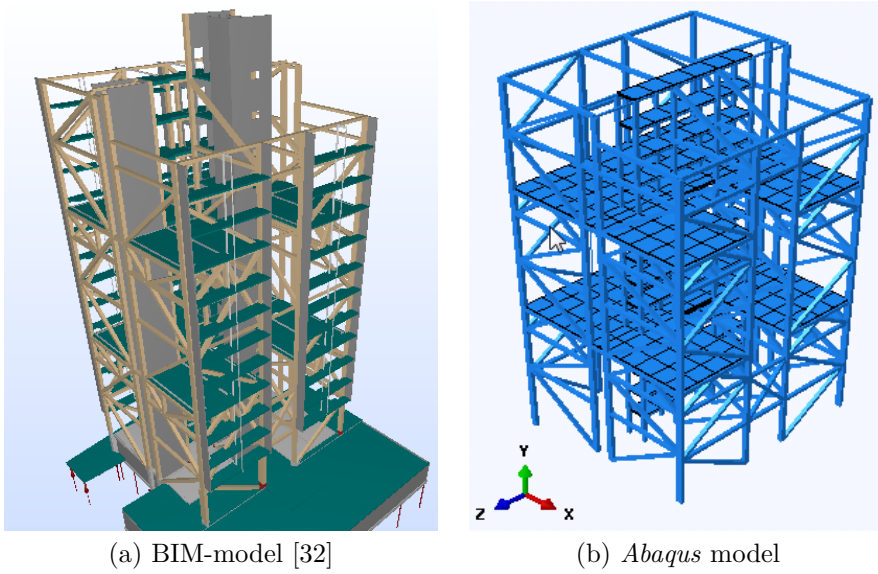


Figure 4.1: Model of the case building

slabs, and foundation. The figure also include the balconies. Not shown in this figure are the timber and glass facades, the apartment modules and the roof. In figure 4.1 (b) the *Abaqus* model of the building is shown. In this model, only the glulam frame, the concrete slabs and corridors are modeled, while all other components are included as increased mass.

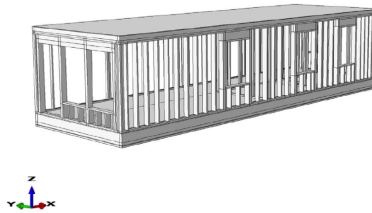


Figure 4.2: A typical module [24]

The modules are stacked both in height and plan, and will then be placed on the concrete slabs. The power-storeys and concrete slabs will transfer the loads from the apartment modules to the frame structure.

4.2 Model in *Abaqus*

The case building is modeled in the finite element program *Abaqus/CAE*. This program is chosen due to its possibilities, especially regarding dynamic analysis. Also the possibilities to define the damping ratios is an advantage. The modeling would have been much simpler using a conventional program like Robot Structures (Autodesk) or FEM-design (Strusoft), but for the purpose of this work, and especially to perform system identification on the model, the abilities of these programs would have been unsatisfactory. *Abaqus* is a general-purpose finite element program, with almost no limitations. The user interface in the program is less developed compared to conventional civil engineering programs, but almost everything may be manually programmed in the keywords function, or input files might be used.

Elements The beams, columns and diagonals in the glulam frame are modeled as wires, and meshed with B33 elements. The B33 element is a cubic beam in space with 2 nodes. This is an Euler-Bernoulli beam element, and should only be used if the cross-sectional dimensions are small compared to the length of the beam. No transverse shear deformation are allowed for these beam elements. They are well suited for dynamic vibration studies, as they use cubic interpolation functions [41].

The slabs are modeled as shells, and meshed with S4R elements. This is a shell element with 4 nodes, using the reduced integration to form the element stiffness. The reduced integration gives more accurate results, and reduces the analyzing time [41].

A mesh convergency test is done to evaluate for which mesh size the eigenfrequency converges. This allows coarse meshing in the beam elements and shell elements, thus the analysis time is reduced. This will reduce the exactness of the solutions, but for global response, and force distribution in the structure, a coarse mesh is good enough. The total number of beam elements (B33) is 3177, and there are 292 shell elements (S4R) in the model.

Constraints The different parts are connected with tie constraints between the columns, simulating the continuity. The concrete slabs are connected to the power stories such that all translations are constrained, while rotations are released.

Boundary Conditions The building is planned on top of a parking garage, which will make a stiff foundation for the glulam frame. The supports are idealized as pinned. The effect of changing the boundary conditions are investigated in chapter 5.

4.2.0.1 Simplifications

Several simplifications are made to make the model easier to work with, and to improve the computation efficiency.

- Foundations are excluded
- The balconies are assumed to have no impact on the structural performance, thus they are represented by increased mass in supporting columns.
- The facade (both timber and glass) are represented as increased mass in the external columns
- The CLT core walls are neglected in the computational model, since they are not coupled to the frame. All forces in the CLT walls are transferred directly to the foundation.
- The concrete slab is simplified to one slab with a simple geometry, neglecting the spacing between the prefabricated slabs.

4.2.0.2 Variations of simplified model

For the parametric study in chapter 6, two additional models were made to modify and test out different properties. The models will be described briefly here, see the results from the parametric study for further explanation.

Model of frame included modules To study the effect of the apartment modules, simplified models representing the stiffness and mass of each apartment module was implemented to the simplified model described previously.

Model with beam segments To evaluate the effect of the connections in the glulam frame, all beams and diagonals was cut into three parts, where the segments at each end was set to be 0.4m long, and the properties of the segment was modified to represent the stiffness in the connections.

4.2.1 Material properties

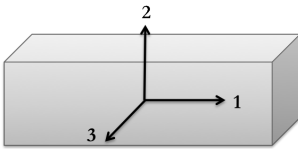


Figure 4.3: Local axis of beam

Glulam The orthotropy of glulam is implemented through engineering constraints in the material module in *Abaqus* with properties as listed in table 4.1. Figure 4.3 shows the local axis of a beam, where direction 1 is the longitudinal direction of the beam. Direction 2 and 3 is the perpendicular directions of the beam, where the strength is significantly lower.

The glulam beams planned to use in this project are produced by Moelven, and the type is CE L40C. The strength properties for this

4.2. MODEL IN ABAQUS

Table 4.1: Material properties of CE L40C [2]

| Young's modulus [Pa] | Poisson's ratio | Shear modulus [Pa] |
|------------------------|-------------------|----------------------------|
| $E_1 = 13 \cdot 10^9$ | $\nu_{12} = 0.35$ | $G_{12} = 7.6 \cdot 10^8$ |
| $E_2 = 4.1 \cdot 10^8$ | $\nu_{13} = 0.35$ | $G_{13} = 7.6 \cdot 10^8$ |
| $E_3 = 4.1 \cdot 10^8$ | $\nu_{23} = 0.10$ | $G_{23} = 1.07 \cdot 10^8$ |

**See figure 4.3 for the local axis of a beam section*

type is in the range of a mean between the typical glulam types GL28c and GL32c given in NS-EN 1194. The properties given in table 4.1 are given by Moelven, see reference [2]. The mean density of CE L40C is $390kg/m^3$.

Concrete, B35 For simplicity the concrete is modeled as an isotropic material, with E-modul 34.5 MPa, and poisson's ratio 0.25. This will not include the effect of the reinforcement, and no cracking of the concrete is considered. The density of the concrete is $2500kg/m^3$. Modeling concrete in a FEM-program such as *Abaqus* is complicated, and not considered as part of the aim of this thesis.

Massive wood The massive wood panels used in the corridors between the apartment modules are modeled as slabs with the material properties given in table 4.2. As with the glulam beams, the massive wood slabs are modeled with orthotropic material properties using engineering constraints. The density of the corridors is $500kg/m^3$.

Table 4.2: Material properties of massive wood panels [6]

| Young's modulus, [Pa] | Poisson's ratio | Shear modulus, [Pa] |
|-------------------------|-------------------|----------------------------|
| $E_1 = 7.72 \cdot 10^9$ | $\nu_{12} = 0.35$ | $G_{12} = 1.06 \cdot 10^8$ |
| $E_2 = 2.37 \cdot 10^9$ | $\nu_{13} = 0.35$ | $G_{12} = 1.06 \cdot 10^8$ |
| $E_3 = 2.37 \cdot 10^9$ | $\nu_{23} = 0.2$ | $G_{12} = 7.9 \cdot 10^8$ |

4.2.2 Modeling of damping

Two approaches to model the damping in the structure are done:

1. Rayleigh - damping
2. Composite modal damping

1 - Rayleigh-damping is implemented in the model by adding the α and β parameter in the material properties. A MATLAB script provided by Ole Øiseth is used to calculate the input values for the material Rayleigh-damping, see figure

5.6 [35]. The damping in the frame structure is assumed to be 1.5%. This gives $\alpha = 0.0752$ and $\beta = 0.0007$ as shown in figure 5.6.

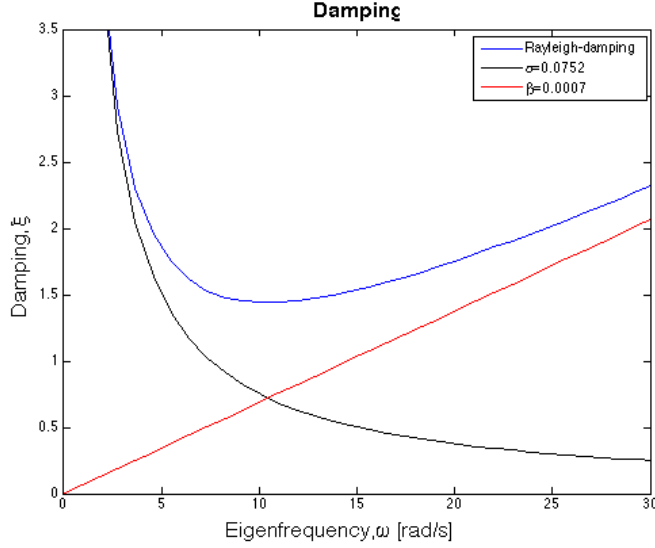


Figure 4.4: Rayleigh-damping in frame structure

2 - Composite modal damping is also implemented in the material properties in *Abaqus*. The damping is assigned to each material as a fraction of the critical damping. Such that for a structure with damping ratio assumed to be 1.5%, the value 0.015 is assigned to the material properties. The damping factors for each material is then combined to a modal damping factor for each eigenfrequency.

The results from both composite damping and rayleigh damping are evaluated in chapter 5.

4.3 Analysis

To examine the dynamic properties of the case building, a modal analysis is done. In *Abaqus/CAE* this is executed with a linear perturbation frequency step. Using linear perturbation, only the linear response is considered. The frequency step extracts eigenfrequencies and eigenmodes to the system. Lanczos method is chosen as the iteration method.

A linear perturbation step, with complex frequencies are also applied to evaluate the damping properties of the structure. The damping ratio is then represented by the complex part.

4.4. MODEL FOR SYSTEM IDENTIFICATION

The results from the dynamic analysis are used to calculate the static wind load on the building. A general static analysis is done to estimate the displacement of the top floor due to wind. In addition, a dynamic step is performed to produce an acceleration time-history for the dynamic wind load. This gives the input for the system identification.

4.4 Model for system identification

The simplified model, where the modules, balconies and facade are represented by increased mass in existing members, is used for the system identification. The background theory for the system identification is presented in section 3.5. The procedure for the system identification will be briefly explained in the following. The MATLAB script used are developed by Ole Øiseth, and are given in the digital appendix for reference.

4.4.1 Retrieving measurement data

Since the building still is in the planning process, no real measurements of the acceleration is available at this point. To simulate this, a dynamic wind load load is applied as described in section 3.2.1. Then a dynamic implicit analysis is run in *Abaqus*, and the acceleration at 7 measurement locations are plotted against time. These plots are used as input for the system identification. Since the wind load is a varying load, no load input is used. The system identification model is therefore to consider as an output-only model.

4.4.2 Preprocessing

First, the measured data is preprocessed by a spectral analysis. The power spectral density is found. This describes how the power of the time series is distributed with frequency. The order of the sampling data is set. Noise, and instabilities in the time histories are filtered. The fast fourier transform of the measured data gives an estimate of the excited frequencies, and thus which modes of the model are excited by the applied wind load.

4.4.3 Identification

The sampled data are modified to achieve the wanted sampling rate. Usually a good sampling rate is in the range of 10 - 20 times the expected frequency. The appropriate test order must be chosen by the user, smaller than the order of the sampled data.

CHAPTER 4. MODELLING AND ANALYSIS

The model order with the best results are usually the order where the largest drop in singular value is found. The number of eigenvalues computed are dependent on the chosen order. To estimate the n first modes, a minimum order of $6n$ is required etc. Figure 4.5 shows how the MATLAB scripts finds the suggestion for the default order.

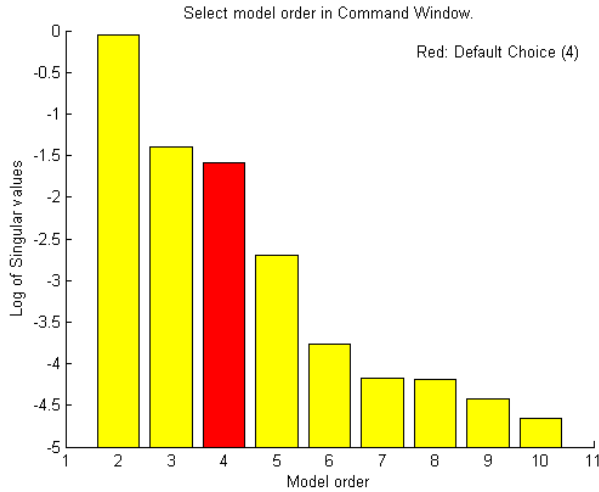


Figure 4.5: Choice of model order in MATLAB script

The identification procedure described in section 3.5.3 is executed by the MATLAB script and the command `n4sid`, based on the sampling data and the chosen model order. The state space data, or the estimated data found from the system identification, are then compared to the sampled data, which is the measurement time histories. System identification is accordingly a curve-fitting method, where the goal is to achieve a good fit of the curves of the sampled and the identified / estimated data.

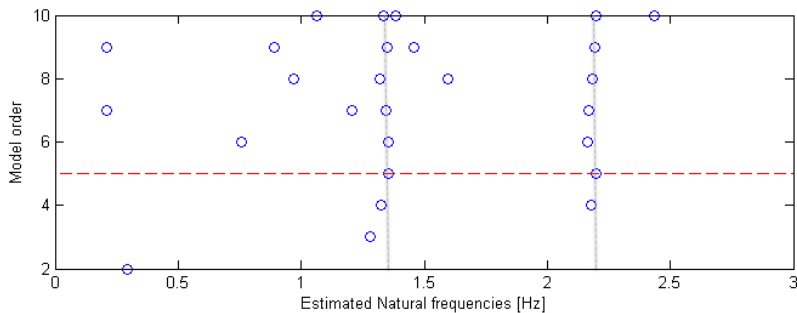


Figure 4.6: Example of estimation of eigenfrequencies from system identification

4.4. MODEL FOR SYSTEM IDENTIFICATION

The estimated eigenvalues are found from the solution of the eigenvalue problem when the system matrix is identified, and the estimated frequencies and damping ratios are found by traditional formulas. The estimated frequencies and damping ratios are plotted versus the model order. As seen in figure 4.6, the choice of order (red dotted line) determines the estimated frequency. The best estimation is achieved when the frequency is more or less independent of the choice of order, and a vertical line for each frequency can be drawn on the plot (grey dotted lines).

4.4.4 Model updating

A mathematical model or data model is only an attempt to give a representation of the reality, with many assumptions and idealizations. If the measurements in section 4.4.1 were real measurements of the acceleration of an actual building subjected to wind load, the results from the system identification might be used to update the data model. Especially the damping ratio used in the model should be evaluated and compared to the damping ratio from the system identification. As mentioned earlier, this is probably the most uncertain value when modelling a structure. Also the stiffness / eigenfrequency of the building is an important property, and the results from system identification should be considered.

5 General results for simplified model

This chapter summarizes some general findings from the analysis. Unless otherwise stated, this chapter presents results from the case building as described in section 4.2. As a first approach, the modules and the permanent part of the live load are represented by increased mass in the concrete slabs. The balconies and the facades are included as increased mass in the columns.

In chapter 6, a more detailed investigation of different components and how they influence the response is presented. Also the effect of including simplified models of the modules is discussed.

5.1 Eigenfrequency

To evaluate the dynamic response of the structure, and what influences the eigenfrequency of the building, several parameters were changed, and the results monitored. The effect of connecting the modules to the structure is discussed in chapter 6.2.

The first four mode shapes and the corresponding eigenfrequency are shown in figure 5.1 - 5.4. For buildings with a height over 50m, a common approximation to the first eigenfrequency is $f_1 = 46/h$ [44]. Using this for the case building, even though not entirely valid, gives an estimate for the expected eigenfrequency: $f_{estimate} = 1.042Hz$.

The modal analysis in *Abaqus* gives higher frequencies than expected. This is probably due to the high complexity of the structure, with numerous connections and beams, that supplies stiffness to the frame structure. Also the use of a truss pattern instead of for example ordinary frames with beams and columns have influence on the increased stiffness.

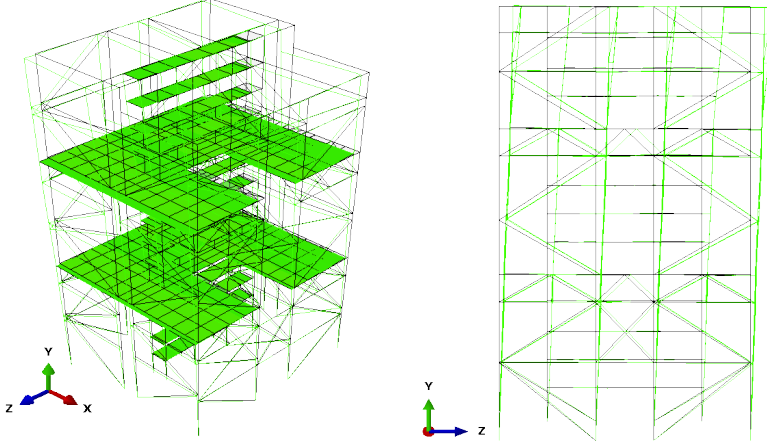


Figure 5.1: Mode 1, $f = 1.245Hz$

Mode shape 1 is, as expected, pure translation in z -direction. The building behaves as a cantilever, and the mode shape is linear.

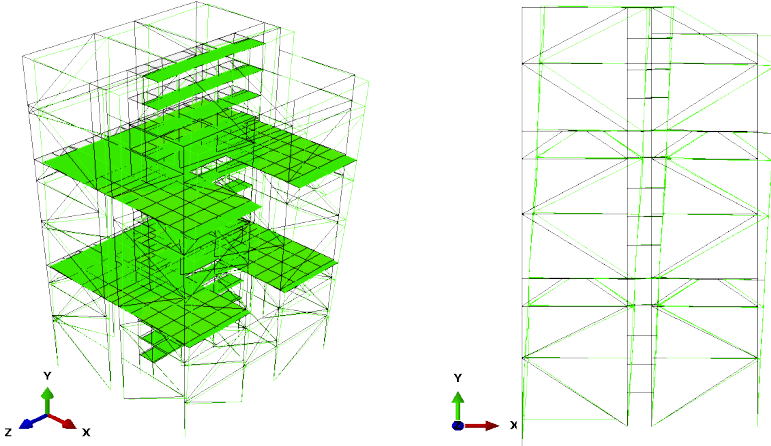


Figure 5.2: Mode 2, $f = 1.351Hz$

Mode 2 is translation in x -direction. The stiffness in x -direction is higher than in z -direction, mostly due to the direction of the truss pattern in the frame, and that there are more internal trusses in x -direction than in z -direction.

5.1. EIGENFREQUENCY

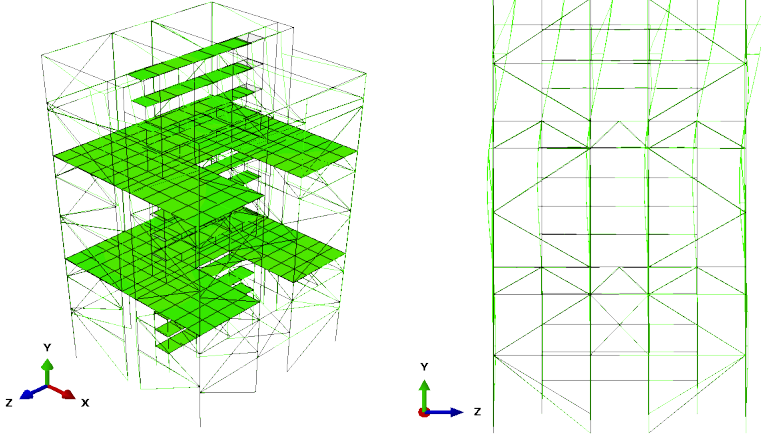


Figure 5.3: Mode 3, $f = 1.975Hz$

Mode 3 is also translation in z-direction. In this case the shape is dominated by motion in the upper 4 storeys, mainly due to the weight of the corridor, and the low stiffness in this direction. Coupling the corridors to the frame with a truss in z-direction will probably reduce this motion.

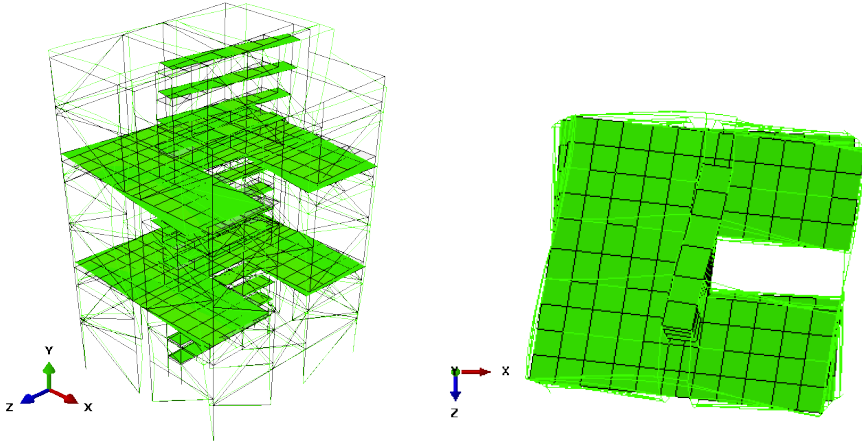


Figure 5.4: Mode 4, $f = 2.223Hz$

Mode 4 describes rotation about the y-axis. Since the plan of the building is nearly symmetrical, the torsional mode is rotation about the center of the building.

The other modes are not presented here, the reader is referred to the digital appendix to study the mode shapes.

5.1.1 Mass

The glulam frame and concrete slabs by itself has a higher frequency than the one where the modules are included. When no extra added mass is included, the eigenfrequencies of the frame structure is as presented in table 5.1.

These frequencies represent the stiffness of the frame structure by itself. The total mass of the structure for these results are: $M_{total} = 5.502 \cdot 10^5 kg$. Comparing to the structure when the modules, balconies, facade and 30% of the live load are included, the total mass is: $M_{total+mass} = 1.434 \cdot 10^6 kg$. The eigenfrequencies are as stated in section 5.1. The global stiffness is found from $\omega^2 = K/M$.

Table 5.1: Eigenfrequency of building with and without additional masses

| Description | With added masses | | Only frame and slabs | | |
|-------------------------|-------------------|--------------------|----------------------|--------------------|------------|
| | <i>Freq [Hz]</i> | <i>K [N/m]</i> | <i>Freq [Hz]</i> | <i>K [N/m]</i> | ΔK |
| Transl in z-dir, f_1 | 1.25 | $88.5 \cdot 10^6$ | 1.88 | $76.7 \cdot 10^6$ | 15% |
| Transl in x-dir, f_2 | 1.35 | $103 \cdot 10^6$ | 2.16 | $101.3 \cdot 10^6$ | 2% |
| Rot about y-axis, f_4 | 2.23 | $281.5 \cdot 10^6$ | 3.68 | $294 \cdot 10^6$ | -4% |

If comparing the frequencies for the three different modes, and the two models, it is obvious that increasing the mass changes the eigenfrequency. When adding the masses, f_1 is reduced with 35%, while f_2 is reduced with 38%, and f_4 is reduced with 40%. Thus, the reduction is higher for increasing frequencies.

The increase in generalized global stiffness when adding the extra masses, and thus accounting for all parts of the structure, is significant. The stiffness is increased with 15% for translation in z-direction, while for the rotation about the y-axis, the global stiffness is reduced with 4%. The stiffness is expected to be independent of the mass, while this shows the opposite. This effect is probably due to the fact that increasing the mass in certain members will change the mode shapes, and the stiffness will be dominated by different parts. The stiffness is dependent on the displacement, in general $F = -k\delta$, thus changing the displacement pattern / mode shape, will also influence the stiffness in each member.

5.1.2 Boundary Conditions at Foundation

The stiffness of the structure seems to be dominated by the frame, and not the boundary conditions. Changing the boundary conditions from pinned to rigid gives almost no change in the eigenfrequencies or the mode shapes. In the proposed concept, the bottom of the frame was planned as concrete member, see figure 5.5. The effect of changing the material in these segments was also evaluated. For modeling reasons, the segments are modeled as a small segment of the original

5.1. EIGENFREQUENCY

member, with same cross section, not as a massive box as in the figure. The segments are tied to the glulam beam.

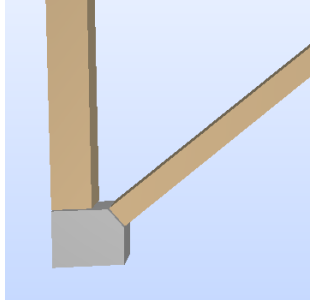


Figure 5.5: Illustration of truss end

Table 5.2: Eigenfrequency of building with respect to boundary conditions

| Boundary condition: | f₁ [Hz] | f₂ [Hz] | f₄ [Hz] |
|----------------------------|---------------------------|---------------------------|---------------------------|
| | <i>Transl. z-dir</i> | <i>Transl. x-dir</i> | <i>Rot. y-axis</i> |
| Pinned | 1.22 | 1.35 | 2.23 |
| Encastre | 1.22 | 1.35 | 2.23 |
| Concrete segments | 1.24 | 1.38 | 2.26 |
| Steel segments | 1.25 | 1.39 | 2.26 |

It is seen from table 5.2 that the boundary conditions have nearly no influence on the stiffness of the structure in x- and z-direction. The increase in eigenfrequency is about only 2% for all three modes, and the different conditions. This is regarded as such a small change that no further analysis is done on the boundary conditions. The stiffness of the building is obviously governed by the stiffness of the frame components and the stiffness in the slabs connecting the frame parts.

5.1.3 Damping

The damping ratio is included in the model with Rayleigh damping, as described in section 3.3 and 4.2. The complex frequency analysis gives the effective damping ratio for each frequency. The damping matrix of the system is found from $[\mathbf{C}] = \alpha[\mathbf{M}] + \beta[\mathbf{K}]$. The effective damping ratios from the calculations in *Abaqus* are compared to the chosen Rayleigh-proportional damping in figure 5.6.

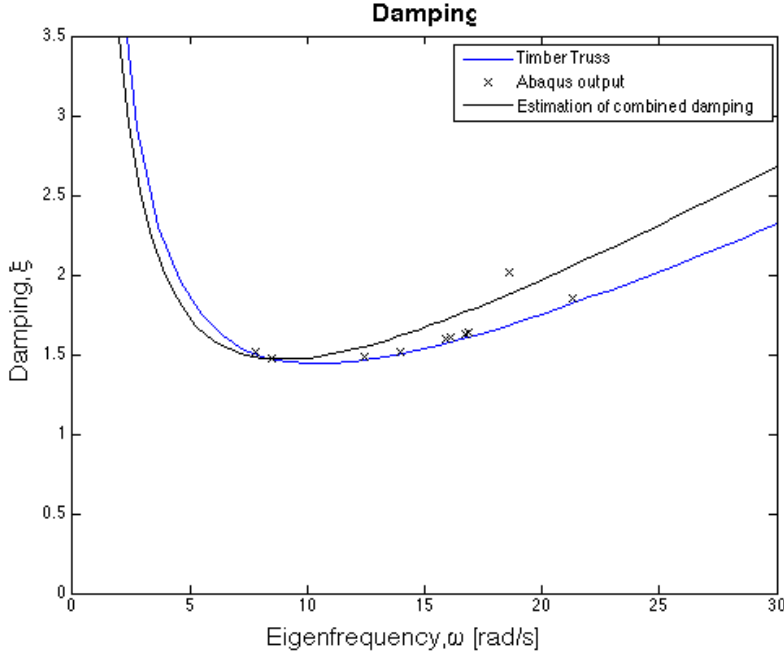


Figure 5.6: Rayleigh-damping in frame structure

Another approach to include the damping in the data model is to use composite modal damping. When using composite modal damping, the modal damping ratio is a weighted average of the damping ratio in each material, see section 3.3. This gives obviously a constant damping ratio for all modes if ξ is the same for all components.

The real difference between the two methods to represent damping is visible when assigning different damping ratios to the different components in the structure. The timber frame is assumed to have higher damping ratios than the concrete slabs and massive wood corridor floors. If the damping in the glulam frame is assumed to be $\xi_{glulam} = 2\%$, and the damping in the concrete slab and massive wood floors are assumed to be $\xi_{concrete} = 1\%$ and $\xi_{CLT} = 1\%$, the results for the estimated damping ratios become as shown in figure 5.7.

The values used in the Rayleigh damping are:

$$\xi = 1\% \rightarrow \alpha = 0.0508, \beta = 0.0005$$

$$\xi = 2\% \rightarrow \alpha = 0.1017, \beta = 0.0009$$

5.1. EIGENFREQUENCY

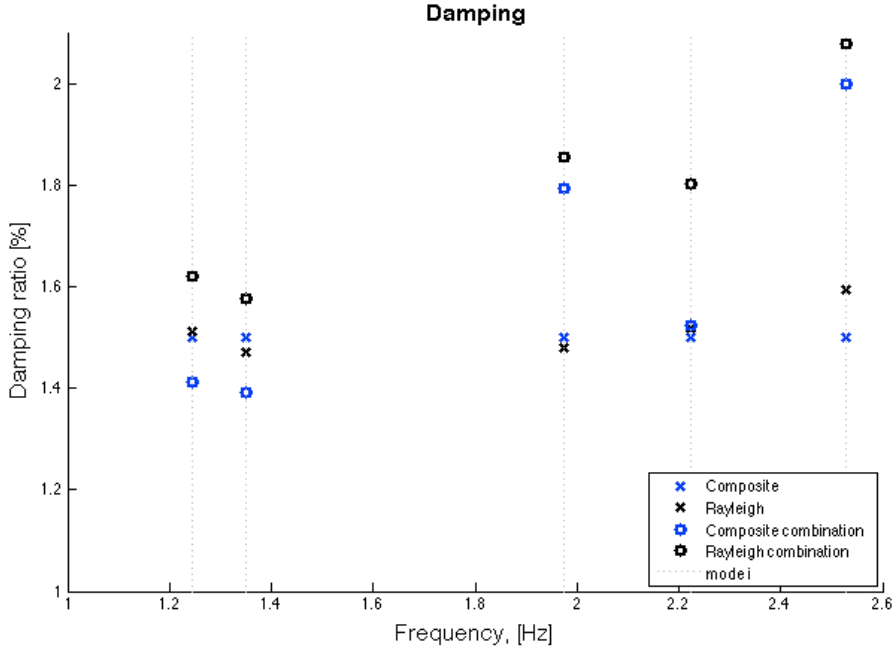


Figure 5.7: Component wise damping in frame structure

As seen in figure 5.7, for the situation when a total damping ratio of $\xi = 1.5\%$ is applied to all components in the structure, the estimated damping ratios are similar for both the composite and rayleigh-damping method. For mode 1-4 the value is constant in the range of 1.5%. For mode 5, the generated mass is lower, thus the stiffness proportional damping is dominating the Rayleigh damping ratio.

For the combination of different components, the composite modal damping method uses a weighting of the components mass. The Rayleigh damping is in fact not useful for combination of different damping ratios, as it is applied to the global mass and stiffness matrix. The estimated damping ratio for combination of different components using the composite modal damping represents how the different components contribute to the damping. Even though the mass in the concrete slabs in total are higher than the mass in the frame, the frame is governing the damping.

The effect of applying different damping ratios to the structure seems to have no significant influence on the calculated frequencies. Table 5.3 shows how the frequency only changes slightly for a damping ratio of 9%. Rayleigh damping is used in this analysis.

Increasing the damping ratio with 500%, which must be considered a huge increase, gives a reduction in the frequency of 0.1% for f_1 and f_4 , and 0.3% for f_2 , which

Table 5.3: Effect of different damping ratios on the eigenfrequency

| Mode | $\xi = 1.5\%$ | $\xi = 3\%$ | $\xi = 6\%$ | $\xi = 9\%$ |
|-------|---------------|-------------|-------------|-------------|
| f_1 | 1.2452 | 1.2451 | 1.2447 | 1.2440 |
| f_2 | 1.3508 | 1.3507 | 1.3503 | 1.3469 |
| f_4 | 2.2230 | 2.2228 | 2.2220 | 2.2209 |

is nothing. Especially when considering all the uncertainties with the model and the assumption of the damping ratio, the effect on damping can be considered negligible.

5.2 Spectral Analysis

To evaluate the response to wind loading a spectral analysis was performed. The resulting plots are shown in figure 5.8.

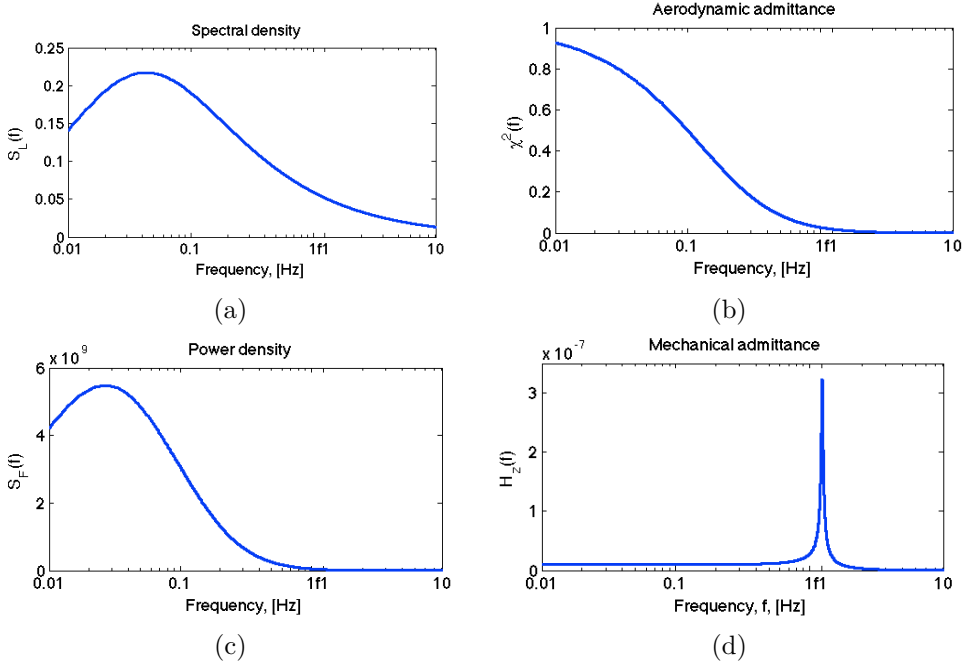


Figure 5.8: Results from spectral analysis

Finally, the response spectrum for wind loading is shown in figure 5.9.

5.2. SPECTRAL ANALYSIS

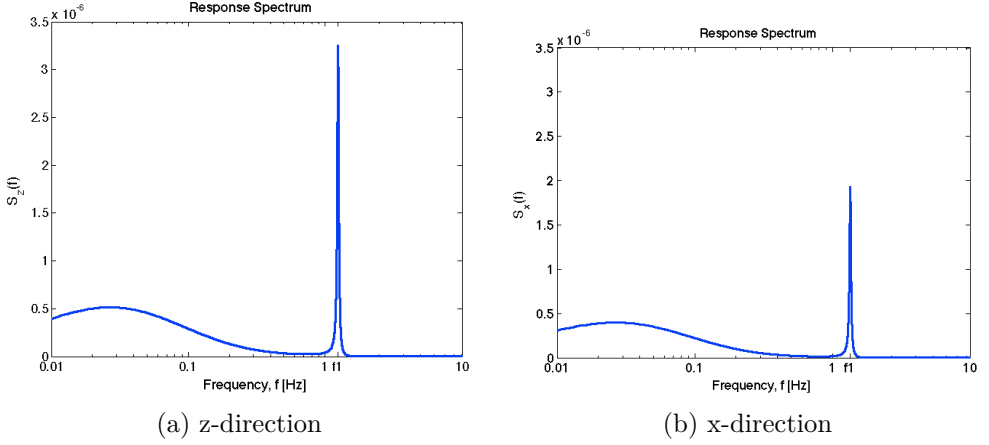


Figure 5.9: Response spectrum

Figure 5.9 (a) illustrates how the response is dominated by the background response for low frequencies. The resonant response for $f=1.262$ Hz is illustrated with the peak. For this situation, the resonant response is about 6 times higher than the background response. Figure 5.10 illustrates how important it is to consider the damping. As the figure shows, the resonance response decays significantly for increasing damping ratios. The considered damping ratios are for timber bridges, given in Eurocode 1-4, and cited in table 3.1.

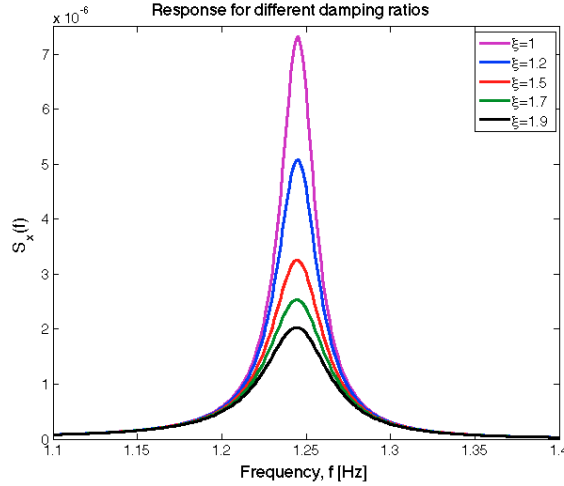


Figure 5.10: Resonance for different damping ratios

As figure 5.8 (a) and (c) shows, the density of the wind load is mainly concentrated

at frequencies lower than 0.1Hz. Since resonance will occur at frequencies around 1.245 Hz, this should not be a problem. This also make reasons to the rule of thumb used for flexible building saying the first eigenfrequency should be above 1 Hz to avoid resonance issues.

The spectral analysis can also be used to calculate displacement and acceleration from the fluctuating wind load. It must be emphasized that the calculated quantities only represent the response from the time-varying load, and not response from the mean wind force. The response calculated in section 5.3 represent the horizontal acceleration and displacement from a static equivalent load, used as an approach to estimate the combination of both the mean and fluctuating wind load on a building, consequently the results presented in section 5.3 are more correct. For the calculations, see the MATLAB script in the digital appendix.

Table 5.4: Displacement and acceleration from spectral analysis

| Direction | Displacement [mm] | Acceleration [m/s ²] |
|------------------|-----------------------------|--|
| z-direction | 1.8 | 0.0308 |
| x-direction | 1.6 | 0.0291 |

Compared to the displacements calculated in 5.3, this is very small. Thus the influence on the total displacement is negligible. To evaluate the total displacement the dynamic displacement calculated here should be added to the static displacements calculated from the formulas given in Eurocode 1-4.

This acceleration is the horizontal acceleration from dynamic wind load on the building. Since the spectral analysis is based on a single-degree of freedom system, this gives a lower acceleration than the acceleration calculated from the formulas in Eurocode 1-4, see section 5.3

5.3 Serviceability

The acceleration from wind load is calculated by the formulas in Eurocode 1 in appendix B, and compared to the numerical acceleration found in *Abaqus* from the dynamic wind load.

Both the wind load and accelerations are dependent on the eigenfrequencies of the building. The eigenfrequencies presented in section 5.1 are used in the following.

5.3. SERVICEABILITY

5.3.1 Maximum Displacement

The wind load calculated in 3.2.1 is applied as a static load on the outer columns of the frame, and a general, static analysis is performed in *Abaqus*.

Wind load in x-direction: For wind load applied in the x-direction the maximum displacement in the along-wind direction is 21.5 mm at the top floor. In the across-wind direction the maximum displacement is 0.04 mm.

Wind load in z-direction: The maximum displacement in x-direction is 1.2 mm, in the top of the frame. The maximum displacement in z-direction, parallel with the applied wind force is 44.5 mm.

The calculated displacements are small compared to the total height of the building, and this should not result in any problems for the design of the building.

5.3.2 Maximum Acceleration

The maximum acceleration is calculated according to annex B, in Eurocode 1-4, with the assumptions in annex F, Eurocode 1-4. A MATLAB script is used to calculate the acceleration on the top of the building.

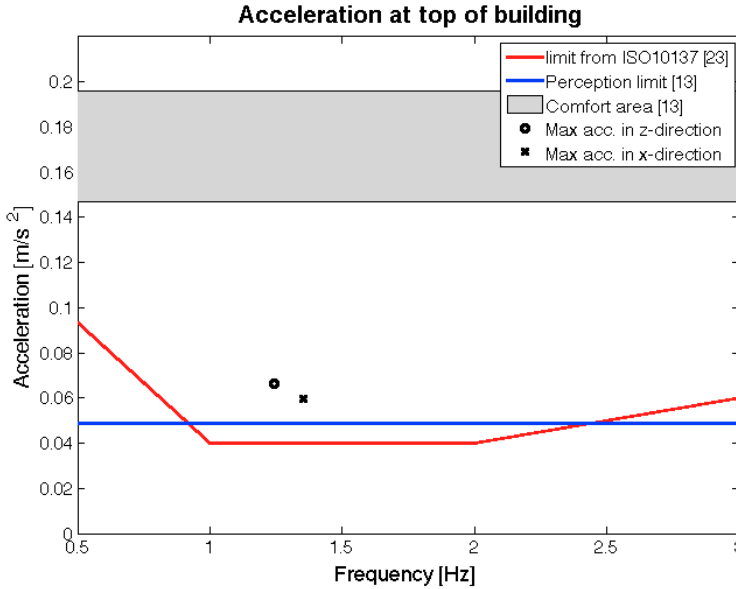


Figure 5.11: Acceleration criteria at top floor

CHAPTER 5. GENERAL RESULTS FOR SIMPLIFIED MODEL

This gives a maximum acceleration of $0.0599m/s^2$ in x-direction, and $0.0663m/s^2$ in z-direction. Figure 5.11 shows the acceleration limit for residential buildings given in ISO 10137 among with the calculated acceleration. The acceleration is about 70 % higher than the allowed acceleration. This might be a problem concerning the proposed design, especially if humans may experience discomfort when staying in the top floor.

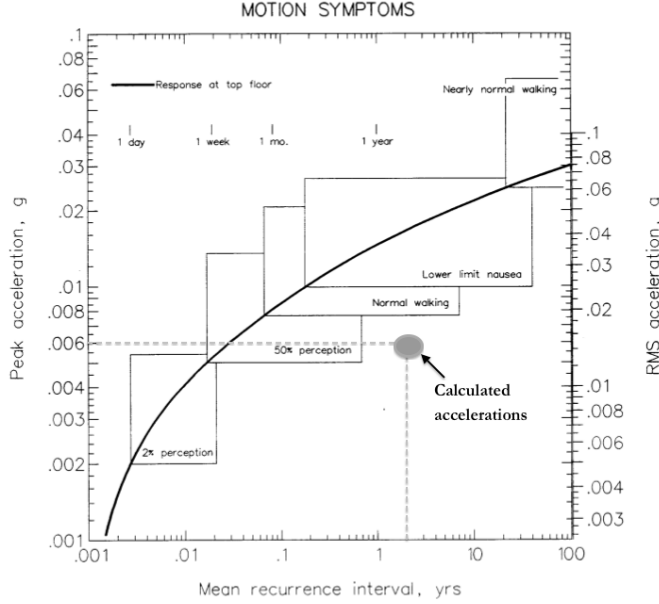


Figure 5.12: Motion symptoms due to acceleration levels [12]

As seen from figure 5.11, the calculated values are just slightly above the perception limit, and below the comfort areas, meaning that the possibility of humans experiencing discomfort is very low. The limits for perception of motion stated by D. Boggs in [12], summarized in figure 5.12 with the calculated accelerations, shows that only about 50% of the humans are expected to even feel the accelerations. The limit to experience nausea and seasickness symptoms are for $0.01g$, equivalent to $0.098m/s^2$.

The calculated accelerations are for the top of the building, while the floor at this story is located about 3 meters below. In addition the apartments will be located in the modules, so the mode shape and frequency is different. The formulas in Eurocode 1-4 only allows for a minimum return period of 2 years, while the acceptance criterium in ISO 10137 is for a 1-year return period. Nevertheless, none of these parameters will influence the acceleration to decrease enough to satisfy the criterium in ISO 10137.

5.3. SERVICEABILITY

5.3.2.1 Means to reduce the Acceleration

To reduce the acceleration below the criterium in ISO 10137, one of the following suggestions might be done to improve the dynamic performance of the structure:

Damping in the structure Assuming higher damping in the structure will reduce the acceleration in the top floor. Figure 5.13 shows how the acceleration in both x- and z- direction is reduced for higher damping ratios. The used damping ratio of 1.5% is assumed based on Eurocode 1-4, while the actual damping in the structure might be higher. Especially when considering the effect of the modules, and the complexity of the structure with regards to the number of connections and members. A damping ratio of 3-5 % does not seem unreasonable.

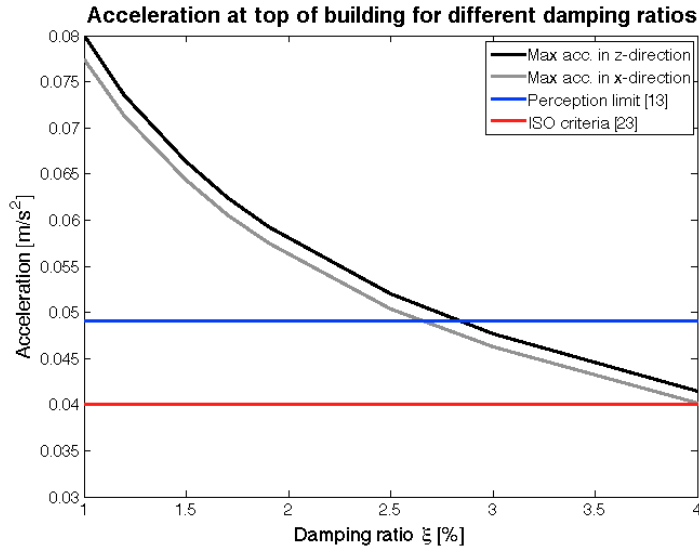


Figure 5.13: Acceleration at top floor with respect to damping

Increasing the mass Increasing the mass of the structure will give lower eigenfrequencies, but the acceleration will be reduced. The mass can be increased by adding a concrete slab at the top of the building, or by using high density concrete. The effect of this is evaluated in section 5.5.

Reducing the height Reducing the number of storeys will give higher eigenfrequencies, but will also reduce the total mass. Consequently the acceleration level at the top story will be reduced.

5.3.2.2 Results from dynamic analysis

Even though the dynamic wind load is not a correct representation of the actual wind load on the structure, the displacement and accelerations from the dynamic wind load are evaluated and compared to the previously presented results. As wanted when generating the load time series, the response is highly fluctuating.

The dynamic load for wind in z-direction gives time histories of the acceleration and displacement in point A at the top of the building. Similarly (but highest amplitudes in x-direction) for the dynamic wind load in x-direction.

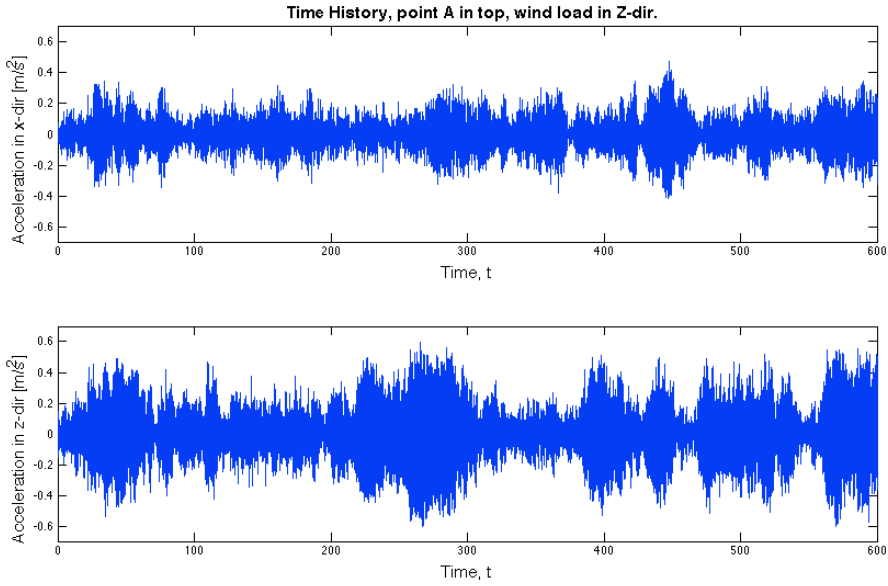


Figure 5.14: Acceleration at top floor in point A

Compared to the calculated acceleration and displacements from the formulas in Eurocode 1, the results here are very different. The acceleration from the dynamic load is in the range of 10 times higher the calculated acceleration. The reason for this is probably the calculation of the wind loading, and the dynamic amplification when considering a dynamic response.

The displacement on the other side is about 1/4 of the static displacement, again showing how the displacement from the fluctuating wind load is significantly lower than from the mean wind load. Also for the displacement the results are expected to be uncorrect due to the load calculations.

5.3. SERVICEABILITY

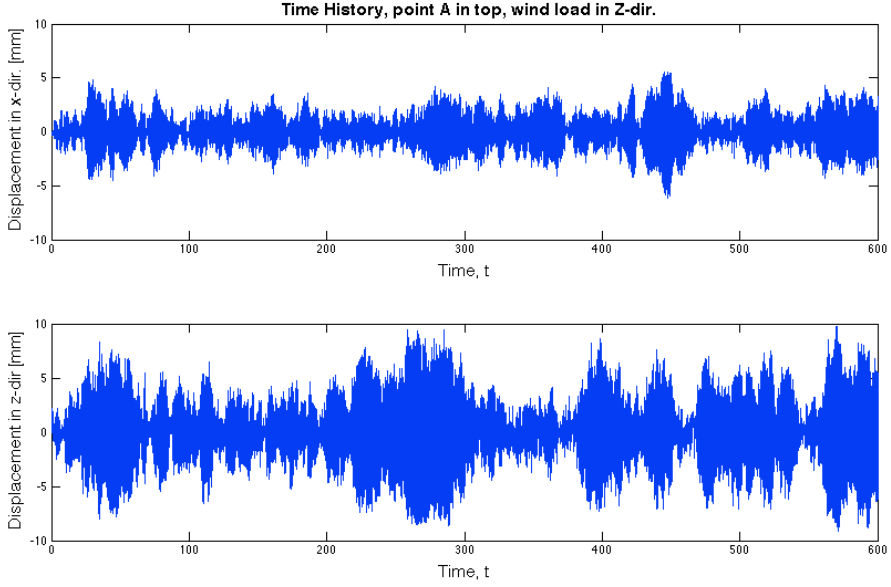


Figure 5.15: Displacement at top floor in point A

Table 5.5: Maximum values from the dynamic analysis

| Direction | Load in x-direction | | Load in z-direction | |
|-------------|---------------------|-----------------|---------------------|-----------------|
| | Displ [mm] | Acc [m/s^2] | Displ [mm] | Acc [m/s^2] |
| z-direction | 9.78 | 0.597 | 4.82 | 0.305 |
| x-direction | 5.52 | 0.472 | 9.95 | 0.695 |

Using the dynamic wind load and generated time histories to evaluate the actual response is consequently not valuable. As mentioned earlier, the purpose of the dynamic analysis is to generate time histories of the acceleration to use in the system identification, and not to evaluate the actual response of the building. For this purpose a more precise calculation of the dynamic wind load must be done.

Another use of the time histories from the dynamic response is to estimate the damping in the structure with the logarithmic decrement. As defined in equation 3.12 in section 3.3, the decay in amplitude of two successive peaks can give an estimate for the damping ratio. To do this time histories from free vibration must be used, and the generated time histories are for forced vibrations due to the applied dynamic wind load. If an analysis with longer time series than the load history was run, it could be possible to see how fast the oscillations of the building diminished, while this would only be relevant for a load that actually stopped immediately.

5.4 Locations of Instruments

Based on the mode shapes from the modal analysis in *Abaqus*, and previous practice on the area instrumentation of buildings, the points for installation of measurement devices are chosen. The locations are assumed to be subjected to high deformations when wind load is applied on the structure. In total 4 points at three different heights are evaluated. The acceleration time history from the dynamic wind load is generated, and system identification is used to validate the locations.

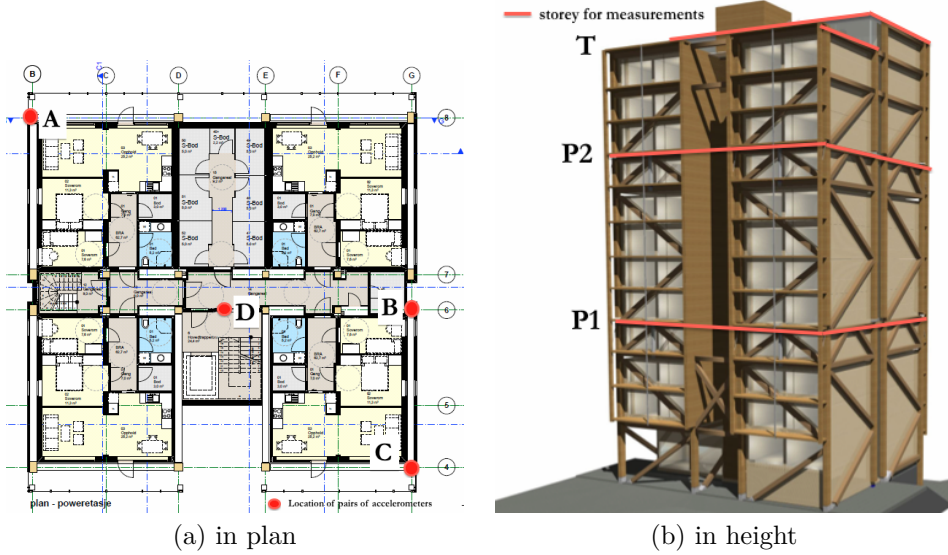


Figure 5.16: Locations of accelerometers, *illustrations from BOB, [9]*

The motion pattern is pretty similar for all heights. To include both torsional and translational motions, the accelerometers should be distributed over the plan of the building, preferably located in the corners. As seen in section 5.1, the third mode shape is dominated by motion of the upper 4 storeys due to the low stiffness in this direction. To capture this effect, point B is suggested.

To evaluate which points should be equipped with accelerometers, the system identification is tested with different combinations of the points, with the generated acceleration time histories. The results from system identification of the points giving the best results are presented in the following.

Suggestions for locations: Based on the results from the optimization of the system identification, and the high accuracy of the results, see section 5.4.1, the measurement locations are decided. The building is suggested equipped with three pairs of orthogonal accelerometers in point A, B and C, at two levels: the top

5.4. LOCATIONS OF INSTRUMENTS

of the building (T) and the 2nd power story (P2). In addition an orthogonal pair is suggested for the center (point D) of the middle slab (P2). This gives 14 accelerometers in total, distributed both in plan and height.

5.4.1 Verification of the Model using System Identification

The dynamic wind load described in section 3.2.1 was applied to the model in *Abaqus* in both x and z-direction. The time history of the acceleration in the chosen measurement points was then extracted and used in the system identification script in MATLAB. See the digital appendix.

Preprocessing Already from the preprocessing of the sampled data the eigenfrequencies could easily be determined. For real measurements this might be more difficult due to present noise. Figure 5.17 shows the frequency spectrum for point A at the top floor for measurements in both z- and x-direction.

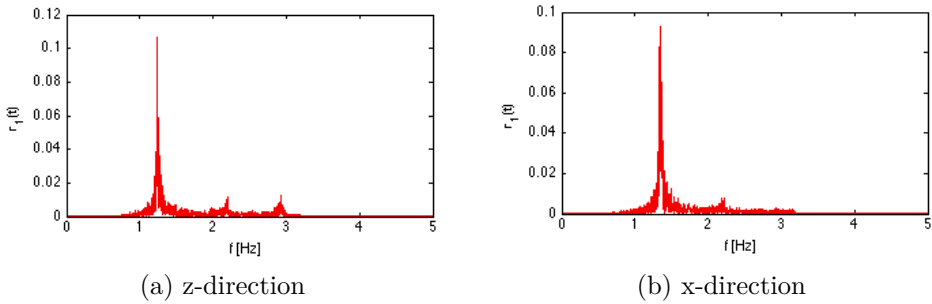


Figure 5.17: Results from fast fourier transform of measurement data

The eigenfrequencies found is a good estimation of the eigenfrequencies of the model. It must be noted that no additional eigenfrequencies than the excited, and thus represented in figure 5.17, can be found in the system identification. The wind load in x-direction will consequently only give results for mode 2 and 4, while the wind load in z-direction will give results for mode 1, 3 and 4, see section 5.1 for descriptions.

Table 5.6: Eigenfrequencies detected by the FFT of acceleration time histories

| acceleration in: | f_1 | f_2 | f_3 | f_4 | f_5 |
|------------------|---------|---------|---------|---------|--------|
| z-direction | 1.237Hz | - | 1.993Hz | 2.199Hz | 2.93Hz |
| x-direction | - | 1.349Hz | - | 2.19Hz | - |

5.4.1.1 Sampling Length

The dynamic analysis, and the system identification procedure, was run for two different time lengths, to see if the results were dependent on the sampled time. Both 60s and 600s were tested. The output was written for every 0.02s for both of the analysis. The effect of increasing the sampling length was not significant, but longer sampling length produced in general better results. The sampling rate for the 60s measurements had to be 50Hz to produce any useful results. 600s are used in the following.

5.4.1.2 Choice of Sampling Rate

The MATLAB script allows for different sampling rate of the input, in this case the acceleration time history. Changing the sampling rate influences the accuracy of the results. In general, a sampling rate in the order of 10-20 times the natural frequency gives the best result. For the case building with $f_1 = 1.245Hz$ this gives an expected optimal sampling rate at 12 - 25 Hz. The effect of changing the sampling rate with regards to the frequency and damping estimation is shown in figure 5.18.

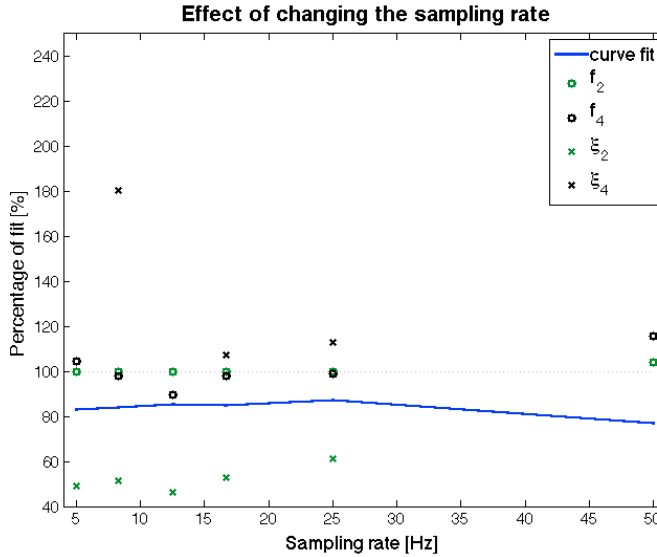


Figure 5.18: Effect of changing the sampling rate

The values in figure 5.18 are results for system identification of response in x-direction, with testorders=2:10, and order=5 for all results. The curve fit line represents the average rate of curve fit of the estimated and measured data. The circles gives the estimated frequencies, and the crosses gives the estimated damping

5.4. LOCATIONS OF INSTRUMENTS

ratios. It is seen that the best approximation is for a sampling rate of 25 Hz. For sampling rates lower than 25Hz, an increase in accuracy is achieved for higher frequencies, while this seems to be the maxima. For a frequency of 50 Hz, the accuracy is lower.

5.4.1.3 Choice of Model Order

The effect of changing the model order is significant. Both too low and too high orders will produce poor estimates of the system matrices. This is easily seen from the plot of estimated frequency versus model order, where the frequencies are spread both for low and high orders.

In general it is sought to choose the model order as low as possible. The curve fit giving a percentage of fit between the identified and measured data, can indicate if the chosen order is a good choice.

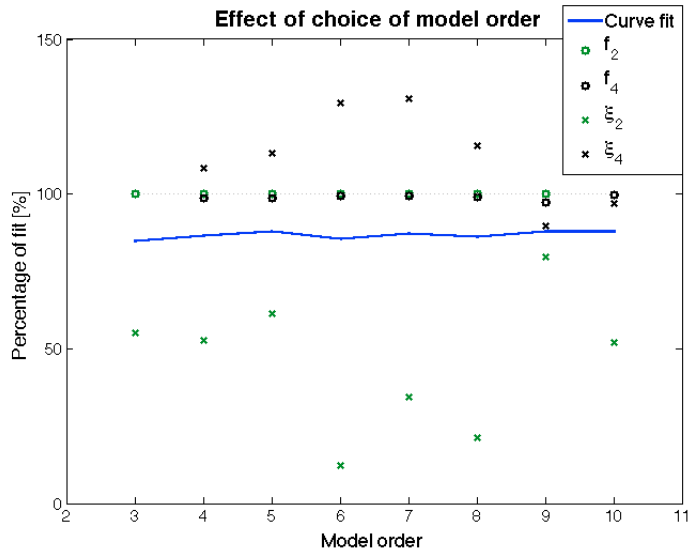


Figure 5.19: Effect of choice of model order

Choosing the right order is of high importance for the exactness of the estimation, as seen in figure 5.19, the results vary significantly for only 1 step in order (for example increasing model order from 5 to 6). Consequently the user must be careful when selecting the model order, and a sensitivity check like the one performed here, is preferable.

5.4.1.4 Results from System Identification

The output from the MATLAB script is eigenfrequencies and corresponding damping ratios, as well as the complex eigenvalues.

The response and system identification from respectively load in z- and x-direction is treated separately. The best estimates was achieved for a sampling rate of 25 Hz, and a model order of 5 and 6 for x- and z-direction respectively.

Z-direction For the estimation of the dynamic properties in z-direction a sampling rate of 25Hz and a model order of 6 gave the best results.

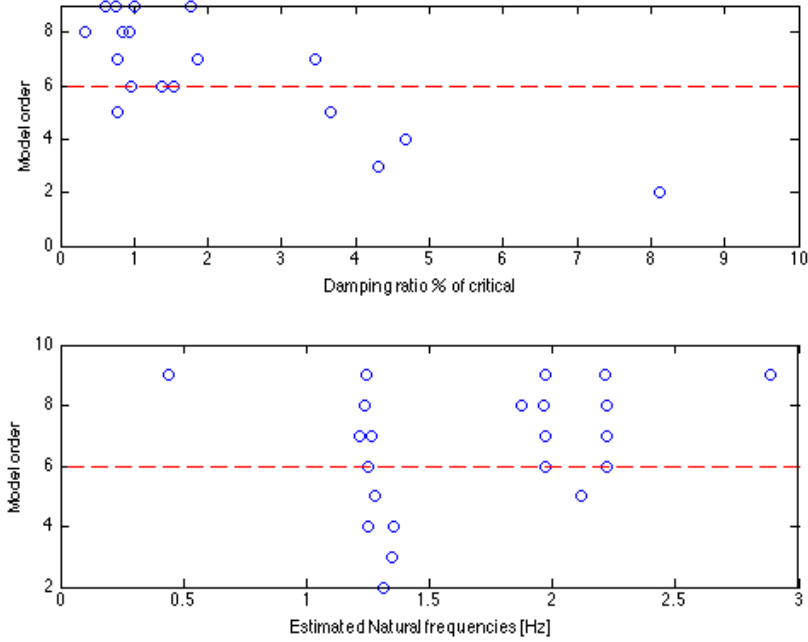


Figure 5.20: Estimates from system identification, Z-direction

As seen in figure 5.20, the eigenfrequencies are more or less independent of the model order, only with some spurious elements for higher modes. A vertical line can be drawn at the three frequencies corresponding to the three mode shapes detected. Regarding the plot of the damping ratio versus model order, the variation in estimated damping ratio is very high. The values are fluctuating between 0.2 and 8, and there are no obvious vertical lines. Many of the points are somewhat concentrated around 1 %, which are reflected in the estimated damping ratios. The scattered points might indicate that the estimation of damping ratio is poor.

5.4. LOCATIONS OF INSTRUMENTS

Table 5.7: Results from system identification, Z-direction

| Mode | Frequency [Hz] | | | Damping [%] | | |
|------|----------------|-------------|--------------|--------------|-------------|--------------|
| | <i>Model</i> | <i>SSID</i> | <i>Error</i> | <i>Model</i> | <i>SSID</i> | <i>Error</i> |
| 1 | 1.245 | 1.244 | -0.1% | 1.51 | 0.76 | -50% |
| 3 | 1.975 | 1.961 | -0.7% | 1.48 | 1.07 | -28% |
| 4 | 2.223 | 2.213 | -0.5% | 1.52 | 1.06 | -30% |

Sampling rate 25Hz, testorders 2:9, order: 6

The accuracy of the estimated eigenfrequencies are very good, only a small error of less than 1%. While for the damping ratios the accuracy is less good, varying between 28 - 50 %. For the three modes detected, two translational and one rotational, the damping ratio was in general estimated below the calculated damping ratio. The average curve fit between the estimated acceleration and measured acceleration in z-direction is 84%, which is good. Since the curve fit is high and the frequency estimation is good, the identification is assumed reasonable.

X-direction For the system identification of response in x-direction, a sampling rate of 25Hz, and a model order of 5 gave the best results. As seen in table 5.8 the estimated frequencies are of high accuracy. The estimation of the damping ratio is ok, with errors of 39% - 13%.

Table 5.8: Results from system identification, X-direction

| Mode | Frequency [Hz] | | | Damping [%] | | |
|------|----------------|-------------|--------------|--------------|-------------|--------------|
| | <i>Model</i> | <i>SSID</i> | <i>Error</i> | <i>Model</i> | <i>SSID</i> | <i>Error</i> |
| 2 | 1.351 | 1.350 | 0% | 1.47 | 0.90 | -39% |
| 4 | 2.223 | 2.197 | -1.2% | 1.52 | 1.72 | 13% |

Sampling rate 25Hz, testorders 2:10, order: 5

The curve fit for these estimations is very good, with an average of 87%, meaning that the estimates are accurate. It is also seen from figure 5.21 that the frequencies more or less are independent of the model order for orders over 5. In contrast, the estimated damping ratios are quite spread, but at a stretch a vertical line can be found at approximately 0.9% and 1.7%. This is also reflected in the estimated damping ratios. Compared to the estimation in z-direction, the variation in the estimated damping ratio with respect to model order is significantly smaller. This indicates that the response in x-direction gives a better approximation.

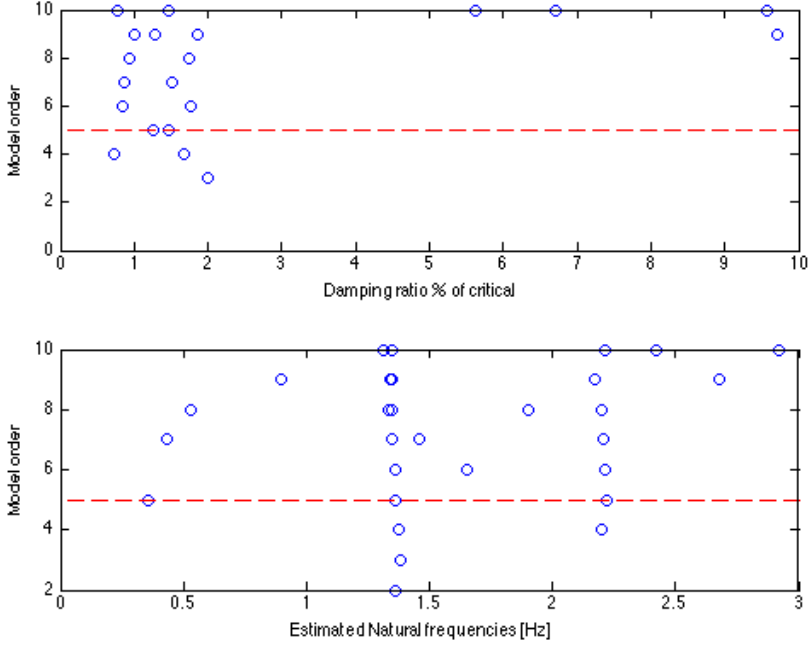


Figure 5.21: Estimates from system identification, X-direction

5.4.2 Effect of damping in model on the results from system identification

The damping ratio estimates from the system identification are poor, with errors ranging from -50% to +13%. Consequently the usefulness of the procedure to determine the damping of an actual building might be questioned. For all that, system identification have through many years and many projects proved that it is a good tool to estimate dynamic properties of a building, including the damping ratio. As discussed earlier, the assumed damping ratio in the building is a very uncertain parameter. A damping ratio of 3% is therefore implemented in the model with Rayleigh-damping ($\alpha = 0.1505, \beta = 0.0014$), and the dynamic analysis is run once again for both load in z- and x-direction. The acceleration time histories are once again used for the system identification. The same points as previously are used.

When increasing the damping ratio in the *Abaqus* model, and running the system identification procedure with the same inputs and choices as described previously, the results for the estimation of the damping ratio is slightly changed. The sampling rate and model order are as previously.

5.4. LOCATIONS OF INSTRUMENTS

Z-direction

Table 5.9: Results from system identification, Z-direction, $\xi = 3\%$

| Mode | Frequency [Hz] | | | Damping [%] | | |
|------|----------------|-------|-------|-------------|------|-------|
| | Model | SSID | Error | Model | SSID | Error |
| 1 | 1.245 | 1.247 | 0.2% | 3.02 | 1.60 | -47% |
| 3 | 1.975 | 1.949 | -1.3% | 2.96 | 2.34 | -21% |
| 4 | 2.223 | 2.225 | 0.1% | 3.04 | 1.73 | -43% |

Sampling rate 25Hz, testorders 2:9, order: 6

The error in the estimates of the damping ratio are slightly reduced for the first two translational modes. Nevertheless, the estimates are still poor. The average curve fit for the estimated time series is only 80%, which is lower than for the previous model with $\xi = 1.5\%$.

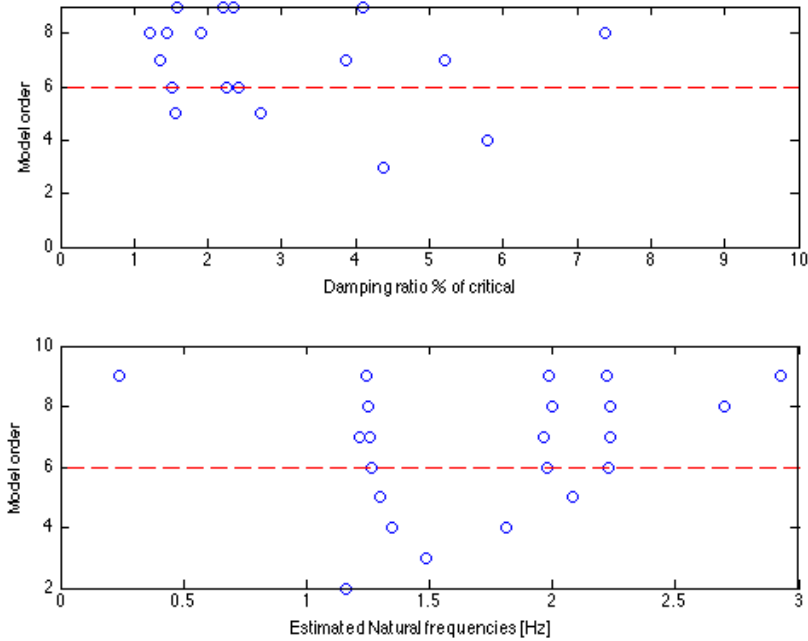


Figure 5.22: Estimates from system identification, Z-direction, $\xi = 3\%$

The frequency estimates are still good, also shown in figure 5.22, where the frequency is more or less independent of the model order. The plot of damping ratio

CHAPTER 5. GENERAL RESULTS FOR SIMPLIFIED MODEL

versus model order still gives scattered points, resulting in the poor estimate of the damping ratios.

X-direction For the response in x-direction, the error of the estimated damping ratio for the first detected eigenfrequency is reduced to 21%. For the rotational mode, the error is increased from +13% to -29%. For an assigned damping ratio of $\xi = 1.5\%$, the system identification gave a too high estimate for the rotational mode, while for a damping ratio of $\xi = 3\%$, the estimation is too low.

Again, the eigenfrequencies are more or less plotted on a vertical line, while the plot for the damping ratio is still scattered. Compared to figure 5.21, the damping ratio is even more fluctuating, and thus the accuracy of the estimates are lower. The curve fit for this estimation is lower than with $\xi = 1.5\%$, averaging on 82.5%.

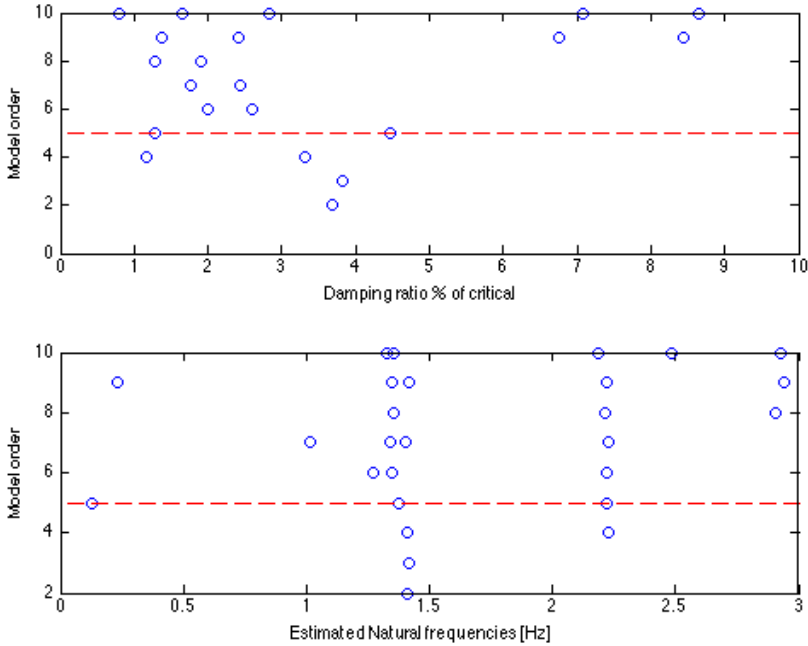


Figure 5.23: Estimates from system identification, X-direction, $\xi = 3\%$

This indicates that the assumed damping ratio influences the estimation results, but it is difficult to draw a conclusion that the estimates are better for higher damping ratios. Increasing the damping ratio in the *Abaqus* model seems to have no positive effect on the accuracy of the system identification. One explanation to the poor damping estimates may be the methods for representation of the damping.

5.5. SUGGESTIONS FOR IMPROVING THE SUPERSTRUCTURE

Table 5.10: Results from system identification, X-direction, $\xi = 3\%$

| Mode | Frequency [Hz] | | | Damping [%] | | |
|--|----------------|-------------|--------------|--------------|-------------|--------------|
| | <i>Model</i> | <i>SSID</i> | <i>Error</i> | <i>Model</i> | <i>SSID</i> | <i>Error</i> |
| 2 | 1.351 | 1.343 | -0.5% | 2.94 | 2.33 | -21% |
| 4 | 2.223 | 2.207 | -0.7% | 3.04 | 2.15 | -29% |
| <i>Sampling rate 25Hz, testorders 2:10, order: 5</i> | | | | | | |

It appears that the generated acceleration time-histories does not detect the applied damping, but consequently finds a lower damping ratio.

When considering all the other uncertainties concerning the assumptions of the damping ratios, these deviation does not seem that big. Maybe choosing other measuring locations, longer time series etc. could estimate the damping ratio with a higher accuracy. Alternatively a consistency check of the damping ratio could be performed by exciting the model with an impulse load and study the displacement time history to estimate the damping with logarithmic decrement.

5.5 Suggestions for improving the Superstructure

To reduce the acceleration levels at the top of the building to satisfy the criteria stated in ISO 10137, several improvements might be done. Some of them are tested out, and new accelerations calculated, and some solutions are just commented. Changing the model in *Abaqus* is very time consuming, as all constraints, section assignments, meshing etc involved in the change must be regenerated manually, thus only a few simple changes were implemented in the model.

1. Increasing the mass in the concrete slabs
2. Using concrete slab as roof
3. Reducing the number of storeys
4. Coupling walls in stair- and elevator shafts to the frame structure
5. Adding a tuned mass damper on the roof

The feasibility of the changes are commented to some extent, but are not considered an important part of this study.

5.5.1 Increasing the mass in the concrete slabs

If the total mass in the building is increased, the eigenfrequency will be reduced, and the acceleration will be reduced due to the higher mass, see appendix B for formulas.

For example can high-density concrete be used in the slabs, increasing the density with $1000\text{kg}/\text{m}^3$, analogous to an increase of 40% of the density in the slabs.

CHAPTER 5. GENERAL RESULTS FOR SIMPLIFIED MODEL

The new total mass is then $1.575 \cdot 10^6 kg$, and the eigenfrequencies will be:

Table 5.11: Frequencies and accelerations from increased mass in concrete slabs

| Mode | Frequency [Hz] | Acceleration [m/s ²] | Deviation [%] |
|-------------|-------------------|-------------------------------------|------------------|
| Trans z-dir | 1.198 | 0.0626 | -5.6% |
| Trans x-dir | 1.298 | 0.0608 | +1.5% |

While using high-density concrete or increasing the mass by a different manner will reduce the accelerations, the effect is not very large. The use of high-density concrete is mainly for special structures such as nuclear plants or offshore structures functioning as ballast. The probability that this should be done for this building is therefore very low. Although the effect of increasing the mass is actual, and other means to increase the mass is possible.

5.5.2 Using concrete slab as roof

The proposed solution by Sweco is to use the roof at the upper apartment modules as roof for the building. While this is feasible, no stiffness is transferred between the external frame at the top. Therefore adding a concrete slab at the top of the building will increase the general stiffness. Since the concrete also increases the mass, the eigenfrequency of the building will be lower. As long as the eigenfrequency is above 1 Hz, such that resonance with the wind load is avoided the reduction is ok.

Adding the concrete mass will increase the total mass of the building with 12 %, while the effective mass will be increased with 30%, since the added mass is within the upper third of the building. Consequently the acceleration at top level will be reduced.

The new total mass is $1.6065 \cdot 10^6 kg$. The eigenfrequencies will then be:

Table 5.12: Frequencies and accelerations from adding slab at top level

| Mode | Frequency [Hz] | Acceleration [m/s ²] | Reduction [%] |
|-------------|-------------------|-------------------------------------|------------------|
| Trans z-dir | 1.09 | 0.0594 | -10.4% |
| Trans x-dir | 1.18 | 0.0579 | -3.4% |

5.5. SUGGESTIONS FOR IMPROVING THE SUPERSTRUCTURE

The 3rd mode described previously is now gone, as the concrete slab will transfer the motions between the corridor and external frame. The mode shapes are exactly as for a cantilevered beam.

This is something the engineers and architects actually are considering as a solution to reduce the accelerations. With reference to the other maximum acceleration criterions mentioned earlier, and the small reduction of 10% achieved, the actual advantage of this change should be considered. The increased weight on the foundation, the lower eigenfrequencies closer to 1Hz, and architectural perspectives might be more important than reducing the acceleration.

5.5.3 Reducing the number of storeys

If reducing the number of storeys the eigenfrequencies will generally be increased. Due to the higher global stiffness, the acceleration values are expected to be lowered. The surface subjected to wind load on the building is also reduced.

5.5.4 Coupling of CLT walls

Coupling the massive wood walls in the staircase and elevator shaft will increase the global stiffness of the structure. The shafts will possibly give a box-function in the center of the building, and the resistance for horizontal motions will be increased. This seems like a more reasonable solution, since the massive wood walls are planned as part of the structure anyway, and not using them for horizontal stiffness is in vain.

5.5.5 Tuned mass damper at roof

Another solution is to install a tuned mass damper at the top of the building. This can be done by connecting a mass to the structure by a spring. The mass-spring system will work as a vibration absorber if tuned corresponding to the properties of the frame structure. The springs will absorb energy due to relative movements between the frame structure and the mass. If the mass is replaced by a water tank, giving the same effect, this can be used as water storage for fire protection in addition. As seen in section 5.3, and section 5.2, an increase of the damping ratio will reduce the response, and thus also reduce the acceleration significantly.

6 Parametric study

To evaluate how different parameters influence the global dynamic response, a parametric study have been performed. The rigidity of the connections are studied, as well as the influence of the modules. In addition, the damping in the structure is evaluated. This chapter presents both the background, process, results, and finally a discussion of the findings.

6.1 Connections

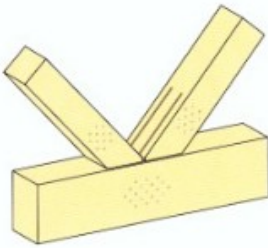


Figure 6.1: Joint with slotted steel plates and dovels [33]

To connect the members in the glulam frame, slotted steel plates are used. These plates will transfer the forces between the members in the joints. A sketch from Moelven shows the solution in figure 6.1. The flexibility of the joints connecting beams and diagonals to the columns in the external truss will influence the deformation pattern of the structure, as well as the dynamic performance. It is especially interesting to find out whether the properties of the joints will influence the overall stiffness of the structure, which can be seen by evaluating the eigenfrequency.

Slip in connections The stiffness of a fastener is represented by the stiffness modulus K_{ser} . This modulus is dependent on the connection type, the density of the timber, and the diameter of the fastener. The slip in the connections are mainly caused by tolerance when drilling holes for the dovels. Also yielding in the fasteners, or compression of the timber are likely to cause slippage in the connections.

Rotational stiffness The rotational stiffness in the connections are dependent on the mutual placing of the fasteners as well as the stiffness of the fasteners.

The stiffness of a typical connection is calculated in appendix C.

6.1.1 Modeling of Connections

Several approaches to model the connections are done to investigate how this parameter changes the dynamic performance of the model:

1 - Fixed This is almost impossible to achieve when the building is assembled, thus this represents an extremity. The results presented in chapter 5, are all with rigid connections.

2 - Hinged The opposite extremity will be releasing the rotational degree of freedom around the local primary axis in all joints. Hinged joints is conservative when detailing the members of the structure. While concerning the dynamics, this will give a too flexible building compared to reality.

3 - Change material parameters By assigning modified material parameters to a small segment of the beam nearest the joint the properties of the connection may be controlled. Two properties are changed for the general section in these beam segments: (a) - Area, A , and (b) - Second moment of area, I .

6.1.2 2D-truss

At first, a 2D-truss similar to one of the end walls are modeled. The three alternatives listed above are compared for this 2D-truss. The complete model of the case model is very complex, with more than 200 joints, modifying all the connections is therefore a cumbersome process. Thus a small 2D-truss as shown in figure 6.3 is used.

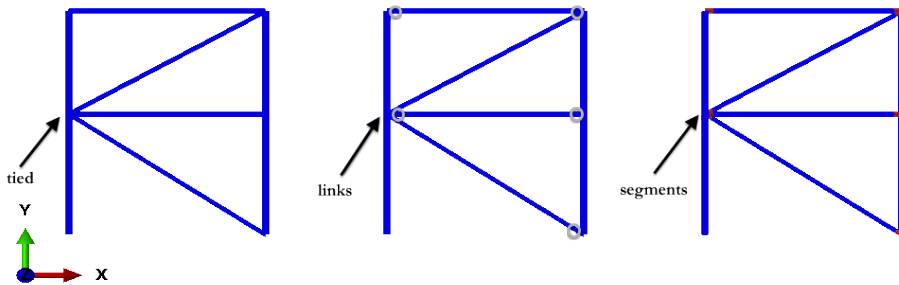


Figure 6.2: 2D-truss

6.1. CONNECTIONS

This truss is analysed with three types of connections:

1. tied / rigid
2. linked / hinged
3. beam segments with $A = 0.2 \cdot A_{beam}$

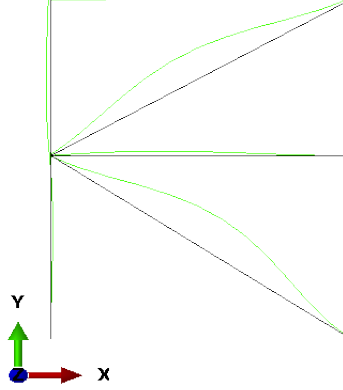


Figure 6.3: Mode shape 1 for 2D-truss with tied connections

Table 6.1: Eigenfrequency of 2D-truss

| Configuration | 1st mode | 2nd mode | Deflection |
|------------------------|----------|----------|------------|
| (1) Tied | 17.17 Hz | 17.87 Hz | 0.202 mm |
| (2) With links | 12.47 Hz | n/a | 0.204 mm |
| (3) With beam segments | 17.07 Hz | 17.65 Hz | 0.243 mm |

What is seen from this preliminary study is that the beam segments reduces the stiffness in the frame compared to the tied frame. As expected the model with the beam segments lies closer to the tied model, and this is also a wanted feature of the beam segments. The stiffness in the connections are only slightly reduced compared to a rigid connection, and the mode shapes are very similar. To use a hinged connection in the frame structure is not wanted, since horizontal bracing effect of the truss-pattern will be reduced. So the fact that the model with beam segments lie closer to the tied model than the hinged model is good. An important observation from this preliminary study of a 2D-frame, is that the deflection of the frame with the beam segments is 20% larger than for the tied and hinged frame. This is obviously due to the reduction of axial stiffness in the beam segments. Consequently the model with the beam segments should only be used for a study of the global stiffness. Not for deformation or to evaluate forces in members.

6.1.3 Reducing A in Beam Segments

The stiffness of the connection is calculated in appendix C, and is calculated to $1.063 \cdot 10^6 N/mm$. For a beam segment of length 0.4m, this gives an equivalent area A_{eq} to represent the stiffness in the connection:

$$k = \frac{A \cdot E}{L} \Rightarrow A_{eq} = \frac{k \cdot L}{E} = \frac{1.063 \cdot 10^6 N/mm \cdot 400mm}{13000 N/mm^2} = 32700 mm^2 \quad (6.1)$$

This is equivalent to a beam segment with $A_{segment} = 0.2 \cdot A_{beam}$. To evaluate the sensitivity of the model regarding stiffness in the connections, a beam segment with equivalent area in the range of 10 - 40% of the beam area is investigated. This gives an interval around the calculated stiffness of the connection, to ensure variation in stiffness in the actual connections.

6.1.3.1 Effect on Frequency

The reduction of the stiffness in the beam segments have influence on the frequency for $A_{segment} = 0.2 \cdot A_{beam}$ or less. The reduction in the frequency is in the area of 5-20 % from the original frequency. The mode shapes are similar to the ones found in section 5.1.

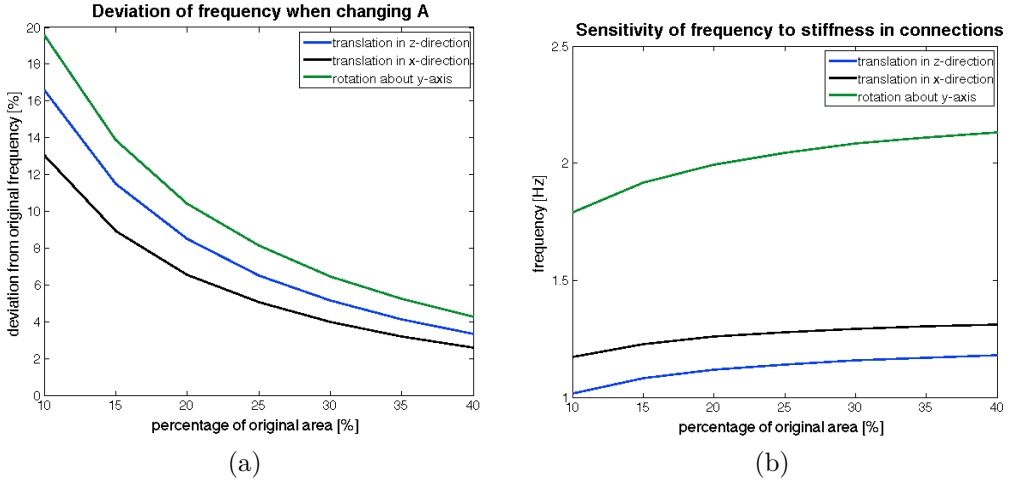


Figure 6.4: Effect on frequency for varying stiffness in beam segments

As seen in figure 6.4, there is almost no change in the frequencies when the area of the beam segment is larger than 25% of the original area. This is partially explained with the short length of the segments compared to the beams. With lengths of 8 - 12 meters for the beams and diagonals, a 400mm segment at each end is equivalent to 10% of the total length. Thus reducing the stiffness in the

6.1. CONNECTIONS

segments, should have only a small effect on the global stiffness. The accelerations as a consequence of the reduced stiffness in the beam sections are given in table 6.2.

Table 6.2: Results for model with beam segments, $A_{segment} = 0.2 \cdot A_{beam}$

| Direction | Frequency [Hz] | Acceleration [m/s ²] | Increase |
|-------------|-------------------|-------------------------------------|----------|
| z-direction | 1.1167 | 0.0751 | 13.3% |
| x-direction | 1.2580 | 0.0698 | 16.5% |

Clearly the effect of reducing the area in the beam segments to imitate the stiffness in the connections will give an increase in the acceleration. The effect is not very big, and the models assuming all connections to be tied are apparently a reasonable approximation.

6.1.4 Reducing I in Beam Segments

The rotational stiffness from equation C.6 can similarly be represented by an equivalent 2. moment of area, I :

$$k = \frac{6 \cdot E \cdot I}{L^2} \Rightarrow I_{eq} = \frac{k \cdot L^2}{6 \cdot E} = \frac{4.356 \cdot 10^{10} Nmm/rad \cdot 400^2 mm^2}{6 \cdot 13000 N/mm^2} = 8.935 \cdot 10^{10} mm^4 \quad (6.2)$$

Compared to the 2. moment of area of the original beam section: $I_{beam} = 2.24 \cdot 10^9 mm^4$, this is significantly higher. Which indicates that the rotational stiffness in the connections are governed by the stiffness in the beams and not in the connections. This was as expected, since the frame is quite similar to a truss, and therefore axial loads are dominating in the connections. No further analysis is therefore done on the rotational stiffness.

6.1.5 Energy dissipation in Connections

Another assumption is that most of the damping in a structure usually is a product of the energy dissipation in joints. Therefore the damping ratio in the beam segments was increased to see if this had any effect on the total damping of the structure. As explained earlier, the Rayleigh damping is for global damping ratios only, while the composite modal damping can be used for component wise damping. Since the summation procedure of the damping ratio in each component is weighted based on generated mass, the effect of increasing the damping ratio in the

beam segments was negligible. To study this effect, another type of damping representation should be used. For example hysteresis damping or frictional damping might give a visible result for this effect. Due to limited time, this is not tested any further.

6.1.6 Summary of Connection Study

As seen in the preliminary study of the 2D-model and the study of the complete 3D-model, the effect of reducing the area in the beam segments does not influence the frequency significantly. The displacements are increased due to the low axial stiffness in the beams, which will not be the case in the actual connections, thus no further evaluation of the displacements are done.

Taking into account the reduced stiffness in the connections, this gives higher acceleration levels at the top of the structure. Nevertheless, it must be emphasized that the connection study is done assuming all connections are similar, with 5x5 dowels in a rectangular pattern, and two slotted steel plates. For the real structure, many of the connections will be designed with less dowels than this, which might result in further reduction of the frequency. The representation of the stiffness in the connections might also be questioned, as it is a very simplified method, and there are several other factors than just the slip in the dowels that affect the stiffness in the connections.

6.2 Modules

As a first approach, only the mass of the modules are included in the model. This will be a good approximation if the modules are supported on the concrete slabs, and not connected in any other way to the frame structure. To evaluate the dynamic response of the frame and modules together, simplified models that represent the dynamic properties of the modules were introduced to the model. The connection between the modules and the frame are modelled with springs and constraints.

6.2.1 Key Properties of the Modules

The modules have been tested and evaluated by fellow student Anders Jørstad. A summary of his findings is presented in the following [24]. The modules are configured in three ways for this building: (a) five modules side-by-side over four stories, (b) two modules side-by-side over four stories, and (c) two modules side-by-side over three stories.

6.2. MODULES

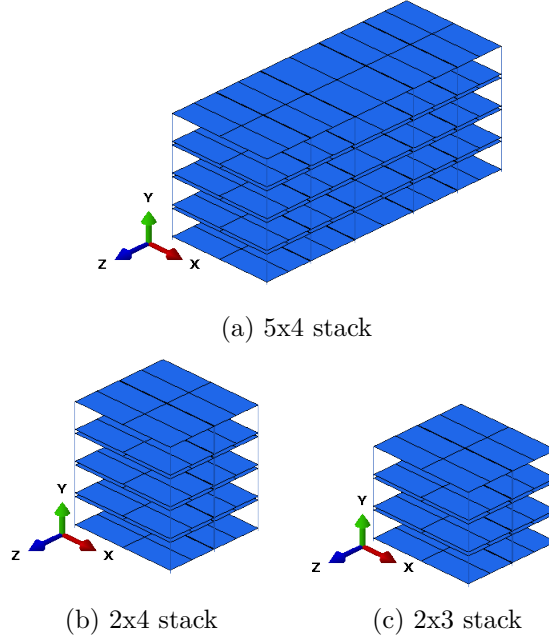


Figure 6.5: Simplified models of the apartment modules [24]

Mass of module The mass of one module is $8050kg$, or $241kg/m^2$.

Damping ratio The damping ratio of the modules are estimated to 3% from the experiments conducted at Kodumaja, Estland.

Eigenfrequencies & modes The first three modes for the two-by-four are shown here. The other two configurations have similar mode shapes.

Table 6.3: Eigenfrequency of module stacks [24]

| Configuration | transl in z-dir | transl in x-dir | rot about y-axis |
|---------------|-----------------|-----------------|------------------|
| (a) 5x4 | 2.64 Hz | 3.35 Hz | 3.89 Hz |
| (b) 2x4 | 2.62 Hz | 3.58 Hz | 4.74 Hz |
| (c) 2x3 | 3.53 Hz | 4.80 Hz | 6.33 Hz |

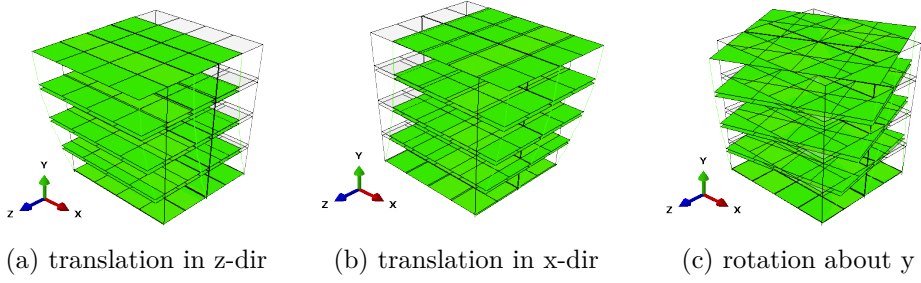


Figure 6.6: Mode shapes of the two-by-four module stack [24]

6.2.2 Modules tied to slab

For the proposed concept where the concrete slabs on the power storeys are used as support for the stacks of modules, the eigenfrequencies and mode shapes are given in the following. The mode shapes for mode 1-4 is similar to the simplified model where the modules are represented by mass only. The eigenfrequencies are in the range of 3-7% lower than the simplified model. Nevertheless, the results verifies that the simplification done, and therefore also the previous results achieved, are valuable and trustworthy. It is seen from figure 6.7 to 6.9 that the modules move as rigid bodies, following the deformation of the rest of the frame. The mode shapes and frequencies are given in the following.

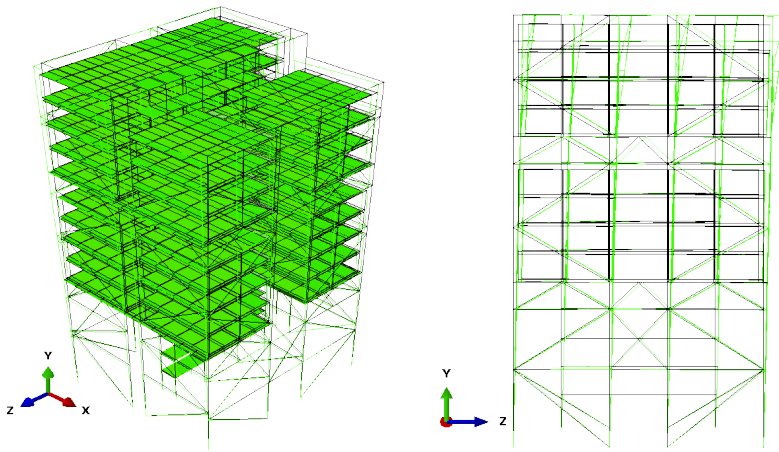


Figure 6.7: Mode 1, $f = 1.193\text{Hz}$ -4% compared to simplified model

6.2. MODULES

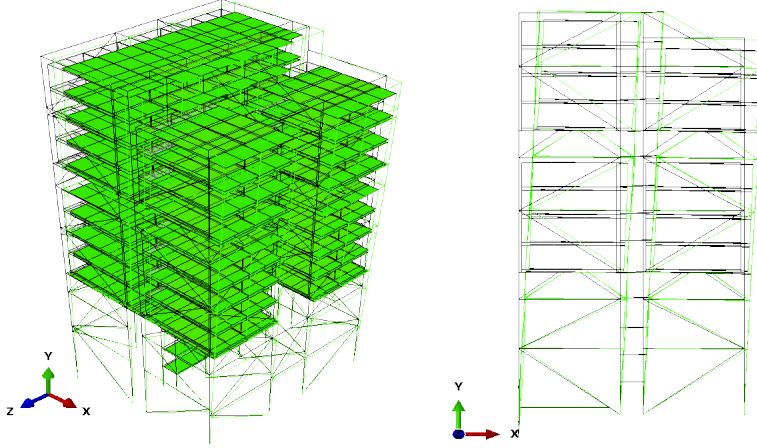


Figure 6.8: Mode 2, $f = 1.311Hz$ -3% compared to simplified model

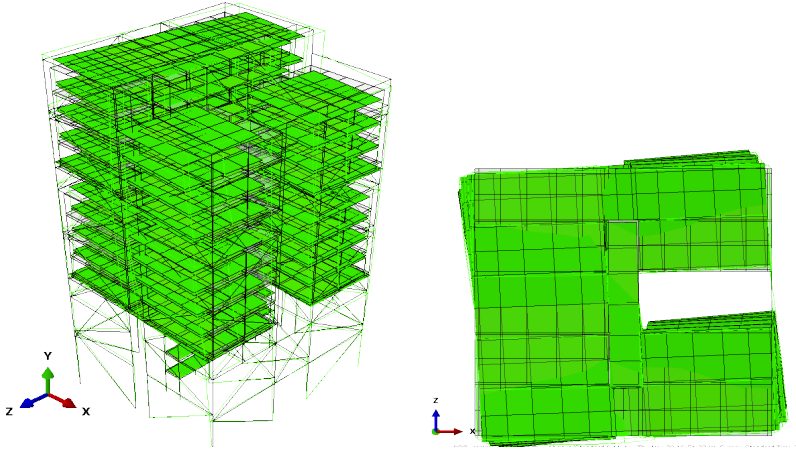


Figure 6.9: Mode 4, $f = 2.076Hz$ -7% compared to simplified model

For mode 5 and 6, both with frequencies in the range of the eigenfrequencies of the modules, see section 6.2, the modules sway in addition to the frame motion. This should not be a problem of any significance, especially since the wind load spectra has almost no density for frequencies at this range. As seen in figure 3.1 in section 3.2, higher frequencies might be excited by an earthquake. This is not a part of this thesis, and the effect will not be further investigated.

CHAPTER 6. PARAMETRIC STUDY

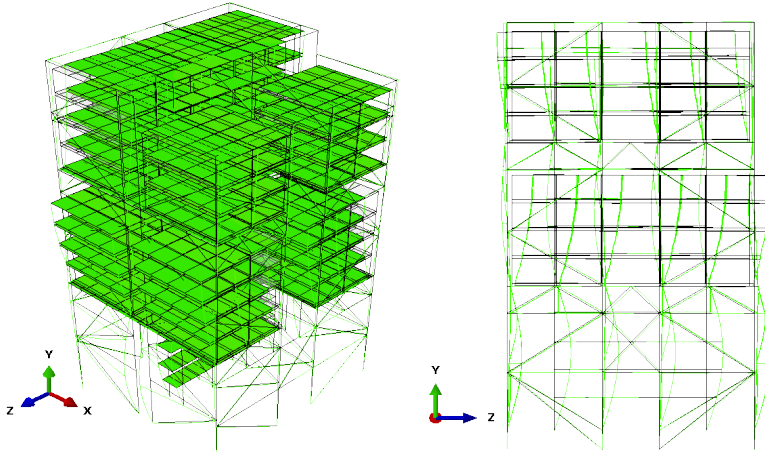


Figure 6.10: Mode 5, $f = 2.363Hz$

It is seen that the apartment modules sway on their own, and the middle modules are actually swaying in the opposite direction of the frame.

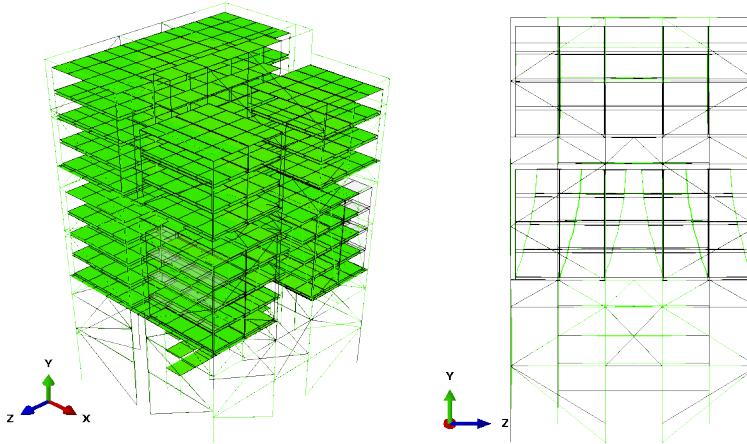


Figure 6.11: Mode 6, $f = 2.527Hz$

For mode 6, the modules in the middle of the building are pounding, which might cause a problem if these frequencies are excited.

Concerning the eigenfrequencies, it is seen that the eigenfrequency is reduced for all modes. This is probably due to the motion in the modules, and since the eigenfrequency is reduced, it seems reasonable to assume that the modules gives

6.2. MODULES

no contribution to the global stiffness of the structure. Since the eigenfrequency is slightly reduced, it is reasonable to assume that the modules contribute in some way to the response, rather than only moving as rigid bodies connected to the concrete slabs. The reduction in eigenfrequency can probably be explained by the distribution of mass over the height.

6.2.3 Damping Ratio by Components

As mentioned in section 3.3, the damping ratio of a structure is highly based on assumptions and previous measurements. There is never built a timber building with this concept and this height, therefore the damping ratio is most likely wrong. For timber structures it is normal to assume a damping ratio at about 1-2 %. Changing the damping ratio will influence the acceleration calculations in section 3.2.3. Since this is an important parameter for the design, an approach to estimate how the modules affect the damping ratio is done in the following.

To evaluate the sensitivity of the damping parameter, each component is designated a different damping ratio, and this is implemented in a separate model. It must be emphasized that this approach is not verified, nor a method to estimate the structural damping. As mentioned earlier, Rayleigh-damping is meant to represent the damping of the structure as a whole, and not for separate components. The summation procedure for Rayleigh-damping in *Abaqus* will not give a damping that represent the total damping in the building. Nevertheless, this is done to reason assumptions regarding each components contribution to damping, as well as the sensitivity of damping. The following damping properties for the different components are used:

Table 6.4: Damping ratios for different components

| Component | Damping ratio | α | β | Composite |
|------------------------|---------------|----------|---------|-----------|
| Timber frame and slabs | 1.5 % | 0.0752 | 0.0007 | 0.015 |
| Modules | 3% | 0.3493 | 0.0005 | 0.030 |

This is implemented in Abaqus in the material module, with α and β values as listed in table 6.4. Figure 3.7 shows the proportional damping in the different components, as well as the output from the complex eigenfrequency analysis in Abaqus. Assuming that the damping ratio for the superstructure (timber frame, concrete slabs and CLT floors) is 1.5%, gives the results shown in figure 6.12.

For the component wise damping ratio using Rayleigh- damping, the calculated damping ratio lies in the middle of the two curves representing the damping in the modules and the truss respectively. Thus the modules are assumed to contribute almost similarly as the frame to the total damping. In reality they will probably contribute to some extent, but maybe not as much as the external frame.

CHAPTER 6. PARAMETRIC STUDY

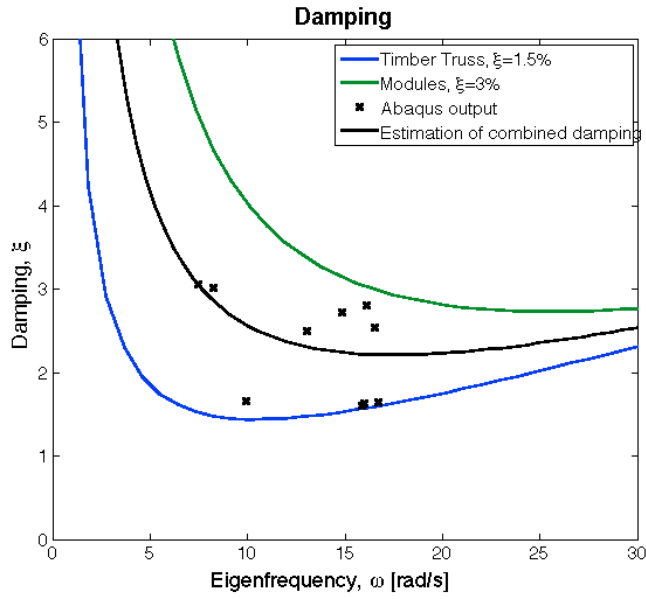


Figure 6.12: Combined rayleigh-damping considering superstructure and modules

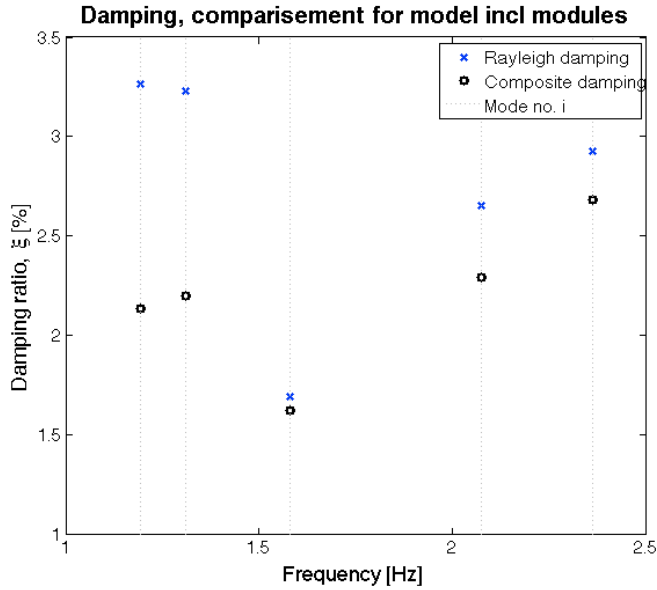


Figure 6.13: Comparison of the combination of component wise damping ratio

It is seen from figure 6.12 and 6.13 that the Rayleigh damping overestimates the effect of the modules due to the high mass of the modules, as a result of rigid body

6.2. MODULES

motions. The modal composite damping seems to give a better approximation to the estimated total damping, still assuming that the damping in the modules contribute significantly to the total damping. This effect is questionable, and further analyzes and real measurements should be done to evaluate how the modules affect the damping in the structure. Even though both the composite modal damping and the Rayleigh damping results in higher effective damping ratios when using component wise damping, the summation of the damping is questionable, and the combination is not a representation of the actual situation.

6.2.3.1 Effect on Acceleration due to assumed increased Damping

Using the increased damping ratio for the combination of the damping in the frame and in the modules, the acceleration at the top floor will be reduced. Even though the summation of the damping ratios not are entirely correct, it is plausible reasonable to assume a higher damping ratio than 1.5% in the structure. The combined damping ratio for the composite modal damping is used, as this is assumed the most correct summation.

Table 6.5: Acceleration for increased damping ratio

| Direction | Frequency | Damping ratio | Acceleration | Reduction |
|-------------|-----------|---------------|----------------|-----------|
| z-direction | 1.193Hz | 2.13% | 0.0610 m/s^2 | -8% |
| x-direction | 1.311Hz | 2.19% | 0.0536 m/s^2 | -10.5% |

Compared to the previously calculated accelerations, these values are lower. As seen previously, increasing the assumed damping ratio in the structure will reduce the accelerations at the top level. Nevertheless, this is the acceleration in the frame. To calculate the acceleration in the apartment modules, a different approach should be used. The fact that the stack of modules are only 4 storeys tall, and moves by them selves inside the frame must be accounted for.

6.2.4 Modules connected to external frame with springs in top

The concept where the modules are connected with spring - dashpots to the timber frame is investigated. The frequency as a function of the spring stiffness is shown in figure 6.14.

The problem with connecting the modules to the external frame is that the motions are transferred between the frame and the modules. The concept without this connection is probably better, since the modules are used for apartments. Therefore the motion in the modules is desired to be smaller than the motion of the frame.

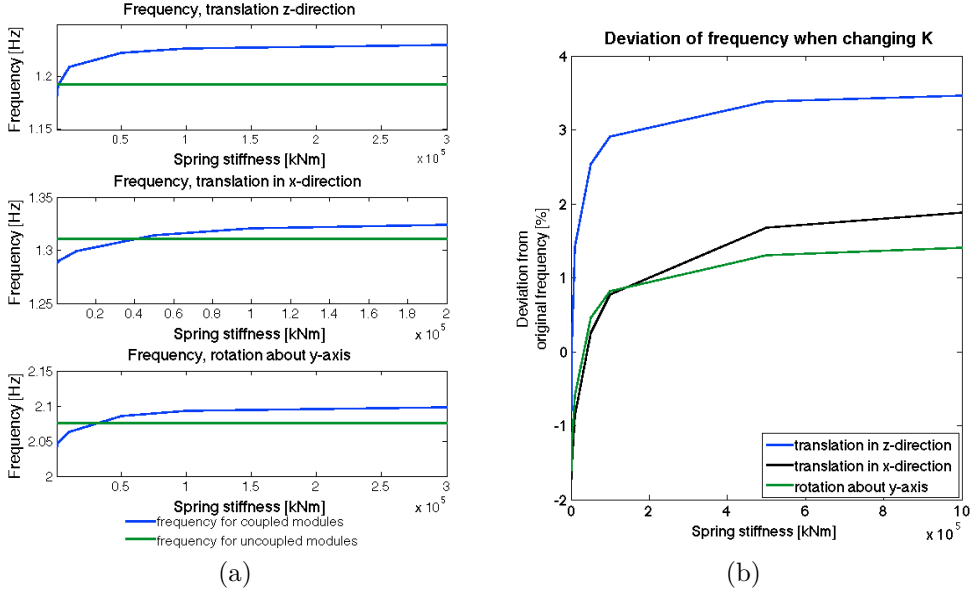


Figure 6.14: Effect on frequency for varying spring stiffness in connections

For a spring stiffness larger than $k = 50000kNm$, the effect is noticeable. For the first eigenfrequency, an increase of 3% is achieved with $k = 100000kNm$. This gives $f_1 = 1.2273Hz$, corresponding to an acceleration of the top floor at $0.0662m/s^2$. Thus the effect of the acceleration when connecting the modules to the structure with springs is minimal.

The damping as a function of the spring stiffness in the spring connecting the modules to the frame was studied, but the effect was very small. Both Rayleigh damping and composite modal damping was tested.

The effect of implementing dashpots in the connections between the modules and the frame seemed to have no significance to either the damping nor the frequency. If structural damping were chosen, and a dynamic analysis was run to evaluate the logarithmic decrement from the displacement time-history the effect from the connections would probably be more visible. Due to time limitations this was not tested.

6.2.4.1 Acceleration at top floor

If using the eigenfrequencies and damping ratios from the calculations with spring stiffness $k = 100000kNm$, this gives a reduction of the acceleration at the top floor given in table 6.6

6.2. MODULES

Table 6.6: Acceleration when connecting modules

| Dir. | Frequency [Hz] | | Damping ratio [%] | | Acceleration [m/s^2] | |
|-------------|-----------------------|-------------------|--------------------------|-------------------|--|-------------------|
| | <i>tied</i> | <i>w/ springs</i> | <i>tied</i> | <i>w/ springs</i> | <i>tied</i> | <i>w/ springs</i> |
| <i>z</i> | 1.193 | 1.228 | 2.13 | 2.22 | 0.0610 | 0.0590 |
| <i>x</i> | 1.311 | 1.321 | 2.19 | 2.20 | 0.0536 | 0.0530 |

The acceleration at the top floor is consequently reduced with 3% when connecting the modules to the frame in the top with springs. The effect is so small, that this is unnecessary. In addition, due to the connection, the acceleration in the apartment modules will probably be higher than the acceleration of the frame. As a result, the concept with springs in top of the modules should probably be rejected.

7 Conclusion

Based on the results found in chapter 5 and 6, a summary of the findings and some remarks are made in the following.

7.1 Summary of Findings

The eigenfrequencies of the structure were higher than expected based on the height of the building, with calculated values in the range of 1.24 - 2.22 for the first mode shapes. The mode shape were as expected more or less similar to the mode shapes of a cantilevered box. The stiffness in z-direction, and especially in the upper third of the building, seems to be somewhat low. Changing the boundary conditions or increasing the damping ratio had no influence on the calculated eigenfrequencies.

The maximum displacement and accelerations of the top of the building was calculated, and found to be at an approved level based on the acceleration criterions given in section 3.2.3. Since the acceleration levels are higher than the accepted levels in ISO 10137, several suggestions for reducing the acceleration are proposed. The most effective solution is to increase the damping in the structure, or reduce the number of storeys.

The curiosity regarding the feasibility of this timber frame concept and the actual damping ratio in the building can in some ways be satisfied by installing the building with accelerometers when finished. The building is therefore suggested to be equipped with in total 14 accelerometers, distributed in orthogonal pairs both in plan and height. The system identification showed good results for the estimation of dynamic properties from generated acceleration time series. Thus this can be used to investigate the dynamic properties of the real building.

The parametric study showed that the stiffness in the connections had low influence on the global stiffness in the structure, while this should probably be investigated more in depth before disregarding the effects in the joints. Furthermore the effect of including simplified models of the modules reduced the eigenfrequency of the building. Due to the high damping in the modules, the global damping ratio is

CHAPTER 7. CONCLUSION

increased when using component wise damping. Connecting the modules to the structure with springs in the top seemed to have no positive effects.

One of the most difficult parameters to estimate in the planning phase of a building is the damping, or amount of dissipated energy. An approach to estimate the global damping in the structure is done, and the effect of using both composite modal damping and Rayleigh - damping is evaluated. The results for the two representation methods are dissimilar, enhancing the estimation issues regarding the damping parameter.

7.2 Remarks

Stiffness The stiffness of the building seems to be high enough to withstand large deformations and accelerations due to dynamic wind loading. Nevertheless, increasing the stiffness in z-direction with for example an internal truss or coupling the massive wood walls is advisable.

Damping Assuring what the actual damping ratio is, will be of high importance, as seen the damping ratio influences the response significantly. If the damping ratio is lower than the assumed $\xi = 1.5\%$, this might cause problems considering the acceleration levels.

Modules The high damping in the modules are expected to increase the global damping in the structure, and therefore reduce the accelerations at top of the building. The actual contribution can not be determined with the damping models used in this thesis. This will be important for the verification of the concept.

System identification The system identification gave good results for the estimation of eigenfrequencies, while less accurate approximations for the damping ratio. Anyway it is suggested as a tool to estimate the dynamic properties of the actual building when finished.

The proposed concept for the case building is apparently a good solution, and the project should be considered feasible based on the dynamic properties investigated in this thesis.

7.3 Further Work

Suggestions for further work are:

- Measuring of the actual accelerations
- Study non-classical damping

7.3. FURTHER WORK

- More thorough connection studies
- Improving the structure

As discussed previously, the damping parameter is difficult to estimate mathematically. Installing accelerometers in the actual building when finished would therefore be very interesting. The system identification could then be used to estimate the damping ratios.

Another approach to study the damping properties of the structure is to introduce non-classical damping. As found in section 5.1 and 6.2.3, neither of the two applied damping models give reasonable results for the combination of the damping ratio in each component.

With regards to the flexibility of the connections, a more thorough study of what influences the properties of the connections, and how this affects the overall dynamic performance of the building would be interesting. Also the effect of the concentration of total energy dissipation in the connections is an area for further investigation.

Furthermore it would be interesting to study several approaches to reduce the vibrations due to wind loading, for example the effect of tuned mass dampers or changing the truss pattern.

Bibliography

- [1] Gateway to the united nations systems work on climate change, 2012. URL <http://www.un.org/wcm/content/site/climatechange/pages/gateway/mitigation>.
- [2] Fasthestverdier for ce 140c, 2012. URL <http://www.moelven.com/no/Produkter-og-tjenester/Limtre/Teknisk-informasjon-og-sertifikater/Fasthetsverdier-for-limtre-og-Kerto/>.
- [3] Explore the world's tallest timber apartments, 2012. URL <http://www.forteliving.com.au/>.
- [4] Murray grove - the world's tallest modern timber residential building, 2012. URL <http://www.waughthistleton.com/project.php?name=murray&img=1>.
- [5] Umeå kommun: Umeå ö - ett signum för umeå, 2012. URL <http://www.umea.se/4.5b0fc44e112e702ab8980008049.html>.
- [6] J. Aarstad, G. Glasø, and A. Bunkholt. Massivtre. *Fokus på tre*, (20), 2011.
- [7] K. Alvin, A. Robertson, G. Reich, and K. Park. Structural system identification: from reality to models. *Computers and Structures*, 81:1149–1176, 2003.
- [8] P. G. Bergan, P. Larsen, and E. Mollestad. *Svingning av konstruksjoner*, volume 2. Tapir Forlag, 1993.
- [9] Bergen og Omegn Boligbyggelag. Verdens høyeste trehus nærmere realisering, 2012.
- [10] Blueprint. Timber towers. <http://www.waughthistleton.com/press/10june20122012>.
- [11] B. Boellard. Design of an outrigger structure for tall timber buildings. Master's thesis, Eindhoven University of Technology, 2012.
- [12] D. Boggs. Acceleration indexed for human comfort in tall buildings - peak or rms. Submitted to CTBUH Monograph Chpt. 13, Motion Perception Tolerance and Mitigation 1997, July 1995.
- [13] D. Boggs and J. Dragovich. The nature of wind loads and dynamic response. *ACI Special Publications*, 240(2):15–44, 2006.

BIBLIOGRAPHY

- [14] R. Brincker and P. Andersen. *Understanding Stochastic Subspace Identification*. University of Aalborg, Denmark, Dept of Structural and Environmental Engineering, 2006.
- [15] A. K. Chopra. *Dynamics of Structures*. Pearson Education, Inc., 3 edition, 2007.
- [16] K. Cock and B. Moor. *Subspace Identification Methods*. K.U. Leuven, Dept of Electrical Engineering, 2003.
- [17] Cook, Malkus, Plesha, and Witt. *Concepts and Applications of Finite Element Analysis*. John Wiley & Sons. Inc, 4 edition, 2002.
- [18] W. Favoreel, B. Moor, and P. Overschee. Subspace state space system identification for industrial processes. *Journal of Process Control*, 10:149–155, 2000.
- [19] G. Glasø. Fleretasjes trehus. *Fokus på tre*, (32), 2008.
- [20] M. Green and J. Karsh. The case for tall wood buildings. <http://webc.smallboxcms.com/database/rte/files/Tall2012>.
- [21] J. Holmes. *Wind Loading of Structures*. Taylor & Francis, 2. edition, 2007.
- [22] H. Imai, C.-B. Yun, O. Maruyama, and M. Shinozuka. Fundamentals of system identification in structural dynamics. *Probabilistic Engineering Mechanics*, 4 (4):162 – 173, 1989.
- [23] *ISO 10137, Bases for design of Structures - Serviceability of Buildings and Walkways against Vibrations*. ISO, 2007.
- [24] A. Jørstad. Preliminary title: Experimental testing and numerical modeling of dynamic properties of building modules. Master’s thesis, NTNU, 2012/2013.
- [25] L. H. Kaasa. Design of an experimental setup for measurements of the aerodynamic properties of bridge decks. Master’s thesis, NTNU, 2012.
- [26] T. Kijewski-Correa and J. Pirnia. Dynamic behavior of tall buildings under wind: Insights from full-scale monitoring. *The structural design of tall and special buildings*, 16:471–486, 2007.
- [27] M. Kochly and T.Kijewski-Correa, editors. *Monitoring tall Buildings under the Action of Wind: the Role of GPS in urban Zones*, July 2005. ITAM AS CR, EACWE4 - The Fourth European & African Conference on Wind Engineering.
- [28] N. Labonnote. *Damping in Timber Structures*. PhD thesis, NTNU, 2012.
- [29] P. Léger and S. Dussault. Seismic-energy dissipation in mdof structures. *Journal of Structural Engineering*, 118(5), 1992.
- [30] S. Liang, S. Liu, Q. Li, L. Zhang, and M. Gu. Mathematical model of across-wind dynamic loads on rectangular tall buildings. *Journal of Wind Engineering and Industrial Aerodynamics*, 90:1757–1770, 2002.
- [31] L. Ljung. *System Identification: Theory for the User*. Prentice-Hall, Inc, 1987.

- [32] M.A. Bjertnæs, Sweco. Personal correspondance, drawings and concept information, Fall 2012.
- [33] Moelven. Fagverk, 2012. URL <http://www.moelven.com/no/Produkter-og-tjenester/Limtre/Bygge-med-Limtre/Konstruksjonsystemer/Fagverk/>.
- [34] Norconsult. Flisa bru, 2010. URL http://www.norconsult.no/arch/_img/9053667.pdf.
- [35] O. Øiseth. Personal correspondance and MATLAB scripts,. Department of Structural Dynamics, NTNU, Fall 2012.
- [36] G. Oosterhout. The wind-induced dynamic response of tall buildings, a comparative study. *Journal of Wind Engineering and Industrial Aerodynamics*, 64:135–144, 1996.
- [37] A. Øvrum. Konstruksjonsvirke. *Fokus på tre*, (43), 2007.
- [38] O. M. Rapp. Vil bygge verdens høyeste trehus, 2011.
- [39] T. Reynolds, R. Harris, and W.-S. Chang. Dynamic response of tall timber buildings to wind load. University of Bath, UK, 2012. URL <http://reynoldstom.files.wordpress.com/2012/04/thomas-reynolds-full-paper1.pdf>.
- [40] E. Simiu and T. Miyata. *Design of Buildings and Bridges for Wind*. John Wiley & Sons. Inc, 2006.
- [41] Simulia. *Abaqus Analysis User’s Manual*. Dassault Systèmes, 2011.
- [42] K. H. Solli and G. Glasø. Trebaserte konstruksjonselementer. *Fokus på tre*, (27), 2002.
- [43] *NS-EN 1194 - Trekonstruksjoner, Limtre, Fasthetsklasser og bestemmelse av karakteristiske verdier*. Standard Norge, 1.edition edition, September 1999.
- [44] *NS-EN 1991-1-1:2002, Eurokode 1: Laster på konstruksjoner, Del 1-1: Allmenne Laster, Tetthet, egenvekt, nyttelaster i bygninger*. Standard Norge, 2002.
- [45] E. Strømmen. *Theory of Bridge Aerodynamics*. Springer, 2. edition, 2010.
- [46] K. Sveen. Moelven limtre as. ppt-presentation, 2012.
- [47] J.-H. Weng and C. Loh. Recursive subspace identification for on-line tracking of structural modal parameter. *Mechanical Systems and Signal Processing*, 25: 2923–2937, 2011.
- [48] C. O. Yigit, C. Inal, and M. Yetkin, editors. *Monitoring of tall Building’s dynamic Behaviour using precision inclination Sensors*, May 2008. LNEC, Symposium on Deformation Measurement and Analysis.

APPENDIX

A Mass properties of *Abaqus* model

A.1 Added mass in model for eigenfrequency analysis

To represent the actual mass of the building in the eigenfrequency analysis, components excluded from the model are implemented as increased density. The components that contribute with mass but not stiffness are summarized in table A.1.

Table A.1: Increased mass from non-structural components

| Component: | Weight: | Increased density: | Applied to: |
|---------------------|--------------|--------------------|------------------|
| Modules | $1.77kN/m^2$ | $\sim 1060kg/m^3$ | Concrete slabs * |
| Balcony | $0.8kN/m^2$ | $\sim 780kg/m^3$ | Columns |
| Cladding glass | $0.45kN/m^2$ | $\sim 830kg/m^3$ | Columns |
| Cladding (timber) | $0.5kN/m^2$ | $\sim 1010kg/m^3$ | Columns |
| Permanent live load | $0.6kN/m^2$ | $\sim 360kg/m^3$ | Concrete slabs * |

* *Increased density in slab, per story*

The cladding is distributed on the columns. For the corner columns, both the weight from timber cladding, glass cladding and balconies are added. The sketch of the building, shown in figure 1.1 is used as a basis to calculate the cladding distributions. The distribution of the cladding is assumed to be equally divided between the columns at one facade.

In addition to the non-structural components, a permanent fraction of the live load must be considered in the eigenfrequency analysis. Eurocode 1 defines this to be 30% of the live load. Eurocode 1 also allows for a reduction factor for imposed loads over several storeys. This will not be used for the eigenfrequency analysis, but if detailing of the column and frame were interesting, a reduction factor should be used.

The residential building categorize as *Category A*, Areas for domestic and residential activities. According to the national annex this gives a distributed load $q_k = 2.0kN/m^2$ for all floors.

A.1.1 Distribution of mass

Since there is no rotation of the concrete slabs, and thus the distribution of the mass over the height is neglectable, the increased mass from the modules and the permanent live load are summarized and added to the concrete slabs. This is also a good representation of the actual concept where the modules are supported by the concrete slabs.

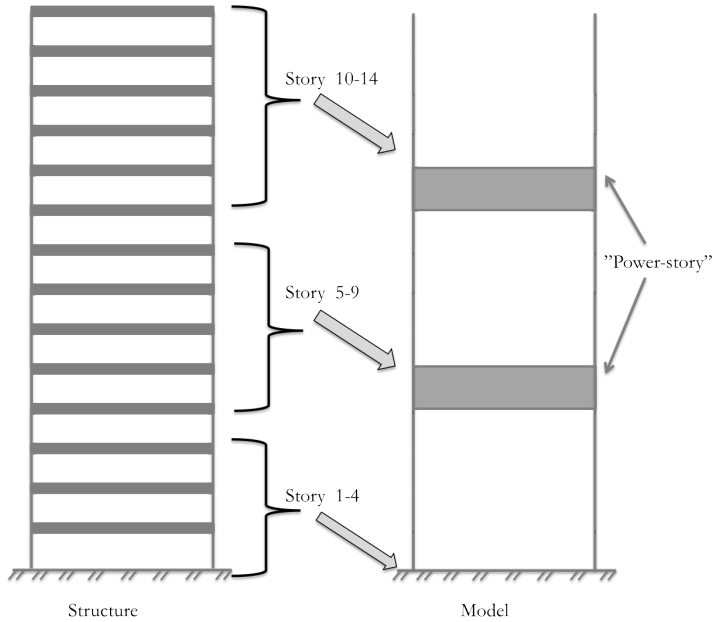


Figure A.1: Simplification of mass and live load in stories

The mass of story 1-4 is neglected since this load is carried entirely by the foundation / basement structure.

B Formulas for wind load and acceleration

To calculate the wind load acting on the building and the resulting acceleration of the top story, a MATLAB script is used. The formulas used in the calculations are presented in the following. The required input for the calculations are:

For simplicity, the concept building is considered rectangular, and no cut outs are included.

The formulas needed for the calculation of wind load, acceleration and response spectrum are to a certain extent similar, each formula will only be given once, while used several times.

The MATLAB scripts for the calculations can be found in appendix E, and in the digital appendix.

Table B.1: Properties for calculation of the wind load

| Property: | | Value: | |
|---------------------------------------|--|--------------|--------------|
| v_b | Basis wind velocity | 26m/s | |
| $0-IV$ | Terrain category | III | |
| h, z | Height of building | 44.15m | |
| m | Mass of upper 1/3 of building | 632770 kg | |
| δ_s | Logarithmic decrement from structural damping | 0.0943 | |
| Direction specific properties: | | x-dir | z-dir |
| b | Dimension of building orthogonal to wind | 22.34m | 20.66m |
| d | Dimension of building parallel with wind | 20.66m | 22.34m |
| n_1 | Eigenfrequency for motion in alongwind direction | 1.351Hz | 1.245Hz |

B.1 Wind load

The wind load on a structure is defined in Eurocode 1 section 5.3. There are several ways of calculating the wind load, here the wind pressure will be used. The internal pressure will neutralize each other, and friction forces from wind are neglected due to similarity. The MATLAB script used to generate the wind forces is given in the MATLAB appendix as well as the digital appendix.

The wind load is found as:

$$F_w = c_s c_d \cdot \sum_{surfaces} w_e \cdot A_{ref} \quad (B.1)$$

where:

| | |
|-----------|------------------------------------|
| $c_s c_d$ | is the structural factor |
| w_e | is the wind pressure at height z |
| A_{ref} | is the reference area |

The first quantity needed is the mean wind velocity v_m , based on the reference wind velocity v_b at the site:

$$v_b = c_{dir} \cdot c_{season} \cdot c_{alt} \cdot c_{prob} \cdot v_{b,0} \quad (B.2a)$$

$$v_m = c_r \cdot c_0 \cdot v_b \quad (B.2b)$$

where:

| | |
|--------------|---|
| c_{dir} | is the directional factor, usually = 1 |
| c_{season} | is the seasonal factor, usually = 1 |
| c_{alt} | is the altitude factor, usually = 1 |
| c_{prob} | is the probability factor, usually = 1 |
| $v_{b,0}$ | is the characteristic wind speed given for the site |
| c_r | is the roughness coefficient |
| c_0 | is the terrain form factor, usually = 1.0 |

The roughness factor c_r is dependent on the terrain roughness defined by k_r is:

$$c_r = k_r \ln\left(\frac{z}{z_0}\right) \quad (B.3)$$

where:

| | |
|-------|--|
| k_r | is the roughness, for terrain category III, $k_r = 0.22$ |
| z | the height where the wind load is calculated for |
| z_0 | roughness length, $z_0 = 0.3$ |

The wind pressure at height z can be found from the mean wind velocity and the

turbulence intensity.

$$I_v = \frac{\sigma_v}{v_m} = \frac{k_l}{c_0 \cdot \ln(\frac{z}{z_0})} \quad (\text{B.4})$$

where:

σ_v is the standard deviation of the wind velocity
 k_l is the turbulence factor, usually = 1
 \ln is the natural logarithm

The peak velocity pressure as a function of the height over ground, z , is dependent of the turbulence intensity, and mean wind speed.

$$q_p = [1 + 7 \cdot I_v] \cdot \frac{1}{2} \cdot \rho \cdot v_m^2 \quad (\text{B.5})$$

where:

I_v is turbulence intensity
 ρ is the air density, usually 1.25 kg/m^3
 v_m is the mean wind velocity

Furthermore, the wind pressure can be found from equation B.6.

$$w_e = q_p(z) \cdot c_{pe} \quad (\text{B.6})$$

where:

q_p is peak velocity pressure
 c_{pe} is pressure coefficient
 z_e is the reference height for external pressure

The forces on the sides orthogonal to the wind, are set to zero, since they will neutralize each other. The pressure coefficient is different for the windward and leeward sides. When accounting for the pressure on the windward side combined with the suction on the leeward side, the pressure coefficient can be found as:

$$c_{pe} = c_{pe}(D) + corr \cdot c_{pe}(E) \quad (\text{B.7})$$

Where *corr* is the correction factor for correlation as stated in Eurocode 1-4, 7.2.2(3). The pressure coefficients $c_{pe}(D)$ and $c_{pe}(E)$ for zone D and E respectively, are found as $c_{pe,10}$ from table 7.1 in Eurocode 1-4, and the values are interpolated in the MATLAB script [44]. See figure B.1 for the zone division.

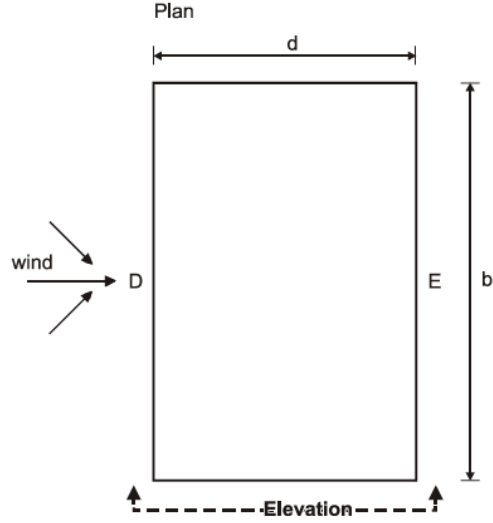


Figure B.1: Pressure zones on the building [44]

The structural factor is given in 6.3.1 in Eurocode 1-4. This factor take into consideration the effect of the wind gust pressure on the surface (c_s) and the oscillation due to turbulence (c_d) [44]. The reference height $z_s = 0.6 \cdot h$ is used to find the structural factor.

$$c_s c_d = \frac{1 + 2 \cdot k_p \cdot I_v(z_s) \cdot \sqrt{B^2 + R^2}}{1 + 7 \cdot I_v(z_s)} \quad (\text{B.8})$$

where:

- k_p is the peak factor
- $I_v(z_s)$ is the turbulence intensity
- B^2 is the background factor
- R^2 is the resonance factor

The background factor B^2 accounts for the lack of full correlation of the pressure on the surface:

$$L = L_t \left(\frac{z}{z_t} \right)^\alpha \quad (\text{B.9a})$$

$$B^2 = \frac{1}{(1 + 0.9 \cdot \left(\frac{b+h}{L} \right)^{0.63})} \quad (\text{B.9b})$$

where:

- L is the turbulence length scale, representing the gust size
- L_t is the reference length scale, $L_t = 300m$
- z_t is the reference height, $z_t = 200m$
- α is a constant depending on the roughness length: $\alpha = 0.67 + 0.05 \ln(z_0)$

The non-dimensional power spectral density function is an expression of the wind distribution over frequencies.

$$f_L = \frac{n \cdot L}{v_m} \quad (\text{B.10a})$$

$$S_L = \frac{6.8 \cdot f_L}{(1 + 10.2 \cdot f_L)} \quad (\text{B.10b})$$

The resonance response factor R^2 accounts for turbulence in resonance with the relevant vibration mode.

$$\eta_h = \frac{4,6 \cdot h \cdot f_L}{L} \quad (\text{B.11a})$$

$$R_h = \frac{1}{\eta_h} - \frac{1 - e^{-2\eta_h}}{2\eta_h^2} \quad (\text{B.11b})$$

$$R^2 = \frac{\pi^2}{2 \cdot \delta} \cdot S_L \cdot R_h \cdot R_b \quad (\text{B.11c})$$

R_b is found in the same manner as R_h , by replacing h with b in the equations for both η_h and R_h . δ is the logarithmic decrement, described previously.

The peak factor is given as:

$$\nu = n_1 \sqrt{\frac{R^2}{B^2 + R^2}} \quad (\text{B.12a})$$

$$k_p = \sqrt{2 \cdot \ln(\nu \cdot T)} + \frac{0.6}{\sqrt{2 \cdot \ln(\nu \cdot T)}} \quad (\text{B.12b})$$

where:

- ν is the up-crossing frequency
- T is the averaging time for the mean wind velocity, $T=600\text{sec}$
- $n_{1,x}$ is the first eigenfrequency in x-direction

Finally, combining all these formulas, the distributed wind load on the building in x- and z-direction can be calculated.

B.1.1 Distribution of wind load

The static wind load applied to the structure in *Abaqus* is generated with a MATLAB code based on the formulas given in Eurocode 1-4 [44]. This load is applied to the columns. The load area for each column varies in the two directions (x and z),

Table B.2: Distribution of static wind forces

| <i>z-direction:</i> | | <i>x-direction:</i> | |
|---------------------|------------|---------------------|------------|
| height | Wind force | height | Wind force |
| [m] | [kN] | [m] | [kN] |
| 20.66 | 462.2 | 22.34 | 553.8 |
| 21.23 | 12.8 | 44.15 | 663.8 |
| 21.79 | 12.9 | | |
| 22.36 | 13.0 | | |
| 22.92 | 13.1 | | |
| 23.49 | 13.2 | | |
| 44.15 | 582.1 | | |

and also between the corner columns and inner columns. The calculated forces are given in table B.2 - B.4.

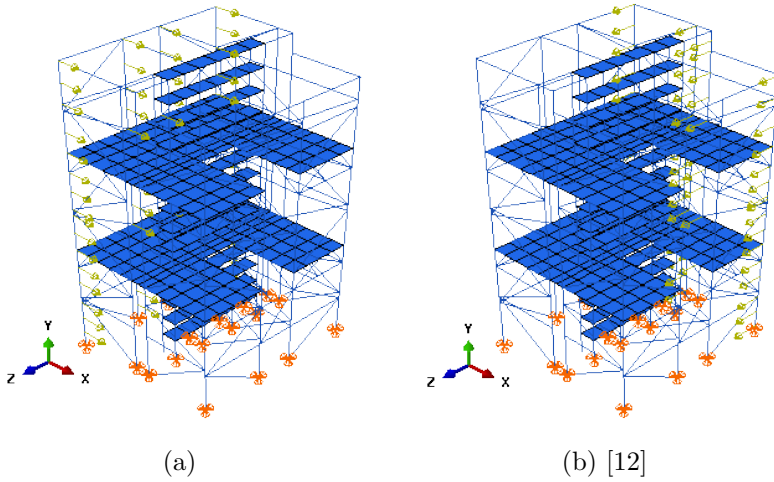


Figure B.2: Applied wind load

Figure B.2 shows the distribution of the wind forces on the columns. Since c_{pe} gives a combination of the windward and leeward pressure, the forces are applied at one of the building faces only.

The distribution of the forces over height are given in table B.2, while the wind load applied in each column is given in table B.3 and B.4. A general static step is performed on the model in *Abaqus* to achieve results for the displacement.

Table B.3: Applied static wind forces in z-direction

| height [m] | Wind load [kN/m ²] | Wind force [kN/m] | |
|----------------|-----------------------------------|----------------------|----------------|
| | | Inner columns | Corner columns |
| 0 - 20.66 | 1.08 | 6.16 | 5.02 |
| 20.66 - 23.49* | 0.798 | 6.58 | 5.37 |
| 23.49 - 44.15 | 1.26 | 7.76 | 6.33 |

* mean value of all h_{strip} calculated

Table B.4: Applied static wind forces in x-direction

| height [m] | Wind load [kN/m ²] | Wind force on columns [kN/m] | |
|---------------|-----------------------------------|---------------------------------|--------|
| | | Inner | Corner |
| 0 - 22.34 | 1.11 | 6.31 | 5.15 |
| 22.34 - 44.15 | 1.36 | 7.75 | 6.32 |

B.2 Calculation of acceleration at top floor:

The acceleration at the top of the building from wind load in x-direction can be calculated from equation B.13, similarly for the z-direction.

$$acc = \sigma_{a,x} \cdot k_p \quad (B.13)$$

where:

$\sigma_{a,x}$ is the standard deviation of the wind induced acceleration
 k_p is the peak factor with $\nu = n_1$

For the calculation of v_m and v_b as given in equation B.2, the probability factor $c_{prob} \neq 1.0$. To account for the reduced return period, set to 2 years, c_{prob} is calculated as:

$$c_{prob} = \left[\frac{1 - K \cdot \ln(-\ln(1 - p))}{1 - K \cdot \ln(-\ln(0.98))} \right]^n \quad (B.14)$$

where:

K is a shape parameter, usually $K = 0.2$
 p is the probability corresponding to the return period, $p = 1/T_{return}$
 n is usually equal to 0.5

The standard deviation is given in equation B.15, and the peak factor is given in

equation B.12b.

$$\sigma_{a,x}(z) = \frac{c_f \cdot \rho \cdot b \cdot I_v(z_s) \cdot v_m^2(z_s)}{m_{1,x}} \cdot R \cdot K_x \cdot \phi_{1,x}(z) \quad (\text{B.15})$$

where:

| | |
|-----------------|--|
| c_f | is the force coefficient, $c_f = c_{f0} \cdot \psi_L$ |
| ρ | is the air density, $\rho = 1.25 \text{ kg/m}^3$ |
| b | is the width of the structure |
| $I_v(z_s)$ | is the turbulence intensity at height z_s |
| $v_m(z_s)$ | is the mean wind velocity for the reference height z_s |
| R | is the square root of resonant response |
| K_x | is a non-dimensional coefficient |
| $m_{1,x}$ | is the equivalent mass |
| $n_{1,x}$ | is the first eigenfrequency of along-wind vibration |
| $\phi_{1,x}(z)$ | is the fundamental mode shape |

The following simplifications and approximations are done for the parameters needed to calculate $\sigma_{a,x}$. The reader is referred to appendix F in Eurocode 1-4 for further reference.

The *fundamental mode shape*, $\phi_{1,x}$ is assumed to be linear, with $\zeta = 1.0$, such that the expression is simply:

$$\phi_1 = \left(\frac{z}{h}\right)^\zeta \quad (\text{B.16})$$

This is assumed a good approximation, since the modal analysis gave almost linear mode shapes for the first translational modes in both z- and x-direction.

The *non-dimensional coefficient* is found with the simplified formula:

$$K_x = \frac{(2 \cdot \zeta + 1) \left[(\zeta + 1) \cdot \left(\ln\left(\frac{z_s}{z_0}\right) + 0.5 \right) - 1 \right]}{(\zeta + 1)^2 \cdot \ln\left(\frac{z_s}{z_0}\right)} \quad (\text{B.17})$$

The *equivalent mass* is approximated as the distributed mass of the upper 1/3 of the building. The mass is calculated in *Abaqus*.

B.3 Spectral analysis

The formulas for calculating the response using a spectral analysis is given in the following. The MATLAB script used for the calculations are given in the digital appendix.

Spectral density of wind velocity $S_L(f_L)$ According to Eurocode 1, the non-dimensional spectral density function of the fluctuating wind can be found from equation B.18a [44]. The magnitude of the wind is a function of the eigenfrequency n , and the height z

$$S_L(z, n) = \frac{6.8 \cdot f_L(z, n)}{(1 + 10.2 \cdot f_L(z, n))^{5/3}} \quad (\text{B.18a})$$

$$f_L(z, n) = \frac{n \cdot Lz}{v_m(z)} \quad (\text{B.18b})$$

where:

$f_L(z, n)$ is the dimensionless frequency
 n is the eigenfrequency
 $L(z)$ is the turbulence length scale: $L(z) = L_t \cdot (z/z_t)^\alpha$
 $v_m(z)$ is the mean wind velocity

The one-sided variance spectrum can then be found according to Eurocode 1:

$$S_v(z, n) = \frac{S_L(z, n) \cdot \sigma_v^2}{n} \quad (\text{B.19})$$

where:

$S_L(z, n)$ is the spectral density function
 σ_v^2 is the variance of the wind: $\sigma_v^2 = [I_v(z) \cdot v_m(z)]^2$
 n is the eigenfrequency

Aerodynamic admittance function $\chi^2(f_L)$ To transform the wind velocities to wind forces, the aerodynamic admittance function acts as a transfer function, see equation B.22. The aerodynamic admittance function is a function of the fundamental mode shapes and the geometry:

$$\chi^2(f_L) = R_h \cdot R_b \quad (\text{B.20})$$

where R_h and R_b can be approximated as: (substitute b for h to get R_b)

$$R_h = \frac{1}{\eta_h} - \frac{1 - e^{-2\eta_h}}{2 \cdot \eta_h} \quad (\text{B.21a})$$

$$\eta_h = \frac{4.6 \cdot h}{L(z_s)} \cdot f_L(z_s, n_{1,x}) \quad (\text{B.21b})$$

where:

h is the building height
 b is the width of the building face perpendicular to the wind direction
 $L(z_s)$ is the turbulence length scale of the reference height z_s
 f_L is the dimensionless frequency

Power density spectrum $\mathbf{S_F(f_L)}$ The power density spectrum of the along-wind load can be found by the formula given in [36].

$$S_F(f_L) = [c_F \cdot C_d \cdot \rho \cdot v_m(z) \cdot A]^2 \cdot \chi^2(f_L) \cdot S_v(z, n) \quad (\text{B.22})$$

where:

| | |
|---------------|---|
| c_F | is the force coefficient |
| C_d | is the drag coefficient |
| ρ | is the density of air, $\rho = 1.25 \text{ kg/m}^3$ |
| $v_m(z)$ | is the mean wind velocity |
| A | is the area subjected to wind load |
| $\chi^2(f_L)$ | is the aerodynamic admittance |
| $S_v(z, n)$ | is the variance spectrum |

Mechanical admittance function $\mathbf{H_x(n)}$ The transfer function between the load and the response spectrum is called the mechanical admittance function. In general, for a harmonic load such as $F(t) = F_0 \cos(2\pi nt)$ the response can be written as $x(t) = H(n) F_0 \cos(2\pi nt - \theta)$. Where $H(n)$ represents the transfer function given by [40]:

$$H_x(n) = \frac{1}{4\pi^2 n_1^2 m \sqrt{(1 - (\frac{n}{n_1})^2)^2 + 4\zeta_1^2 (\frac{n}{n_1})^2}} \quad (\text{B.23})$$

where:

| | |
|-----------|------------------------------|
| n_1 | is the first eigenfrequency |
| n | is the frequency |
| m | is the mass of the structure |
| ζ_1 | is the damping ratio |

Response spectrum $\mathbf{S_x(f_L)}$ Finally the response spectrum can be given by the transfer function $H_x(n)$ and the load spectrum $S_F(f_L)$:

$$S_x(f_L) = [H_x(n)]^2 \cdot S_F(f_L) \quad (\text{B.24})$$

where:

| | |
|------------|--------------------------------|
| $H_x(n)$ | Mechanical admittance function |
| $S_F(f_L)$ | Power density spectrum |

B.4 Displacements and accelerations

The dynamic response is a resultant of the quasi-static and resonance component [11]. The dynamic displacement is calculated from equation B.25, and the acceler-

ation from B.26 [11].

$$\sigma_{stat} = \frac{c_d \cdot A \cdot v_m \cdot \sigma_v}{k} \quad (\text{B.25a})$$

$$\sigma_{res} = \frac{1}{k} \sqrt{\frac{\pi \cdot n_1 \cdot S_F(f_L)}{4 \cdot \xi}} \quad (\text{B.25b})$$

$$\sigma_{dyn} = \sqrt{\sigma_{stat}^2 + \sigma_{res}^2} \quad (\text{B.25c})$$

where:

| | |
|------------|---------------------------------------|
| c_d | is the drag coefficient |
| A | is the area subjected to wind load |
| v_m | is the mean wind velocity |
| σ_v | is the standard deviation of the wind |
| k | is the global stiffness |
| n_1 | is the first eigenfrequency |
| ξ | is the damping ratio of the structure |
| $S_F(f_L)$ | is the power density spectrum |

The acceleration can be found as:

$$\sigma_{acc} = \sqrt{\frac{S_F(f_L) \cdot \pi \cdot n_1}{4 \cdot \xi \cdot m^2}} \quad (\text{B.26})$$

where:

| | |
|------------|---------------------------------------|
| m | is the total mass |
| n_1 | is the first eigenfrequency |
| ξ | is the damping ratio of the structure |
| $S_F(f_L)$ | is the power density spectrum |

C Calculation of the stiffness of the connection

A sketch of a typical connection for a glulam truss is used to calculate the stiffness in the connection. The connection is used in a bridge designed by SWECO, and an example is shown in the figure. It is assumed in the following that all connections are of the same type, with 5x5 dowels with diameter 12mm used as fasteners, and 2 slotted steel plates.

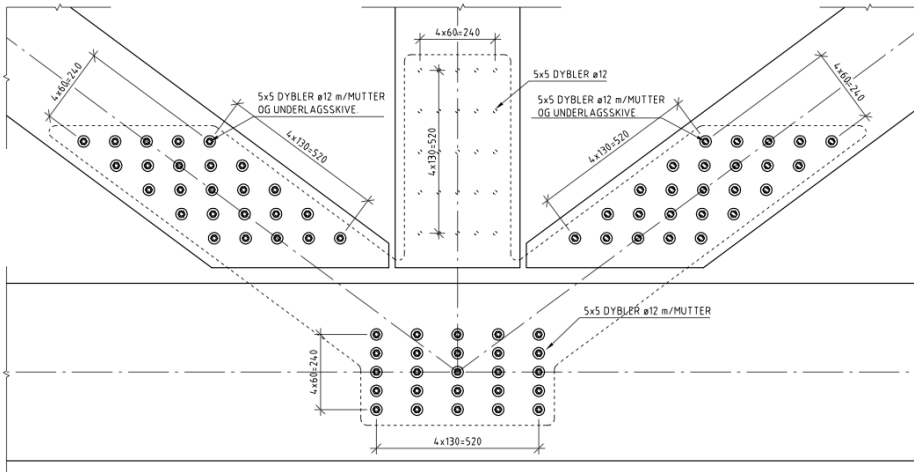


Figure C.1: Sketch of a connection in a timber bridge [32]

C.1 Axial stiffness

The stiffness module for a connection is found in chapter 7 in Eurocode 5-1, and given in equation C.3.

$$K_{ser} = \sum_{i=1}^s \sum_{j=1}^n \cdot \rho_m^{1.5} \cdot \frac{d}{23} \quad (C.1)$$

where:

- n is the number of fasteners in the connection: $n = 25$
- s is the number of sections in the connection: $s = 4$
- ρ_m is the mean density of the timber, $\rho_m = 400 \text{ kg/m}^3$
- d is the diameter of the fastener: $d = 12 \text{ mm}$

For a connector with steel or concrete, only the timber will deform, thus the stiffness can be multiplied with 2 according to Eurocode 1-4, 7.1(3). For 2 slotted steel plates, the stiffness of one fastener is:

$$K_{ser,fasteners} = 2 \cdot 4 \cdot 470^{1.5} \cdot \frac{12}{23} = 42530 \text{ N/mm} \quad (C.2)$$

This gives a total stiffness in each connection:

$$K_{ser,connection} = 25 \cdot 42530 \text{ N/mm} = 1.063 \cdot 10^6 \text{ N/mm} \quad (C.3)$$

C.2 Rotational stiffness

The rotational stiffness in the connections are found as:

$$K_{rot,connection} = K_{ser,fastener} \cdot I_p \quad (C.4)$$

where:

- $k_{ser,fastener}$ is the stiffness in one fastener
- I_p is the polar 2. moment of area

The polar 2. moment of area of a group of fasteners can be found as:

$$I_p = \sum x_i^2 + \sum z_i^2 \quad (C.5)$$

where x_i and z_i is the distance from the center of the group to fastener i in x- and z-direction respectively.

The rotational stiffness in the connection can then be found as:

$$K_{rot} = 42530 \cdot (2 \cdot 5 \cdot (130^2 + 260^2) + 2 \cdot 5 \cdot (60^2 + 120^2)) = 4.356 \cdot 10^{10} \text{ Nmm/rad} \quad (C.6)$$

D Digital appendix

In the digital appendix the following folders and contents can be found:

Models

Abaqus models of the frame structure, including important odb.-files

VHT_simple.cae

VHT_beamsegments.cae

VHT_incl_modules.cae

Dynamic wind

MATLAB script to calculate the dynamic wind forces and generate input files for *Abaqus*. Files are provided by Ole Øiseth unless otherwise stated.

SystemID

MATLAB script to perform the system identification, and the generated acceleration time histories from the dynamic analysis. The MATLAB files are provided by Ole Øiseth.

Static wind

MATLAB scripts to calculate static wind load, accelerations, Rayleigh-damping and spectral analysis. The self-produced scripts are also given in appendix E.

Presentation

Power-point presentation as presented at the department of Structural Engineering December 5th 2012.

E Matlab scripts

The MATLAB scripts written during the work with this thesis, and used for calculations of the wind response are given in the following for reference.

E.1 Calculation of distributed static Wind Load

```
%%%%%%%%%%%%%%%%%%%%%%%%%%%%%%%%%%%%%%%%%%%%%%%%%%%%%%%%%%%%%%%%%%%%%%%%%%%%%%
%                               Wind loading and acceleration           %
%                               Ingunn Utne, NINU                        %
%%%%%%%%%%%%%%%%%%%%%%%%%%%%%%%%%%%%%%%%%%%%%%%%%%%%%%%%%%%%%%%%%%%%%%%%%%%%%%
clear all
close all
clc

%% Input:
vb0= 26; %[m/s^2] Basis wind velocity
kat = 3; %[] Terrain categori, 0-4

%geometry:
h=44.15; %[m]
b=20.66; %[m] direction orthogonal with wind (x-dir: 22.34)
d=22.34; %[m] direction parallel with wind (x-dir: 20.66)

%frequency in alongwind direction:
f=1.245; %[Hz] x-dir: 1.351

%structural damping, represented with logarithmic decrement
delta=0.0943; %damping ratio=1.5

%% Distribution over height:
B=2*b;
if h>B
    zstrip=(h-B)/5;
    z=[b (b+zstrip) (b+2*zstrip) (b+3*zstrip) (b+4*zstrip) (h-b) h];
elseif (h<=B) & (h>b)
    z=[b h];
else
    z=[h];
end

%% Constants:
rho = 1.25; %kg/m^3

c_dir=1;
```



```

c_season=1;
c_alt=1;
c_prob=1;

z_0=[0.003 0.01 0.05 0.3 1.0];
z0=z_0(1+kat);
z_min=[2 2 4 8 16];
zmin=z_min(1+kat);
k_r=[0.16 0.17 0.19 0.22 0.24];
kr=k_r(1+kat);
z0ii=0.05;

co=1.0;
kl=1.0;

zt=200;
Lt=300;

T=600;

zeta=1.0;

%% Wind pressure:
vb=c_dir*c_season*c_alt*c_prob*vb0;

if z<zmin
    lnZ=log(zmin/z0);
else
    lnZ=log(z./z0);
end

cr=kr.*lnZ;

%mean wind velocity:
vm=cr.*co.*vb;

%Turbulence intensity:
I=kl./(co.*lnZ);

%wind pressure:
q=(1+(7.*I)).*0.5.*rho.*vm.^2;

%form factor:
H=h/d;
if H>=1
    c_peD=0.8;
elseif H<=0.25
    c_peD=0.7;
else
    c_peD=0.7+(H-0.25)*(0.8-0.7)/(1-0.25);
end

if H>5
    c_peE=0.7;
elseif H<=0.25
    c_peE=0.3;
else
    if H>=1
        c_peE=0.5+(H-1)*(0.7-0.5)/(5-1);
    elseif H<1
        c_peE=0.3+(H-0.25)*(0.5-0.3)/(1-0.5);
    end
end

korr=0.85+(H-1)*(1-0.85)/(5-1);
c_pe=c_peD+korr*c_peE;

% external wind pressure: %

```

```

w_e = q.*c_pe;

%% construction factor (from appendix B in Eurokode 1-4):
zs=0.6*h;

%Turbulence intensity:
Izs=k1/(co*log(zs/z0));

%Mean wind velocity for zs:
vm_z=kr*log(zs/z0)*co*vb;

%Turbulence lenght:
alpha=0.67+0.05*log(z0);
L=Lt*(zs/zt)^alpha;

%background factor (B^2):
B2=1/(1+0.9*((b+h)/L)^0.63);

%non-dimensional frequency:
fL=f*L/(vm_z); %wm=cr*co*vb, cr=kr*ln(zs/z0)

%force factor:
D=d/b;
if D>10
    cf0=0.9;
elseif D<0.2
    cf0=2.0;
elseif (D>=0.2) & (D<=0.7)
    cf0=2.0+(D-0.2)*(2.4-2.0)/(0.7-0.2);
elseif (D>0.7) & (D<5)
    cf0=2.4+(D-0.7)*(1.0-2.4)/(5-0.7);
elseif (D>5) & (D<10)
    cf0=1.0+(D-5)*(1.0-0.9)/(10-5);
end

lambda=(1.0+((h-15)*(0.7-1)/(50-15)))*(h/d);
if (lambda<10) & (lambda>=1)
    psiL=0.6+(lambda-1)*(0.7-0.6)/(10-1);
elseif (lambda>=10) & (lambda<70)
    psiL=0.92+(lambda-10)*(0.92-0.7)/(70-10);
end
cf=cf0*psiL;

%non-dimensional spectral density function:
S=6.8*fL/((1+10.2*fL)^(5/3));

%aerodynamic admittance function:
etah=4.6*h*fL/L;
etab=4.6*b*fL/L;

if etah>0
    Rh=(1/etah)-((1-exp(-2*etah))/(2*etah^2));
else
    Rh=1;
end

if etab>0
    Rb=(1/etab)-((1-exp(-2*etab))/(2*etab^2));
else
    Rb=1;
end

%resonance response factor (R^2):
R2=pi^2/(2*delta)*S*Rh*Rb;

%up-crossing frequency:
v=f*sqrt(R2/(B2+R2));

```

```

%top factor:
kp=sqrt(2*log(v*T))+(0.6/sqrt(2*log(v*T)));

% construction factor: %
cscd=(1+2*kp*Izs*sqrt(B2+R2))/(1+7*Izs);

%% Wind force on wall orthogonal to wind direction:
z_ny=[0 z];
no=length(z_ny);
F=zeros(1,length(z));
A=zeros(1,length(z));
for i=1:no-1
    hi=z_ny(i+1)-z_ny(i);
    F(i)=cscd*w_e(i)*hi*b/1000;
    A(i)=hi*b;
    f_w(i)=F(i)/A(i);
    fic(i)=f_w(i)*5.689;
    fcc(i)=f_w(i)*4.639;
end
results=[z' F' f_w' fic' fcc'];

disp('
disp('      Height      Wind force Load      Inner col      Corner col')
for i=1:length(z)
disp(results(i,:))
end

```

E.2 Calculation of maximum Acceleration

```

%%%%%%%%%%%%%%%%%%%%%%%%%%%%%%%%%%%%%%%%%%%%%%%%%%%%%%%%%%%%%%%%%%%%%%%%%%%%%%
%                               Wind loading and acceleration                               %
%                               Ingunn Utne, NTNU                                         %
%%%%%%%%%%%%%%%%%%%%%%%%%%%%%%%%%%%%%%%%%%%%%%%%%%%%%%%%%%%%%%%%%%%%%%%%%%%%%%
clear all
close all
clc

%% Input:
vb0= 26; %[m/s^2] Basis wind velocity
kat = 3; %[] Terrain categori, 0-4

% Z-direction: %

%geometry:
h=44.15; %[m]
b=20.66; %[m] direction orthogonal with wind (x-direction: 22.34)
d=22.34; %[m] direction parallel with wind (x-direction:20.66)

%frequency in alongwind direction: approximation: f=46/h
f=1.245; %[Hz] x-direction: 1.351

%returperiode:
retur=2; %eurocode=50yr, acceleration: 1yr

%structural damping, represented with logarithmic decrement
xi=1.5/100;
delta_s=2*pi*xi/sqrt(1-xi^2)

%distributed mass in upper 1/3 of structure:
m=632772/(44.15/3); %[kg] mass from Abaqus, from below the top of the 2nd←
power story to the top.

```

```

%% Constants:
rho = 1.25; %kg/m^3

c_dir=1;
c_season=1;
c_alt=1;

z_0=[0.003 0.01 0.05 0.3 1.0];
z0=z_0(1+kat);
z_min=[2 2 4 8 16];
zmin=z_min(1+kat);
k_r=[0.16 0.17 0.19 0.22 0.24];
kr=k_r(1+kat);
z0ii=0.05;

co=1.0;
kl=1.0;

zt=200;
Lt=300;

T=600;

zeta=1;
z=h;

%% Return period:
K=0.2;
n=0.5;
p=1/retur;

c_prob=((1-(K*log(-log(1-p)))))/(1-(K*log(-log(0.98))))^n;

%% Mean wind:
vb=c_dir*c_season*c_alt*c_prob*vb0;

%% construction factor (from appendix B in Eurokode 1-4):
zs=0.6*h;

%%Turbulence intensity:
Izs=kl/(co*log(zs/z0));

%%Mean wind velocity for zs:
vm_z=kr*log(zs/z0)*co*vb;

%%Turbulence lenght:
alpha=0.67+0.05*log(z0);
L=Lt*(zs/zt)^alpha;

%%background factor (B^2):
B2=1/(1+0.9*((b+h)/L)^0.63);

%%non-dimensional frequency:
fL=f*L/(vm_z); %vm=cr*co*vb, cr=kr*ln(zs/z0)

%%force factor:
D=d/b;
if D>10
    cf0=0.9;
elseif D<0.2
    cf0=2.0;
elseif (D>=0.2) & (D<=0.7)
    cf0=2.0+(D-0.2)*(2.4-2.0)/(0.7-0.2);
elseif (D>0.7) & (D<5)
    cf0=2.4+(D-0.7)*(1.0-2.4)/(5-0.7);
elseif (D>5) & (D<10)
    cf0=1.0+(D-5)*(1.0-0.9)/(10-5);

```

```

end

lambda=(1.0+((h-15)*(0.7-1)/(50-15)))*(h/d);
if (lambda<10) & (lambda>=1)
    psiL=0.6+(lambda-1)*(0.7-0.6)/(10-1);
elseif (lambda>=10) & (lambda<70)
    psiL=0.92+(lambda-10)*(0.92-0.7)/(70-10);
end

cf=cf0*psiL;

%logarithmic decrement from damping:
delta_a=cf*rho*b*vm_z/(2*f*m);
delta=delta_s+delta_a;

%non-dimensional spectral density function:
S=6.8*fL/((1+10.2*fL)^(5/3));

%aerodynamic admittance function:
etah=4.6*h*fL/L;
etab=4.6*b*fL/L;

if etah>0
    Rh=(1/etah)-((1-exp(-2*etah))/(2*etah^2));
else
    Rh=1;
end

if etab>0
    Rb=(1/etab)-((1-exp(-2*etab))/(2*etab^2));
else
    Rb=1;
end

%resonance response factor (R^2):
R2=pi^2/(2*delta)*S*Rh*Rb;

%up-crossing frequency:
v=f*sqrt(R2/(B2+R2));

%top factor:
kp=sqrt(2*log(v*T))+(0.6/sqrt(2*log(v*T)));

kp_a=sqrt(2*log(f*T))+(0.6/sqrt(2*log(f*T))); %v=f for acceleration

%construction factor:
cscd=(1+2*kp*Izs*sqrt(B2+R2))/(1+7*Izs);

%% standard deviation for wind-induced acceleration:
%dimensionless factor:
Kx=((2*zeta)+1)*((zeta+1)*(log(zs/z0)+0.5)-1)/(((zeta+1)^2)*log(zs/z0)+1); %assuming phi=(z/h)^zeta

%simplified first fundamental mode
phi=(z/h)^zeta; %preferably: use input from modal analysis

%standard deviation:
sigma=cf*rho*b*Izs*vm_z^2*sqrt(R2)*Kx*phi/m;

%% Acceleration
disp('Acceleration in z-direction, at height y')
acc=sigma*kp_a;
resultsA=[z acc];
disp(resultsA)

```

E.3 Spectral Analysis

```

%%%%%%%%%%%%%%%%%%%%%%%%%%%%%%%%%%%%%%%%%%%%%%%%%%%%%%%%%%%%%%%%%%%%%%%%%%%%%%
%                               Spectral analysis                               %
%                               Ingunn Utne, NINU                               %
%%%%%%%%%%%%%%%%%%%%%%%%%%%%%%%%%%%%%%%%%%%%%%%%%%%%%%%%%%%%%%%%%%%%%%%%%%%%%%
clear all
close all
clc
%% input:
vb0= 26; %[m/s^2]  Basis wind velocity
kat = 3; %[]      Terrain categori, 0-4

%geometry:
h=44.15; %[m]
b=20.66; %[m]    direction orthogonal with wind, x-dir: b=22.34
d=22.34; %[m]    direction parallel with wind, x-dir: d=20.66

%frequency in alongwind direction: approximation: f=46/h
fn=1.245; %[Hz]
%fn=1.351; % for x-retning
f=0:0.001:10; %vector with different frequencies
%f=fn; % for calculation of displacement and acceleration from
%% fluctuating wind load, see line 145-163.

%Total building mass:
M=1.687e+6; %[kg]

%Damping ratio:
xi=1.5/100;

% CONSTANTS:
rho = 1.25; %kg/m^3

c_dir=1;
c_season=1;
c_alt=1;
c_prob=1;

z_0=[0.003 0.01 0.05 0.3 1.0];
z0=z_0(1+kat);
z_min=[2 2 4 8 16];
zmin=z_min(1+kat);
k_r=[0.16 0.17 0.19 0.22 0.24];
kr=k_r(1+kat);
z0ii=0.05;

co=1.0;
kl=1.0;

zt=200;
Lt=300;

T=600;

% WIND PROPERTIES:
z=0.6*h;
%z=h;
%% Wind pressure:
vb=c_dir*c_season*c_alt*c_prob*vb0;

if z<zmin
    lnZ=log(zmin/z0);
else
    lnZ=log(z/z0);

```

```

end

cr=kr*lnZ;

%mean wind velocity:
vm=cr*co*vb;

%Turbulence intensity:
I=k1/(co*lnZ);

%variance of wind:
var=(I*vm)^2;

%Turbulence lenght:
alpha=0.67+0.05*log(z0);
L=Lt*(z/zt)^alpha;

%force factor:
cf=1.2;

% non-dimensional frequency:
fL=f.*(L/vm);
fL1=fn*(L/vm);

%aerodynamic admittance function:
etah=(4.6*h/L).*fL;
etab=(4.6*b/L).*fL;

Rh=zeros(1,length(fL));
for i=1:length(fL)
    Rh(i)=(1/etah(i))-((1-exp(-2*etah(i)))/(2*(etah(i))^2));
end

Rb=zeros(1,length(fL));
for i=1:length(fL)
    Rb(i)=(1/etab(i))-((1-exp(-2*etab(i)))/(2*(etab(i))^2));
end
Rh2=(1./etah)-((1-exp(-2.*etah))/(2.*etah.^2));
Rb2=(1./etab)-((1-exp(-2.*etab))/(2.*etab.^2));

%%%%%%%%%%%%%%%%%%%%%%%%%%%%%%%%%%%%%%%%%%%%%%%%%%%%%%%%%%%%%%%%%%%%%%%% SPECTRAL ANALYSIS: %%%%%%%%%%%%%%%%%%%%%%%%%%%%%%%%%%%%%%%%%%%%%%%%%%%%%%%%%%%%%%%%%%%%%%%%%
% Spectral density of wind velocity %
S_L=6.8.*fL./((1+(10.2.*fL)).^(5/3));

% Aeodynamic admittance function %
chi2=Rh.*Rb;

% Power density spectrum %
S_v=S_L.*var./fn;

S_F=(cf*rho*vm*h*b)^2.*chi2.*S_v;

% Mechanical admittance function %
rot=(1-(f./fn).^2+(4*xi^2.*(f./fn).^2);

Hx=1./((4*pi^2*fn^2*M).*sqrt(rot));

% Response spectrum %
Hx2=Hx.^2;
Ha=abs(Hx2);
S_x=Ha.*S_F;

% Displacements: %
% k=M*(2*pi*fn)^2;
% x_stat=cf*h*b*vm*sqrt(var)/k;
% x_res=1/k*sqrt(pi*fn*S_F/(4*xi));
% x_dyn=sqrt(x_stat^2+x_res^2);

```

```

%
% disp('dynamic displ.:')
% disp(x_dyn)
%
%
% %           Accelerations:           %
% k=M*(2*pi*fn)^2;
% a_dyn=sqrt(pi*fn*S_F/(4*M^2*xi));
%
% disp('dynamic accel.:')
% disp(a_dyn)

%%%%%%%%%%%%%%%%%%%%%%%%%%%%%%%%%%%%%%%%%%%%%%%%%%%%%%%%%%%%%%%%%%%%%%%%% PLOTTING: %%%%%%%%%%%%%%%%%%%%%%%%%%%%%%%%%%%%%%%%%%%%%%%%%%%%%%%%%%%%%%%%%%%%%%%%%%
figure('color',[1 1 1]);
subplot(2,2,1)
    semilogx(f,S_L,'LineWidth',2)
    title('Spectral density','FontWeight','bold','FontSize',18)
    axis([0.01 10 0 0.25])
    xlabel('Frequency, [Hz]','FontSize',18)
    ylabel('S_L(f)','FontSize',18)
subplot(2,2,2)
    semilogx(f,chi2,'LineWidth',2)
    title('Aerodynamic admittance','FontWeight','bold','FontSize',18)
    axis([0.01 10 0 1])
    xlabel('Frequency, [Hz]','FontSize',18)
    ylabel('\chi^2(f)','FontSize',18)
subplot(2,2,3)
    semilogx(f,S_F,'LineWidth',2)
    title('Power density','FontWeight','bold','FontSize',18)
    axis([0.01 10 0 6e9])
    xlabel('Frequency, [Hz]','FontSize',18)
    ylabel('S_F(f)','FontSize',18)
subplot(2,2,4)
    semilogx(f,Hx,'LineWidth',2)
    title('Mechanical admittance','FontWeight','bold','FontSize',18)
    axis([0.01 10 0 3.5e-7])
    xlabel('Frequency, f, [Hz]','FontSize',18)
    ylabel('H_z(f)','FontSize',18)
figure('color',[1 1 1]);
semilogx(f,S_x,'LineWidth',2)
title('Response Spectrum','FontWeight','bold','FontSize',18)
axis([0.01 10 0 3.5e-6])
xlabel('Frequency, f [Hz]','FontSize',18)
ylabel('S_z(f)','FontSize',18)

```